High resolution MRI in patients with stroke or Cushing's disease

Alexandra Aleida Jeichien de Rotte

High resolution MRI in patients with stroke or Cushing's disease

Hoge resolutie MRI in patiënten met
een beroerte of de ziekte van Cushing
(met een samenvatting in het Nederlands)

Proefschrift

ter verkrijging van de graad van doctor aan de Universiteit Utrecht op
gezag van de rector magnificus, prof. dr. G.J. van der Zwaan, ingevolge
het besluit van het college voor promoties
in het openbaar te verdedigen
op dinsdag 14 april 2015 des ochtends te 10.30 uur

Alexandra Aleida Jeichien de Rotte

geboren op 19 maart 1986
te Nijmegen

Promotor:	Prof. dr. P.R. Luijten
Copromotoren:	Dr. J. Hendrikse Dr. G.J. de Borst

The research in this thesis was financially supported by the Center for Translational Molecular Medicine (CTMM) and by the Dutch Heart Foundation.

Financial support by the Dutch Heart Foundation for the publication of this thesis is gratefully acknowledged.
In addition financial support was provided by Brain Center Rudolf Magnus, Röntgenstichting, Philips and ABN AMRO.

CONTENTS

Chapter 1

General introduction

MRI in clinical practice

Imaging is fundamental in modern medicine and is used in different stages of the healthcare process, from diagnosis to therapeutic monitoring. The most important imaging modalities for anatomical imaging are conventional X-ray, ultrasound, computed tomography (CT) and magnetic resonance imaging (MRI). Each of these modalities has certain advantages and disadvantages, which in turn results in specific applications. Three major advantages of MRI are the high spatial resolution, the high contrast in soft tissue imaging, and MRI is not based on ionizing radiation, which makes MRI a harmless imaging modality used to depict small anatomical or pathological structures. On the other hand, two important disadvantages of MRI are the long scanning time and the high costs, compared to the other imaging modalities.

MRI is a technique with a broad spectrum of indications, from anatomical to more functional, in different organ systems.[1-4] In the clinical setting standard MRI is being performed on scanners with a field strength of 1.0 to 3.0 Tesla (T). However, the increasing number of clinical applications often demand a higher spatial resolution than, within an acceptable scanning time, is currently possible with the standard MRI field strengths. A growing number of imaging sites world-wide make use of scanners with a field strength up to 7.0 T. This increase in magnetic field strength enables to increase the signal-to-noise ratio (SNR) and the contrast-to-noise ratio (CNR) of the obtained images. Consequently, imaging with a higher spatial resolution becomes possible within an acceptable scanning time.[5-7]

The current thesis will focus on the use of MRI in patients with stroke and patients with Cushing's disease. In both areas MRI is crucial for diagnosis and in both areas the outcome of MRI contributes to the therapeutic consequences.

Stroke

Stroke is one of the leading causes of morbidity and mortality in the world.[8,9] In 15-20% of stroke patients the origin of the event is a vulnerable atherosclerotic plaque in the extracranial arteries.[10] Large randomized controlled trials have demonstrated that carotid endarterectomy (CEA) is highly beneficial in patients with a symptomatic carotid artery stenosis of 70-99% and moderately beneficial in patients with a symptomatic carotid artery stenosis of 50-70%.[11,12] Consequently, in patients with a carotid origin of ischemic stroke the stenosis grade is leading for therapeutic decision making in routine clinical practice.[11-14]

Although the severity of stenosis is an accurate determinant for (recurrent) cerebral event prediction, atherosclerotic plaques can also be classified according to their components.[15-17] Histology studies have demonstrated that some of the plaque

components are an important determinant in risk assessment for stroke.[18,19] Two of these plaque components are: intraplaque hemorrhage and a thin/ruptured fibrous cap on top of a lipid core, which are demonstrated to be predictive for (recurrent) cerebral ischemia.[20,21] Since these plaque components are sub-millimeter structures, a high spatial resolution is needed in order to visualize them within the plaque. MRI studies with standard field strengths have until now demonstrated that MRI enables visualization of the plaque composition in vivo in high detail.[20-28] However, 7.0 T MRI has the potential to increase the spatial resolution even further, which might enable even more accurate plaque assessment.[29-31]

Additionally, MRI is used for the assessment of brain damage. A high spatial resolution is needed to detect the smallest cerebral infarcts. In routine clinical practice standard MRI enables good results, even for the visualization of microinfarcts. However, to detect the smallest microinfarcts a very high field strength appears to be necessary, which could be provided by the 7.0 T MRI.

Cushing's disease

Endogenous Cushing's syndrome is a clinical condition in which the adrenal glands secrete excessive amounts of cortisol. Patients classically present with non-pathognomonic and nonspecific symptoms and signs (eg. centripetal obesity, full-moon face, buffalo hump in the neck, abdominal striae, facial plethora, a thin skin, easy bruising and fatigue), which makes diagnosis of the presence and the origin of Cushing's syndrome challenging.

In Cushing's disease, which is responsible for 80-85% of adrenocorticotrophic hormone (ACTH)-dependent Cushing's syndrome, an ACTH producing adenoma located in the anterior lobe of the pituitary gland stimulates the adrenal glands to secrete the excessive amounts of cortisol.[32] In the majority of cases these adenomas are small microadenomas, which are challenging to diagnose.[33] Therefore, the final diagnosis is often based on central venous sampling and on MRI.[34] If a pituitary origin of Cushing's syndrome can be confirmed, the treatment of choice is surgical removal of the lesion, for which the visualization of the pituitary lesion is essential.[35-37] Consequently, it is important to visualize the pituitary gland with the highest possible spatial resolution, which enables correct delineation of small anatomical structures and pathological lesions.

In routine clinical practice, MRI is the preferred imaging technique, since MRI enables to attain the highest spatial resolution, SNR, and CNR of the pituitary gland.[38-40] MRI at a field strength of 1.5 T is most commonly used, but the smallest microadenomas remain undetected in 36 - 63% of patients when scanning with this field strength.[41-45]

The higher attainable SNR and spatial resolution at higher field strengths – for instance 3.0 T or 7.0 T – theoretically has the potential to significantly improve the tumor detection rate.[46,47]

Outline of this thesis

In **Part I**, first the cerebrovascular burden will be evaluated in relation to vulnerable carotid atherosclerotic plaque. Subsequently, the feasibility of high-resolution carotid MRI at 7.0 T will be evaluated. Finally, 7.0 T MRI is used to visualize microinfarcts. All chapters evaluate patients with a symptomatic carotid artery disease. **Chapter 2** describes the relation between high-risk plaque components and cerebral infarcts on 3.0 T MRI in patients with a moderate carotid artery stenosis. **Chapter 3** describes the relation between high-risk plaque components, visualized with 3.0 T MRI, and microembolic signals, detected with Transcranial Doppler, also in patients with a moderate carotid artery stenosis. To assess the feasibility of 7.0 T MRI of the carotid arteries, **Chapter 4** describes a quantitative comparison between 3.0 T MRI and 7.0 T MRI in healthy volunteers. Moreover, **Chapter 5** describes the first evaluation of 7.0 T carotid MRI in a series of patients with a severely stenosed carotid artery. Finally, **Chapter 6** describes the presence of cortical microinfarcts, visualized with 7.0 T MRI, in patients with a severely stenosed carotid artery.

In **Part II**, a high resolution 7.0 T MRI protocol dedicated for the pituitary gland will be evaluated. Firstly, in **Chapter 7**, the protocol is presented, the feasibility is demonstrated in healthy volunteers and a small series of patients is demonstrated. Secondly, in **Chapter 8**, the same MRI protocol will be used for the detection of pituitary microadenomas in a group of patients with clinically an biochemically proven Cushing's disease.

The studies presented in this thesis were based on the following research questions:

- Are intraplaque hemorrhage and a thin/ruptured fibrous cap associated with infarcts on MRI and microembolic signals with transcranial Doppler? (Chapter 2, 3)
- Is it possible to visualize atherosclerotic carotid plaque with 7.0 T MRI? (Chapter 4, 5)
- Are cortical microinfarcts related to macroinfarcts in patients with extracranial atherosclerosis? (Chapter 6)
- Is it possible to visualize pituitary microadenomas with 7.0 T MRI? (Chapter 7, 8)
- Is high resolution 7.0 T MRI of the carotid arteries, the brain and the pituitary gland clinically relevant? (Chapter 4, 5, 6, 8)

References

1. El Aidi H, Adams A, Moons KG, et al. Cardiac magnetic resonance imaging findings and the risk of cardiovascular events in patients with recent myocardial infarction or suspected or known coronary artery disease: a systematic review of prognostic studies. J Am Coll Cardiol. Mar 25 2014;63:1031-1045.
2. Knuttel FM, Menezes GL, van den Bosch MA, et al. Current clinical indications for magnetic resonance imaging of the breast. Journal of surgical oncology. Jul 2014;110:26-31.
3. Chundru S, Kalb B, Arif-Tiwari H, et al. MRI of diffuse liver disease: the common and uncommon etiologies. Diagn Interv Radiol. Nov-Dec 2013;19:479-487.
4. Murphy G, Haider M, Ghai S, et al. The expanding role of MRI in prostate cancer. AJR Am J Roentgenol. Dec 2013;201:1229-1238.
5. Moser E. Ultra-high-field magnetic resonance: Why and when? World journal of radiology. Jan 28 2010;2:37-40.
6. Umutlu L, Ladd ME, Forsting M, et al. 7 Tesla MR imaging: opportunities and challenges. Rofo. Feb 2014;186:121-129.
7. Ladd ME. High-field-strength magnetic resonance: potential and limits. Top Magn Reson Imaging. Apr 2007;18:139-152.
8. Neurologie NVv. Richtlijn 'Diagnostiek, behandeling en zorg voor patiënten met een beroerte'. 2008; https://www.nvvc.nl/media/richtlijn/13/Richtlijn%20Beroerte%20def-2009.pdf.
9. Committee TESOEECatEW. Guidelines for management of ischaemic stroke and transient ischaemic attack 2008. Cerebrovasc Dis. 2008;25:457-507.
10. Chaturvedi S, Bruno A, Feasby T, et al. Carotid endarterectomy--an evidence-based review: report of the Therapeutics and Technology Assessment Subcommittee of the American Academy of Neurology. Neurology. Sep 27 2005;65:794-801.
11. Rothwell PM, Eliasziw M, Gutnikov SA, et al. Analysis of pooled data from the randomised controlled trials of endarterectomy for symptomatic carotid stenosis. Lancet. Jan 11 2003;361:107-116.
12. Rothwell PM, Gutnikov SA, Warlow CP. Reanalysis of the final results of the European Carotid Surgery Trial. Stroke. Feb 2003;34:514-523.
13. Group ECSTC. Randomised trial of endarterectomy for recently symptomatic carotid stenosis: final results of the MRC European Carotid Surgery Trial (ECST). Lancet. May 9 1998;351:1379-1387.
14. North American Symptomatic Carotid Endarterectomy Trial. Methods, patient characteristics, and progress. Stroke. Jun 1991;22:711-720.
15. Virmani R, Kolodgie FD, Burke AP, et al. Lessons from sudden coronary death: a comprehensive morphological classification scheme for atherosclerotic lesions. Arterioscler Thromb Vasc Biol. May 2000;20:1262-1275.
16. Davies MJ, Thomas AC. Plaque fissuring--the cause of acute myocardial infarction, sudden ischaemic death, and crescendo angina. British heart journal. Apr 1985;53:363-373.
17. Stary HC, Chandler AB, Dinsmore RE, et al. A definition of advanced types of atherosclerotic lesions and a histological classification of atherosclerosis. A report from the Committee on Vascular Lesions of the Council on Arteriosclerosis, American Heart Association. Circulation. Sep 1 1995;92:1355-1374.
18. Hellings WE, Peeters W, Moll FL, et al. Composition of carotid atherosclerotic plaque is associated with cardiovascular outcome: a prognostic study. Circulation. May 4 2010;121:1941-1950.
19. Redgrave JN, Lovett JK, Gallagher PJ, et al. Histological assessment of 526 symptomatic

carotid plaques in relation to the nature and timing of ischemic symptoms: the Oxford plaque study. Circulation. May 16 2006;113:2320-2328.
20. Saam T, Hetterich H, Hoffmann V, et al. Meta-analysis and systematic review of the predictive value of carotid plaque hemorrhage on cerebrovascular events by magnetic resonance imaging. J Am Coll Cardiol. Sep 17 2013;62:1081-1091.
21. Gupta A, Baradaran H, Schweitzer AD, et al. Carotid plaque MRI and stroke risk: a systematic review and meta-analysis. Stroke. Nov 2013;44:3071-3077.
22. Underhill HR, Yarnykh VL, Hatsukami TS, et al. Carotid plaque morphology and composition: initial comparison between 1.5- and 3.0-T magnetic field strengths. Radiology. Aug 2008;24:550-560.
23. Cai J, Hatsukami TS, Ferguson MS, et al. In vivo quantitative measurement of intact fibrous cap and lipid-rich necrotic core size in atherosclerotic carotid plaque: comparison of high-resolution, contrast-enhanced magnetic resonance imaging and histology. Circulation. Nov 29 2005;112:3437-3444.
24. Cappendijk VC, Cleutjens KB, Kessels AG, et al. Assessment of human atherosclerotic carotid plaque components with multisequence MR imaging: initial experience. Radiology. Feb 2005;234:487-492.
25. Moody AR, Murphy RE, Morgan PS, et al. Characterization of complicated carotid plaque with magnetic resonance direct thrombus imaging in patients with cerebral ischemia. Circulation. Jun 24 2003;107:3047-3052.
26. Millon A, Mathevet JL, Boussel L, et al. High-resolution magnetic resonance imaging of carotid atherosclerosis identifies vulnerable carotid plaques. J Vasc Surg. 2013;57:1046-1051
27. Leiner T, Gerretsen S, Botnar R, et al. Magnetic resonance imaging of atherosclerosis. Eur Radiol. Jun 2005;15:1087-1099.
28. Kerwin WS, Hatsukami T, Yuan C, et al. MRI of carotid atherosclerosis. AJR Am J Roentgenol. Mar 2013;200:W304-313.
29. Kroner ES, van Schinkel LD, Versluis MJ, et al. Ultrahigh-field 7-T magnetic resonance carotid vessel wall imaging: initial experience in comparison with 3-T field strength. Invest Radiol. Dec 2012;47:697-704.
30. Kraff O, Bitz AK, Breyer T, et al. A transmit/receive radiofrequency array for imaging the carotid arteries at 7 Tesla: coil design and first in vivo results. Invest Radiol. Apr 2011;46:246-254.
31. Koning W, Bluemink JJ, Langenhuizen EA, et al. High-resolution MRI of the carotid arteries using a leaky waveguide transmitter and a high-density receive array at 7 T. Magn Reson Med. Jul 3 2012;69:1186-1193.
32. Juszczak A, Grossman A. The management of Cushing's disease - from investigation to treatment. Endokrynol Pol. 2013;64:166-174.
33. Newell-Price J, Trainer P, Besser M, et al. The diagnosis and differential diagnosis of Cushing's syndrome and pseudo-Cushing's states. Endocr Rev. Oct 1998;19:647-672.
34. Potts MB, Shah JK, Molinaro AM, et al. Cavernous and inferior petrosal sinus sampling and dynamic magnetic resonance imaging in the preoperative evaluation of Cushing's disease. Journal of neuro-oncology. Feb 2014;116:593-600.
35. Maio SD, Biswas A, Vezina JL, et al. Pre- and postoperative magnetic resonance imaging appearance of the normal residual pituitary gland following macroadenoma resection: Clinical implications. Surg Neurol Int. 2012;3:67.
36. Witek P, Zielinski G. Predictive value of preoperative magnetic resonance imaging of the pituitary for surgical cure in Cushing's disease. Turk Neurosurg. 2012;22:747-752.
37. Yamada S, Fukuhara N, Nishioka H, et al. Surgical management and outcomes in patients with Cushing disease with negative pituitary magnetic resonance imaging. World Neurosurg. Mar-Apr 2012;77(3-4):525-532.

38. Escourolle H, Abecassis JP, Bertagna X, et al. Comparison of computerized tomography and magnetic resonance imaging for the examination of the pituitary gland in patients with Cushing's disease. Clin Endocrinol (Oxf). Sep 1993;39:307-313.
39. Guy RL, Benn JJ, Ayers AB, et al. A comparison of CT and MRI in the assessment of the pituitary and parasellar region. Clin Radiol. Mar 1991;43:156-161.
40. Davis WL, Lee JN, King BD, et al. Dynamic contrast-enhanced MR imaging of the pituitary gland with fast spin-echo technique. J Magn Reson Imaging. May-Jun 1994;4:509-511.
41. Patronas N, Bulakbasi N, Stratakis CA, et al. Spoiled gradient recalled acquisition in the steady state technique is superior to conventional postcontrast spin echo technique for magnetic resonance imaging detection of adrenocorticotropin-secreting pituitary tumors. J Clin Endocrinol Metab. Apr 2003;88:1565-1569.
42. Bartynski WS, Lin L. Dynamic and conventional spin-echo MR of pituitary microlesions. AJNR Am J Neuroradiol. May 1997;18:965-972.
43. Buchfelder M, Nistor R, Fahlbusch R, et al. The accuracy of CT and MR evaluation of the sella turcica for detection of adrenocorticotropic hormone-secreting adenomas in Cushing disease. AJNR Am J Neuroradiol. Sep-Oct 1993;14:1183-1190.
44. Ludecke DK, Flitsch J, Knappe UJ, et al. Cushing's disease: a surgical view. Journal of neuro-oncology. Sep 2001;54:151-166.
45. Wolfsberger S, Ba-Ssalamah A, Pinker K, et al. Application of three-tesla magnetic resonance imaging for diagnosis and surgery of sellar lesions. J Neurosurg. Feb 2004;100:278-286.
46. Pinker K, Ba-Ssalamah A, Wolfsberger S, et al. The value of high-field MRI (3T) in the assessment of sellar lesions. Eur J Radiol. Jun 2005;54:327-334.

Part I

High resolution MRI in patients with stroke

Chapter 2

Plaque components in symptomatic moderately stenosed carotid arteries related to cerebral infarcts; the PARISK study

AAJ de Rotte, MTB Truijman, AC van Dijk, MI Liem, FHBM Schreuder, AG van der Kolk, JR de Kruijk, MJAP Daemen, AFW van der Steen, GJ de Borst, PR Luijten, PJ Nederkoorn, ME Kooi, A van der Lugt, J Hendrikse

Stroke. 2015;46:568-576

Abstract

Background and purpose:
Carotid plaque composition is a major determinant of cerebrovascular events. In the present analysis we evaluated the relation between intraplaque hemorrhage (IPH) and a thin/ruptured fibrous cap (TRFC) in moderately stenosed carotid arteries and cerebral infarcts on magnetic resonance imaging (MRI) in the ipsilateral hemisphere.
Methods:
101 patients with a symptomatic 30 - 69% carotid artery stenosis underwent MRI of the carotid arteries and the brain, within a median time of 45 days from onset of symptoms. The presence of ipsilateral infarcts in patients with and without IPH and TRFC was evaluated.
Results:
IPH was seen in 40 out of 101 plaques. TRFC was seen in 49 out of 86 plaques (post-contrast series were not obtained in 15 patients). In total, 51 infarcts in the flow territory of the symptomatic carotid artery were found in 47 patients. Twenty-nine of these infarcts were cortical infarcts found in 24 patients. No significant relationship was found between IPH or TRFC and the presence of ipsilateral infarcts.
Conclusion:
MRI detected IPH and TRFC are not related to the presence of old and recent cortical and subcortical infarcts ipsilateral to a symptomatic carotid artery stenosis of 30-69%.

Introduction

Large randomized controlled trials have demonstrated that patients with a symptomatic 70 - 99% stenosis of the carotid artery benefit most from carotid endarterectomy (CEA).[1] In line with these results, decision-making for patients with a symptomatic carotid artery stenosis is currently based on the degree of stenosis. Nevertheless, in the last decades research has demonstrated that atherosclerotic plaque components may also play a role in risk assessment of these patients.[2]

Previous magnetic resonance imaging (MRI) studies suggest a correlation between specific carotid plaque components and the presence of cerebral infarcts on MRI as well as clinical events during follow-up.[3-6] The aim of the present cross-sectional study is to evaluate the association between intraplaque hemorrhage (IPH) and a thin/ruptured fibrous cap (TRFC) and the presence of infarcts on MRI in patients with a symptomatic 30 - 69% carotid artery stenosis. Vulnerable plaque components like IPH remain detectable in the plaque even after 18 months.[7] We therefore hypothesize that both old and recent infarcts might be related to vulnerable carotid plaque components as assessed on MRI. Since not all subcortical infarcts are considered to be a result from large vessel disease, in contrast to cortical infarcts, we evaluate both cortical and total amount of infarcts.

Methods

Study population

The current study was based on the Plaque At RISK (PARISK) study, a prospective diagnostic cohort study.[8] In- and exclusion criteria are previously described.[8] A detailed description of the stenosis calculation can be found in the supplementary materials. Institutional review board approval was obtained and all patients gave a written informed consent.

Imaging

Brain and carotid imaging was performed on the same day. Imaging was performed on 3.0 Tesla whole-body MRI scanners, with an imaging protocol described previously.[8] A brief description of the imaging protocol can be found in the supplementary material.

Image analysis

Two trained readers (MT and AD), blinded for the brain MRI results, performed the carotid MRI analysis in VesselMASS (Leiden University Medical Center, Leiden, The Netherlands). Analysis was performed according to previously published criteria,

which demonstrated a moderate to good intra- and interobserver reproducibility (kappa coefficient = 0.60 – 1.00).[9] A detailed description can be found in the supplementary material.

All brain MRI scans were evaluated for the presence of infarcts. Of all scored infarcts, the localization in the brain (cortical or subcortical) and the flow territory was subsequently determined. Brain images were assessed by a single experienced neuroradiologist (JH), blinded for the carotid MRI and clinical characteristics.

Statistical analysis

The association between plaque components and the presence of infarcts on MRI was evaluated with a Fisher's Exact test. Statistical analyses were performed in IBM SPSS Statistics version 20 (IBM Corporation, Armonk, NY, USA).

Results

IPH was present in 40 of 101 patients. In 15 patients the fibrous cap status could not be assessed because no post-contrast MRI was obtained (n = 6) or the post-contrast series had inferior image quality (n = 9). Consequently, the fibrous cap status could be evaluated in 86 patients and a TRFC was present in 49 of these patients. In 8 patients both a TRFC and IPH was present. (Figure 1) In total, 51 infarcts in the flow territory of the symptomatic carotid artery were found in 47 patients. Twenty-nine of these infarcts, found in 24 patients, were located cortical. (Figure 2) An overview of baseline characteristics is given in Table 1. In the supplementary material a distribution of infarcts, compared to the classification of the index event is demonstrated.

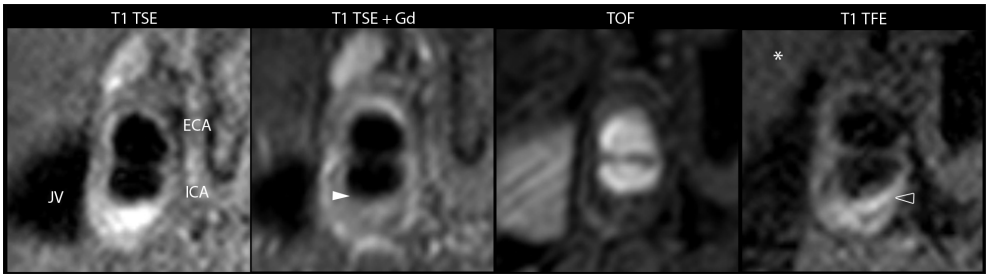

Figure 1. Overview of T_1 turbo spin echo (TSE) before and after Gadolinium (Gd) administration, time-of-flight (TOF) sequence and a T_1 ``Turbo `Field Echo (TFE) sequence. Internal carotid artery (ICA), external carotid artery (ECA) and jugular vein (JV) are marked. The intraplaque hemorrhage is pointed out with an open arrowhead, visible as a high signal intensity relative to the signal intensity of the sternocleidomastoid muscle (*) and a thin/ruptured fibrous cap is pointed out with a white arrowhead. No infarct was visible on MRI of the brain (not demonstrated).

In total, 22 of the 40 patients (55%) with IPH had ≥1 infarcts on MRI and 25 of the 61 patients (41%) without IPH had ≥1 infarcts on MRI (P = 0.22). In total, 22 of the 49 patients (45%) with a TRFC had ≥1 infarcts on MRI and 18 of the 37 patients (49%) with a thick fibrous cap had ≥1 infarcts on MRI (P = 0.83). Analysis based only on cortical infarcts, resulting from large vessel disease, did not change the significance of the results. In 13 of the 40 patients (33%) with IPH ≥1 cortical infarcts were present on MRI and in 11 of the 61 patients (18%) without IPH ≥1 cortical infarcts were present on MRI (P = 0.10). In 9 of the 49 patients (18%) with a TRFC ≥1 cortical infarcts were present on MRI and in 10 of the 37 patients (27%) with a thick fibrous cap ≥1 infarcts were present on MRI (P = 0.43).

Table 1. Baseline characteristics of all patients

Gender, male	70 (69%)
Age, years	69 ± 9
BMI, kg/m^2	26.5 ± 3.6
Classification of ndex event	
Stroke	49 (49%)
TIA	42 (42%)
AFX	10 (10%)
Interval event – imaging, days	45 (7 - 100)
Current smoker	24 (24%)
Hypertension	67 (66%)
Hypercholesterolemia*	
no	35 (35%)
Yes, statin on admission -	16 (16%)
Yes, statin on admission +	50 (50%)
Diabetes Mellitus	26 (26%)
Family history cerebrovascular disease <60 years	13 (13%)

Total (n = 101); Data are mean ± SD, median (range), or absolute number of patients (%)
BMI = body mass index, TIA = transient ischemic attack; AFX = amaurosis fugax
*hypercholesterolemia based on clinical history

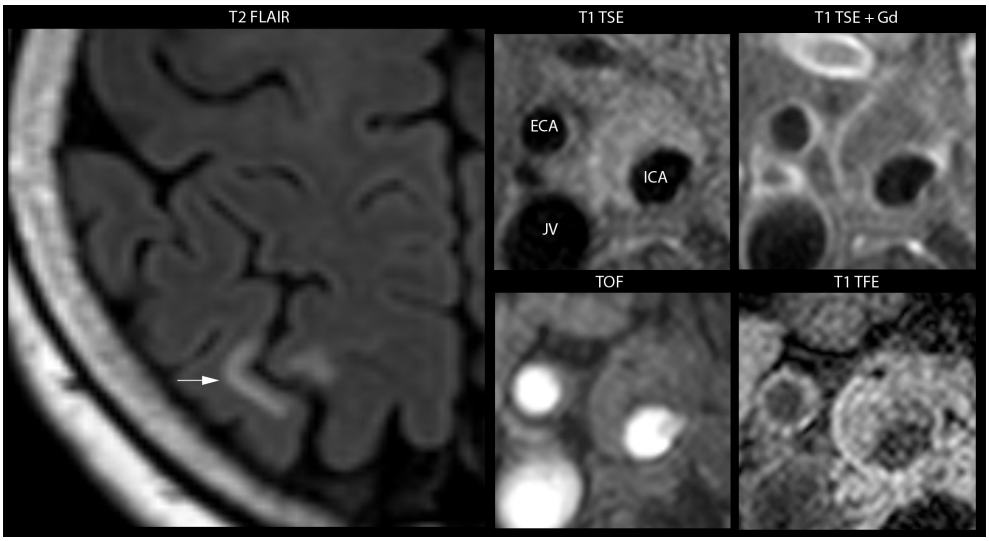

Figure 2. T_2 fluid-attenuated inversion recovery (FLAIR) sequence of the brain. A cortical infarct in the ipsilateral hemisphere is pointed out with a white arrow. Overview of the T_1 TSE sequence before and after Gadolinium (Gd) administration, time-of-flight (TOF) sequence and a T_1 turbo field echo (TFE) sequence of the symptomatic carotid artery. The internal carotid artery (ICA), external carotid artery (ECA) and jugular vein (JV) are marked. No intraplaque hemorrhage or thin/ruptured fibrous cap was present in this patient.

Discussion

The current study demonstrates that the presence of IPH and a TRFC in the stenosed carotid artery is not related to the presence of old and recent infarcts in the flow territory of the symptomatic carotid artery.

The current results are in contrast with previously published studies.[3,5,10] IPH and TRFC are demonstrated to be significantly associated with the presence of acute infarcts on diffusion weighted imaging (DWI). Regarding infarcts on FLAIR imaging, which represent both old and recent infarcts, controversial associations are demonstrated.[4,10] Ouhlous et al. demonstrated a statistically significant correlation between the presence of a lipid core in the carotid plaque and infarcts on FLAIR.[10] However, the presence of a lipid core lacks information about the status of a possible fibrous cap. The current study results are in line with Lindsay et al. demonstrating no statistically significant association between TRFC and infarcts on FLAIR.[4]

In the current study, imaging of the carotid plaque and the brain was performed on the same day, which implies that both MRI of the carotid plaque and MRI of the brain were obtained after the acute phase. Although histology studies demonstrated that vulnerability stabilizes after the acute phase[11], literature regarding in vivo imaging of this process is controversial. On the one hand, MRI enables to visualize different

stages of plaque vulnerability.[12] On the other hand, however, previous MRI studies have demonstrated that the presence of IPH and TRFC on MRI does not change significantly over time within one year.[7,13,14] Additionally, infarct volume on FLAIR images is found to decrease over time within one month, but disappearance of infarcts on FLAIR has, to the best of our knowledge, never been reported.[15] These results suggest that the absence of a relationship between a high-risk plaque with IPH and/or TRFC components and the presence of infarcts on FLAIR images could not be explained by the rather long time interval between index event and imaging (median: 45 days; range: 7 - 100 days). Nevertheless, since FLAIR images also show infarcts older than the index event, this might explain why in the current study the presence of IPH and TRFC does not correlate with cerebral infarcts on MRI, in contrast to previously published studies on DWI positive infarcts in an early phase after the ischemic symptoms.

Conclusion

The current study demonstrates that MRI detected IPH and TRFC are not related to the presence of both old and recent cortical and subcortical infarcts ipsilateral to a symptomatic carotid artery stenosis of 30-69%.

References

1. Rothwell PM, Eliasziw M, Gutnikov SA, et al. Analysis of pooled data from the randomised controlled trials of endarterectomy for symptomatic carotid stenosis. Lancet. 2003;361:107-116
2. Gupta A, Baradaran H, Schweitzer AD, et al. Carotid plaque mri and stroke risk: A systematic review and meta-analysis. Stroke. 2013;44:3071-3077
3. Zhao H, Zhao X, Liu X, et al. Association of carotid atherosclerotic plaque features with acute ischemic stroke: A magnetic resonance imaging study. Eur J Radiol. 2013;82:e465-e470
4. Lindsay AC, Biasiolli L, Lee JM, et al. Plaque features associated with increased cerebral infarction after minor stroke and tia: A prospective, case-control, 3-t carotid artery mr imaging study. JACC Cardiovasc Imaging. 2012;5:388-396
5. Altaf N, Goode SD, Beech A, et al. Plaque hemorrhage is a marker of thromboembolic activity in patients with symptomatic carotid disease. Radiology. 2011;258:538-545
6. Saam T, Hetterich H, Hoffmann V, et al. Meta-analysis and systematic review of the predictive value of carotid plaque hemorrhage on cerebrovascular events by magnetic resonance imaging. J Am Coll Cardiol. 2013;62:1081-1091
7. Underhill HR, Yuan C, Yarnykh VL, et al. Arterial remodeling in [corrected] subclinical carotid artery disease. JACC Cardiovasc Imaging. 2009;2:1381-1389
8. Truijman MT, Kooi ME, van Dijk AC, et al. Plaque at risk (parisk): Prospective multicenter study to improve diagnosis of high-risk carotid plaques. Int J Stroke. 2013;9:747-754
9. Kwee RM, Teule GJ, van Oostenbrugge RJ, et al. Multimodality imaging of carotid artery plaques: 18f-fluoro-2-deoxyglucose positron emission tomography, computed tomography, and magnetic resonance imaging. Stroke. 2009;40:3718-3724
10. Ouhlous M, Flach HZ, de Weert TT, et al. Carotid plaque composition and cerebral infarction: Mr imaging study. AJNR Am J Neuroradiol. 2005;26:1044-1049
11. Peeters W, Hellings WE, de Kleijn DP, et al. Carotid atherosclerotic plaques stabilize after stroke: Insights into the natural process of atherosclerotic plaque stabilization. Arterioscler Thromb Vasc Biol. 2009;29:128-133
12. Chu B, Kampschulte A, Ferguson MS, et al. Hemorrhage in the atherosclerotic carotid plaque: A high-resolution mri study. Stroke. 2004;35:1079-1084
13. Kwee RM, Truijman MT, van Oostenbrugge RJ, et al. Longitudinal mri study on the natural history of carotid artery plaques in symptomatic patients. PLoS One. 2012;7:e42472
14. Takaya N, Yuan C, Chu B, et al. Presence of intraplaque hemorrhage stimulates progression of carotid atherosclerotic plaques: A high-resolution magnetic resonance imaging study. Circulation. 2005;111:2768-2775
15. Tourdias T, Renou P, Sibon I, et al. Final cerebral infarct volume is predictable by mr imaging at 1 week. AJNR Am J Neuroradiol. 2011;32:352-358

Chapter 3

Intraplaque hemorrhage, fibrous cap status, and microembolic signals in symptomatic patients with mild to moderate carotid artery stenosis; the PARISK study

MTB Truijman, AAJ de Rotte, R Aaslid, AC van Dijk, J Steinbuch, MI Liem, FHBM Schreuder, AFW van der Steen, MJAP Daemen, RJ van Oostenbrugge, JE Wildberger, PJ Nederkoorn, J Hendrikse, A van der Lugt, ME Kooi, WH Mess

Stroke. 2014;45:3423-3426

Abstract

Background and purpose:

In patients with mild to moderate symptomatic carotid artery stenosis, intraplaque hemorrhage (IPH) and a thin/ruptured fibrous cap (FC) as evaluated with MRI, and the presence of microembolic signals (MESs) as detected with transcranial Doppler, are associated with an increased risk of a (recurrent) stroke. The objective of the present study is to determine whether the prevalence of MES differs in patients with and without IPH and thin/ruptured FC, and patients with only a thin/ruptured FC without IPH.

Methods:

In this multicenter, diagnostic cohort study, patients with recent transient ischemic attack or minor stroke in the carotid territory and an ipsilateral mild to moderate carotid artery plaque were included. IPH and FC status were dichotomously scored. Analysis of transcranial Doppler data was done blinded for the MRI results. Differences between groups were analyzed with Fisher's exact test.

Results:

A total of 113 patients were included. Transcranial Doppler measurements were feasible in 105 patients (average recording time, 219 minutes). A total of 26 MESs were detected in 8 of 105 patients. In 44 of 105 plaques IPH was present. In 92 of 105 plaques FC status was assessable, 36 of these had a thin/ruptured FC. No significant difference in the prevalence of MES between patients with and without IPH ($P = 0.46$) or with thick versus thin/ruptured FC ($P = 0.48$) was found.

Conclusion:

In patients with a symptomatic mild to moderate carotid artery stenosis, IPH and FC status are not associated with MES. This suggests that MRI and transcranial Doppler provide different information on plaque vulnerability.

Introduction

To date, the degree of luminal narrowing by a carotid artery plaque is used to estimate the risk of recurrence of cerebrovascular events and to stratify therapeutic options.[1] However, other plaque characteristics have gained interest. Detection of atherosclerotic plaques, which are prone to rupture, the socalled vulnerable plaques, might help in determining the best therapeutic approach, especially for patients with a mild to moderate carotid artery stenosis. Intraplaque hemorrhage (IPH) and fibrous cap (FC) status, as evaluated with MRI, are important features of plaque vulnerability and are associated with an increased risk of future ischemic stroke or transient ischemic attack.[2,3]

Also microembolic signals (MES) as measured with transcranial Doppler (TCD) ultrasound are predictors of combined transient ischemic attack and ischemic stroke in patients with symptomatic carotid stenosis.[4,5] Consequently, MRI and MES detection are both promising techniques to more precisely identify those patients who are at increased risk of a recurrent cerebrovascular event. As MRI visualizes morphological aspects of the plaque, while TCD is based on physiological aspects, this may imply that these techniques study plaque characteristics in a different way. The aim of the present study was to investigate the association between the occurrence of MES and the presence of IPH and a thin/ruptured FC (TRFC) in patients with a symptomatic mild to moderate carotid artery stenosis.

Methods

Study Population

Patients were included consecutively in the Plaque At RISK (PARISK) study, a multicenter diagnostic cohort study. Details on inclusion and exclusion criteria have been described earlier.[6] For details on the quantification of the luminal stenosis, see supplement material. The study was approved by the institutional Medical Ethical Committees. All patients gave written informed consent.

MRI Protocol

All patients were scanned using 3.0 T scanners as previously described.[6] For details on the MRI protocol, see supplementary material.

Ambulatory TCD

With transcranial duplex ultrasound (IU22, Philips Healthcare, Best, The Netherlands) the main stem of the middle cerebral artery ipsilateral to the symptomatic carotid artery was located and the ultrasound transparency of the transtemporal bone window was investigated. Subsequently, the 1.5 MHz probe of a portable ambulatory TCD instrument (TCD-X, Hemodynamics AG, Bern, Switzerland) was positioned at the location where the window was found. For details on the TCD recording, see supplementary material.

Data Analysis

MR images were analyzed according to previously published criteria by a trained observer (MT) using dedicated vessel wall analysis software (VesselMASS, Leiden University Medical Center, Leiden, The Netherlands) blinded to the TCD results.[7] TCD recordings were semiautomatically analyzed with dedicated software (TCDemb, Hemodynamics AG, Bern, Switzerland). For details on the MRI and TCD analysis, see supplementary material.

Statistical Analysis

To determine whether IPH and FC status were associated with MES, a Fisher's Exact test was performed. All calculations were made using SPSS (Version 20; IBM SPSS Inc, Chicago, IL).

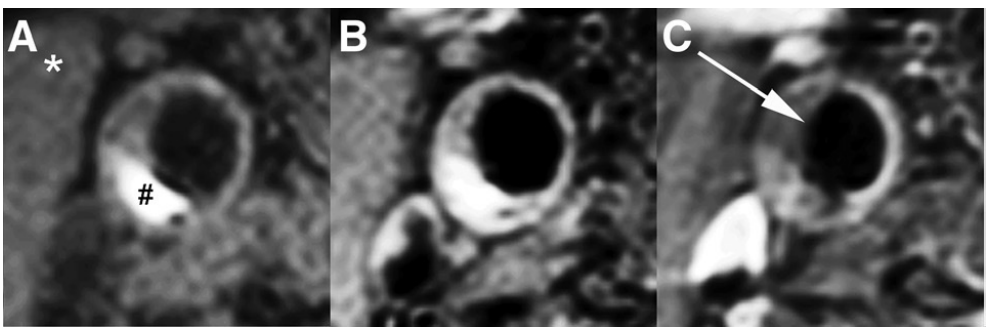

Figure 1. MR images showing T_1 inversion recovery turbo field echo (IR-TFE; A), T_1 quadruple inversion recovery turbo spin echo precontrast (B) and postcontrast (C). Note hyperintense signal (#) in the IR-TFE image compared with the sternocleidomastoid muscle (*) indicating intraplaque hemorrhage. The absence of signal enhancement between lipid-rich necrotic core and lumen (arrow) indicates a thin/ruptured fibrous cap.

Results

A total of 113 patients were included. Eight patients were excluded because of too much noise artifacts in the TCD signal. Clinical characteristics of the 105 patients are summarized in the Table. Time interval between clinical event and MRI was 53 ± 20 days (range, 12 - 100) and 52 ± 20 days (range, 11 - 100) between clinical event and TCD. Because of absence (n = 7) or poor image quality (n = 6) of postcontrast images, FC status could be analyzed in 92 patients.

IPH was detected in 44 of 105 (42%) of the patients, and 36 of 92 (39%) plaques had a TRFC. A total of 44 of 92 (48%) had neither IPH nor a TRFC and 28 of 92 (30%) plaques showed both IPH and a TRFC. (Figure 1) In total, 23,034 minutes of TCD signal were recorded (mean, 219; range, 21 - 379 minutes). Twenty-six MES were detected in 8 of 105 (8%) patients (Figure 2). Every first MES was detected within 175 minutes after commencing the record. Time interval between clinical event and TCD for these 8 patients was 54.1 ± 20.5 days (range, 34 - 100). Two of the 61 patients (3%) with IPH and 6 of the 44 patients (14%) without IPH had MES ($P = 0.46$). Two of the 49 patients (4%) with a TRFC and 6 of the 43 patients (14%) with a thick FC had MES ($P = 0.48$). Noteworthy, even in the case of abundant MES, as in patient 3, there was no IPH or TRFC present on MRI.

Table 1. Baseline characteristics of all included patients (n = 21)

Gender, male	84 (80%)
Age, years	67 ± 8
Smoking	
Current	26 (25%)
Former	59 (56%)
Never	18 (17%)
Unknwon	2 (2%)
Diabetes Mellitus	26 (25%)
Hypertension	68 (65%)
History in coronary artery disease	25 (24%)
Statin therapy	
Before event	48 (46%)
After event	92 (88%)

Data are number of patients (% from total) or mean ± standard deviation.

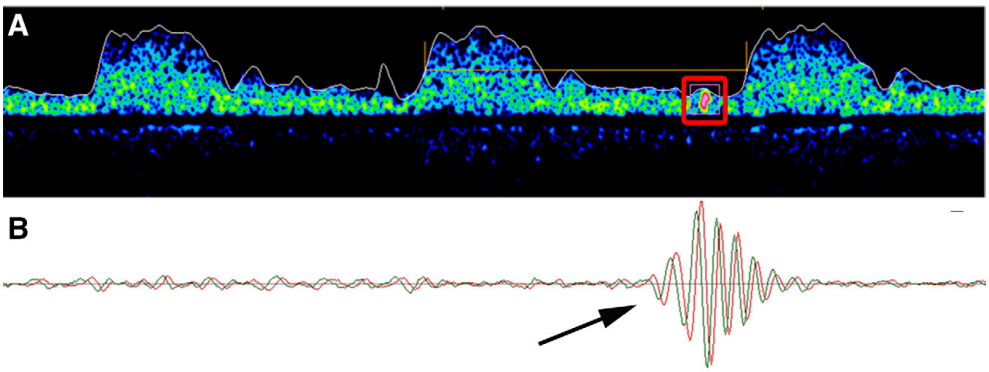

Figure 2. Transcranial Doppler signal showing both the frequency (A) and the time (B) domain. The red box delineates a microembolic signal, with a typical time domain signal (arrow).

Discussion

In the present study, we did not find an association between the presence of MES and IPH in patients with mild to moderate symptomatic carotid artery stenosis. The same applied for the relationship between MES and a TRFC and for the combination of IPH and a TRFC.

These findings are in contrast with previously published results by Altaf et al[8] in which they studied patients with highgrade carotid stenosis (60 – 99%). Their main finding was a highly significant relationship between MES occurrence and the presence of a vulnerable plaque on MRI. There are several possible explanations for this difference between the study results.

First, Altaf et al. studied patients with a high-grade carotid stenosis, whereas we investigated symptomatic patients with a mild to moderate stenosis. MESs are more common in patients with a severe carotid artery stenosis than in those with a mild to moderate stenosis.[9] This might explain the difference between studies in prevalence of MES-positive patients (44% versus 8%). Another difference in the selected patient population concerns potential cardiac sources of MES alike atrial fibrillation and in patients with heart valve prostheses.[10] In our study, we excluded patients with possible causes of MES other than the carotid arteries. Furthermore, the majority of our patients (88%) used lipid-lowering therapy, which is known to decrease the presence of MES.[11]

Finally, the time window between event and TCD recording differs between studies. MES are highly dependent on the latency between clinical event and TCD recording.[12] In the present study, the latency is relatively long (52 ± 20 days) as compared with the one reported by Altaf et al (19 days; interquartile range, 12 - 27 days). Yet, in our study,

no MES were found in the 14 patients who had their TCD recording within 30 days of the neurological event (21.7 ± 5.4 days), whereas we would expect 6 of 14 patients to be MES positive based on the prevalence mentioned by Altaf et al. The number of MES might even have been higher than 6 of 14 because we recorded ≈3.5 hours, which was 3.5 times longer than in the previous study. This longer recording time, made possible by the use of the mobile TCD device, is known to increase the number of MES-positive patients.[13]

On the contrary, IPH and the FC status on MRI have shown to be much more stable in time.[14] So, the difference between the incidence of MES on the one hand and the presence of IPH or a TRFC on the other hand fits with that concept and underlines that both techniques have a different approach toward studying plaque features.

Another plaque feature of interest other than the degree of stenosis might be inflammation. Moustafa et al.[15] studied the correlation between MES and signs of plaque inflammation by means of ^{18}F-fluorodeoxyglucose positron emission tomography and they were able to show an association between the 2 parameters in recently symptomatic patients. So, ^{18}F-fluorodeoxyglucose positron emission tomography might be another modality for identifying high-risk carotid artery plaques.

To conclude, our study suggests that, in symptomatic patients with mild to moderate stenosis, IPH presence and TRFC on MRI do not relate to the presence of MES. Hence, MRI and TCD are likely to provide different information on plaque vulnerability. The present study concerns a baseline analysis of the PARISK study.[6] The clinical follow-up data on clinical events will become available in the summer of 2016. We expect to determine which imaging approach allows for the best individual risk stratification and has the highest predictive value for a (recurrent) stroke in patients with mild to moderate carotid artery stenosis.

References

1. Rothwell PM, Eliasziw M, Gutnikov SA, et al; Carotid Endarterectomy Trialists' Collaboration. Analysis of pooled data from the randomised controlled trials of endarterectomy for symptomatic carotid stenosis. Lancet. 2003;361:107–116.
2. Hosseini AA, Kandiyil N, Macsweeney ST, et al. Carotid plaque hemorrhage on magnetic resonance imaging strongly predicts recurrent ischemia and stroke. Ann Neurol. 2013;73:774–784.
3. Gupta A, Baradaran H, Schweitzer AD, et al. Carotid plaque MRI and stroke risk: a systematic review and metaanalysis. Stroke. 2013;44:3071–3077.
4. Babikian VL, Wijman CA, Hyde C, et al. Cerebral microembolism and early recurrent cerebral or retinal ischemic events. Stroke. 1997;28:1314–1318.
5. Markus HS, MacKinnon A. Asymptomatic embolization detected by Doppler ultrasound predicts stroke risk in symptomatic carotid artery stenosis. Stroke. 2005;36:971–975.
6. Truijman MT, Kooi ME, van Dijk AC, et al. Plaque At RISK (PARISK): prospective multicenter study to improve diagnosis of high-risk carotid plaques. Int J Stroke. 2014;9:747–754.
7. Kwee RM, Teule GJ, van Oostenbrugge RJ, et al. Multimodality imaging of carotid artery plaques: 18F-fluoro-2-deoxyglucose positron emission tomography, computed tomography, and magnetic resonance imaging. Stroke. 2009;40:3718–3724.
8. Altaf N, Goode SD, Beech A, et al. Plaque hemorrhage is a marker of thromboembolic activity in patients with symptomatic carotid disease. Radiology. 2011;258:538–545.
9. Jayasooriya G, Thapar A, Shalhoub J, et al. Silent cerebral events in asymptomatic carotid stenosis. J Vasc Surg. 2011;54:227–236.
10. Sliwka U, Job FP, Wissuwa D, et al. Occurrence of transcranial Doppler high-intensity transient signals in patients with potential cardiac sources of embolism. A prospective study. Stroke. 1995;26:2067–2070.
11. Spence JD, Coates V, Li H, et al. Effects of intensive medical therapy on microemboli and cardiovascular risk in asymptomatic carotid stenosis. Arch Neurol. 2010;67:180–186.
12. Forteza AM, Babikian VL, Hyde C, et al. Effect of time and cerebrovascular symptoms of the prevalence of microembolic signals in patients with cervical carotid stenosis. Stroke. 1996;27:687–690.
13. Mackinnon AD, Aaslid R, Markus HS. Long-term ambulatory monitoring for cerebral emboli using transcranial Doppler ultrasound. Stroke. 2004;35:73–78.
14. Kwee RM, Truijman MT, van Oostenbrugge RJ, et al. Longitudinal MRI study on the natural history of carotid artery plaques in symptomatic patients. PLoS One. 2012;7:e42472.
15. Moustafa RR, Izquierdo-Garcia D, Fryer TD, et al. Carotid plaque inflammation is associated with cerebral microembolism in patients with recent transient ischemic attack or stroke: a pilot study. Circ Cardiovasc Imaging. 2010;3:536–541.

Chapter 4

MRI of the carotid artery at 7.0 T: quantitative comparison with 3.0 T

W Koning, AAJ de Rotte, JJ Bleumink, TA van der Velden,
PR Luijten, DWJ Klomp, JJM Zwanenburg

Journal of Magnetic Resonance imaging. 2014 February 27
(Epub ahead of print)

Abstract

Background and purpose:

To evaluate the 7.0 Tesla (T) MRI of the carotid arteries, as quantitatively compared with 3.0 T.

Methods:

The 7.0 T MRI of the carotid arteries was performed in six healthy subjects and in two patients with carotid stenosis. The healthy group was scanned at 3.0 T and at 7.0 T, using current coil setups at both field strengths. T_1 and T_2 values of the normal carotid vessel wall were assessed at both field strengths. B_1^+ maps and signal to noise ratio (SNR) maps were obtained, as well as T_1 weighted images with a resolution as high as 0.4 x 0.4 x 1.5 mm^3.

Results:

The T_1 of the normal carotid vessel wall was found to be 1227 ± 47 ms at 3.0 T and 1628 ± 130 ms at 7.0 T, while a T_2 of 55 ± 11 ms at 3T and 46 ± 4 ms at 7.0 T was found. A twofold average gain in SNR at the carotid arteries was found with 7.0 T. T_1 weighted images demonstrated an increased SNR at 7.0 T for all subjects.

Conclusion:

Evaluation between 3.0 T and 7.0 T carotid MRI with optimized setups at both field strengths showed improved SNR at 7.0 T, an increase in vessel wall T_1 and a decrease in vessel wall T_2.

Introduction

Imaging the carotid vessel wall is important for risk assessment and intervention decisions.[1,2] In general, the resolution of current MRI is insufficient to reflect plaque detail.[3–5] Current 1.5 Tesla (T) and 3.0 T MR scanners are operating at their limits in terms of maximizing image resolution for a given scan time. Increasing the field strength to 7.0 T can increase the signal to noise ratio (SNR)[6], which can be used to increase resolution. Due to the field strength dependence of T_1 and T_2, image contrast may change at 7.0 T. Hence, T_1 and T_2 measurements in the carotid vessel wall might need to be performed, and coils optimized. The goal of this study was twofold. First, to validate the receive and transmit performance of a current setup of 7.0 T MRI, and second, to measure the change in T_1 and T_2 in the normal carotid vessel wall, relative to 3.0 T MRI, as relaxation parameters depend on field strength.

Methods

The performance and potential of 7.0 T carotid MRI was evaluated using a series of quantitative and qualitative experiments in six healthy subjects (two male, four female, mean age 27 ± 3) that were scanned at both 3.0 T and 7.0 T. Additionally, the feasibility of 7.0 T MRI was demonstrated in two patients with carotid stenosis (both male, mean age 60 and 76). Institutional Review Board (IRB) approval was obtained for this study. All participants signed an informed consent according to the regulations of the IRB.

3.0 T MRI

The 3.0 T scans were performed on a whole body MRI scanner (Achieva 3.0 T, Phillips Healthcare, Best, The Netherlands). The body coil was used for transmission, and an additional dedicated bilateral eight-channel phased array receive array (Shanghai Chenguang Medical Technologies Co., Shanghai, China) was used for reception. Outer dimensions of the receiver array were 12.8 x 10.3 cm^2. The automatic power optimization provided by the MRI vendor was used for flip angle calibration.

7.0 T MRI

The 7.0 T scans were performed on a whole body MRI scanner (Achieva 7.0 T, Philips Healthcare, Cleveland, OH). A 2-element leaky waveguide transmitter [7] was used in combination with a 30-element bilateral receiver array (15 elements per side) with total outer dimensions of 15 x 10 cm per side (MR coils BV, Drunen, The Netherlands). For all subjects, flip angle calibration was performed locally on the carotid arteries, as follows: transversal complex $B1^+$ maps were acquired for each of the two transmit elements (Actual Flip angle Imaging (AFI) [8], $T_{R,1}/T_{R,2}$ = 25/125 ms, flip angle: 50°, gradient echo

(GE), 220 x 220 x 55 mm^3. To avoid slice profile effects, a three-dimensional acquisition was performed, acquiring five slices of which the middle slice was used. Because both elements contribute significantly to both regions of interest (left and right carotid arteries), inhouse built software was used to perform $B1^+$ shimming. Complex weighting factors were calculated iteratively, based on manually selected regions of interest (ROIs). Both left and right carotid arteries were selected as target ROIs for the shimming procedure. The calculated weighting factors were used for all the subsequent exams of the same subject. After shimming, a $B1^+$ shimmed transversal $B1^+$ map was acquired. The B0 field was shimmed for the neck using third order image based shimming.[9] A specific absorption rate (SAR) model developed for this transmit array [7] was used to ensure that all scans remained within the SAR guidelines.[10]

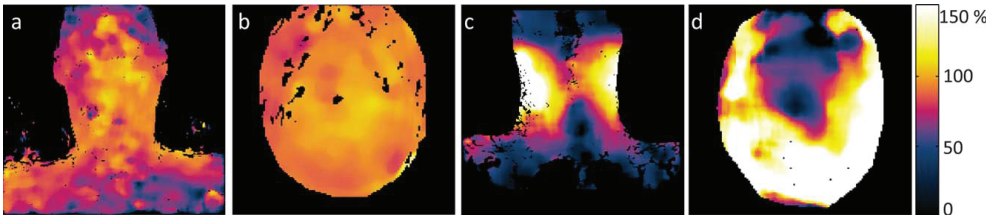

Figure 1. Actual flip angle maps of the neck at 3.0 T (a,b) and 7.0 T (c,d). Coronal (a,c) and transverse (b,d) slices of the neck. The actual flip angle map is shown as a percentage of the nominal flip angle.

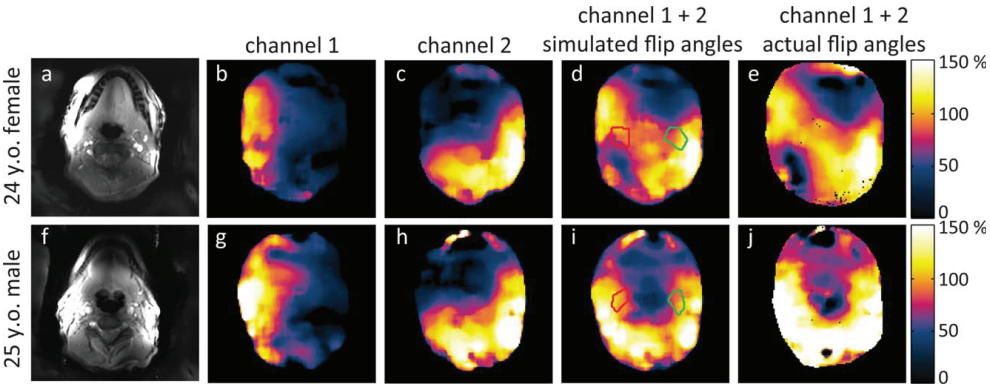

Figure 2. Examples of the bilateral $B1^+$ shimming procedure in two volunteers (24-year-old female and a 25-year-old male) (anatomical images a,f). Actual flip angle maps are shown as a percentage of the nominal flip angle. In b, c, g, and h, the actual flip angle maps of the single channels are shown. In d and i the simulated combined flip angle field after $B1^+$ shimming is shown, with the red and green regions of interest indicating the locations for which the $B1^+$ was optimized. In e and j the correspondingactually measured flip angle maps are shown.

Signal to Noise Ratio Maps

Signal to noise ratio (SNR) maps of a transverse slice of the neck were acquired at both field strengths. Identical protocols were designed to acquire a proton density weighted gradient echo image with minimal T_1 and T_2 weighting, with the following parameters: TR/TE = 200/2.1 ms, flip angle = 6° (calibrated as described above), $BW_{readout}$ = 858 Hz, field of view (FOV) = 200 x 200 mm^2, acquired voxel size = 1.0 x 1.0 mm^2, slice thickness = 3 mm. An additional noise image was acquired by repeating the scan with the same receive gain settings, phases and weightings in coil combination, but without the application of any radiofrequency (RF) or gradients. The standard deviation of the noise in the local ROI in the real-part image of the noise scan was taken as the noisemetric to calculate the SNR of the corresponding image. SNR maps were corrected for differences caused by flip angle inhomogeneity. This was done using the measured actual flip angle from the $B1^+$ shimmed $B1^+$ map, according to Eq. [1],

$$SNR_{corrected} = SNR_{measured} \cdot \sin(\alpha)/\sin(c \cdot \alpha) \quad [1]$$

where α is the nominal flip angle, and c is the ratio of the actual and the nominal flip angle, following directly from the $B1^+$ map. From the corrected SNR maps of all subjects, profiles were measured from the edge of the neck inward to evaluate SNR as a function of penetration depth. The mean and standard deviation (over the subjects) of the SNR was calculated at each depth.

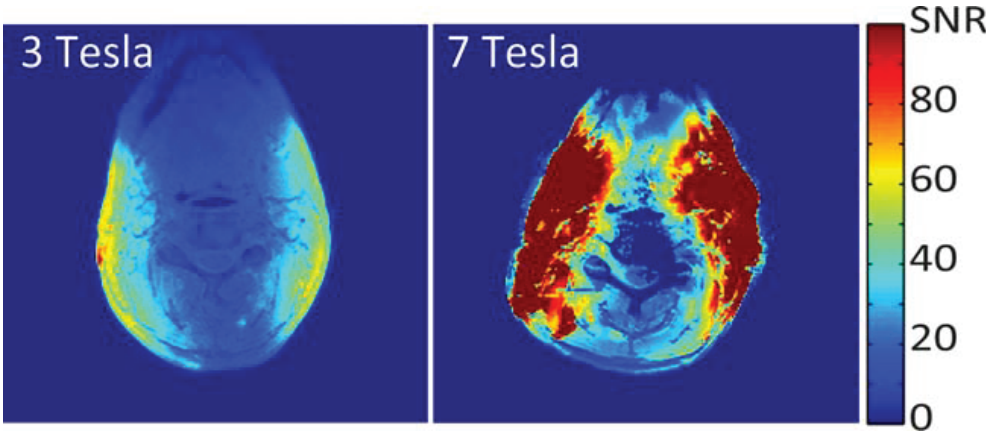

Figure 3. SNR maps in a transverse slice of the neck at 3.0 T and 7.0 T.

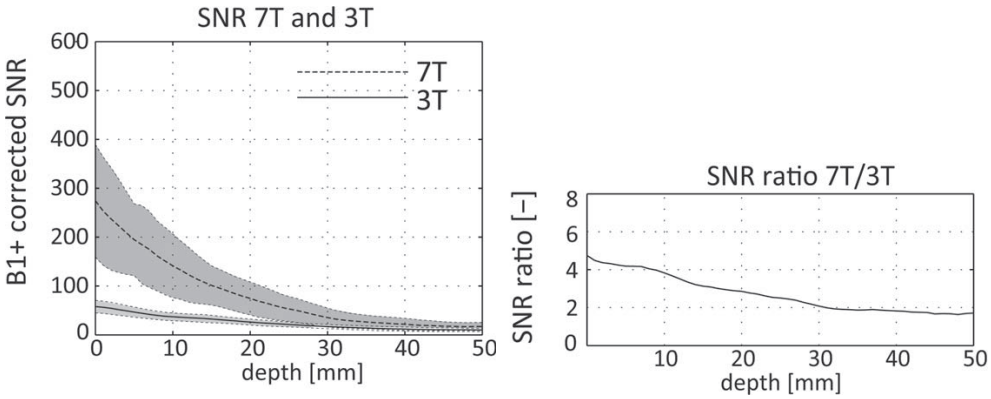

Figure 4. Mean SNR in the neck of all healthy subjects as a function of depth at 3.0 T and 7.0 T (a), and the ratio between these two curves (b). The centered lines demonstrate the inter subject average, and the filled area demonstrates the inter subject standard deviation.

T_1 and T_2 Maps

T_1 and T_2 measurements in the vessel wall of the healthy subjects were acquired by means of T_1 and T_2 maps. T_1 was acquired by three subsequent high resolution inversion recovery turbo spin echo (IR-TSE) images with three different inversion times (50, 700, and 2000 ms) and the following parameters: TR = 8000 ms, echo train length = 10 (including 2 startup echoes), refocusing angle = 80°, FOV = 150 x 150 mm^2, slice thickness = 2 mm, acquired voxel size = 0.5 x 0.5 mm^2, SENSE acceleration factor = 3 (7.0 T) and 2 (3.0 T), total scan time = 6 minutes and 48 seconds (7.0 T) and 9 minutes and 36 seconds (3.0 T). T_2 relaxation time in the vessel wall was acquired using a high resolution multi echo spin echo sequence with the following parameters: 15 echos, echo spacing = 9 ms, TR = 1600 ms, slice thickness = 2 mm, acquired voxel size = 0.5 x 0.5 mm^2, FOV = 150 x 150 mm^2. No electrocardiograph gating was applied in either T_1 or T_2 measurements. Only even echo numbers were used for T_2 determination. For both T_1 and T_2 maps, slices were positioned 2 cm below the bifurcation to facilitate a perpendicular planning of the slice through the vessel. Because the asymmetric transmit pattern of the 7.0 T setup could not always guarantee sufficient $B1^+$ on the left side of the neck at this low position for all volunteers, only the right side carotid arteries were taken into account for T_1 and T_2 analysis.

Anatomical Scans

Multi-slice T_1 weighted turbo spin echo (TSE) sequences were acquired at both field strengths for each subject. Scan parameters: 15 slices, TR = 1000 ms, TSE factor 11 (including three startup echoes), reduced refocusing angles: min angle = 80°, $T_{E,k}$ = 0.28 ms, $T_{E,eq}$ = 18 ms calculated for a given reference tissue with a T_1 and T_2 of 2000 and 50 ms, respectively ($T_{E,eq}$ is the equivalent echo time of a plain spin echo, yielding similar T_2 weighting[11]), acquired voxel size = 0.4 x 0.4 mm^2, slice thickness = 1.5 mm, FOV = 180 x 180 mm^2, SENSE acceleration factor = 2, acquisition time = 3 minutes and 52 seconds. In the two patients, an additional multi slice dual echo TSE scan was performed, providing proton density weighted (PDW) and T_2 weighted (T2W) images. Scan parameters: 15 slices, TR = 3000 ms, TSE factor 16, $T_{E,eq}$ = 27 and 70 ms for first and second echo, respectively, acquired voxel size = 0.5 x 0.5 mm^2, slice thickness = 2.0 mm, FOV = 150 x 179 mm^2, acquisition time = 4 minutes and 36 seconds.

Image Analysis

T_2 maps were calculated by fitting the two parameter model shown in Eq. [2] to the individual TE images by fitting to the two parameter model shown in Eq. [2],

$$SI(TE) = \alpha \cdot e^{-TE/T2} \quad [2]$$

where SI is the signal intensity and a is the amplitude of the curve. The mean and standard deviation T_2 over the vessel wall was calculated for each subject. The T_1 was calculated from three subsequently acquired images with different inversion times. To avoid errors from small deformation and displacement between the acquisitions, a circumferential center line was drawn in the vessel wall in each of the three IR images. Signal intensities were taken at this center line. The lengths of the three lines of the different acquisitions were normalized, and the data were interpolated to equal dimensions. A two parameter (amplitude and T_1) fit resulted in a circumferential T_1 line, of which the mean T_1 of each subject was taken for comparison between 3.0 T and 7.0 T. Equation [3] shows the two parameter inversion recovery model, where SI is the signal intensity as a function of inversion time TI, and a is the amplitude of the curve.

$$SI(TI) = \alpha \cdot (1 - 2e^{-TI/T1}) \quad [3]$$

To evaluate the performance of 7.0 T compared with 3.0 T imaging, the combined effect of gain in SNR, and changed T_1 and T_2 relaxation time constants was computed for a plain spin echo sequence. This was done by combining the effects of SNR and the

changes in T_1 and T_2 as described in Eq. [4], derived from Eqs. [2] and [3],

$$SNR_{act}(T_R, T_E) = SNR_{PD} \cdot (1 - e^{-TR/T1}) \cdot e^{-TE/T2} \quad [4]$$

where SNR_{act} is the actual SNR for a given TR and TE and SNR_{PD} is the proton density weighted SNR corrected for $B1^+$. A map with the actual ratio of 7.0 T over 3.0 T SNR_{act} as function of TE and TR was computed following Eq. [4], accounting for the measured gain in SNR_{PD}, and the observed T_1 and T_2 values of the carotid vessel wall at both field strengths.

Coupling Loss

An additional experiment was performed at 7.0 T to quantify the potential loss of SNR due to coupling effects of the high density receiver array. Coupling effects were measured on a spherical phantom with a diameter of 12 cm containing a solution of 120 mg/mL $CuSO_4$ in water. Two images were acquired as follows: (i) "coupled": the image was acquired with all elements connected simultaneously and combined with sum of squares (ii) "uncoupled": the image was acquired for each element separately, while detuning all other elements, and combining the separate element images with sum of squares, creating an ideally uncoupled and perfect noise decorrelated image. The ratio of the coupled image to the uncoupled image was calculated providing a spatial indication of losses due to combined coupling effects.

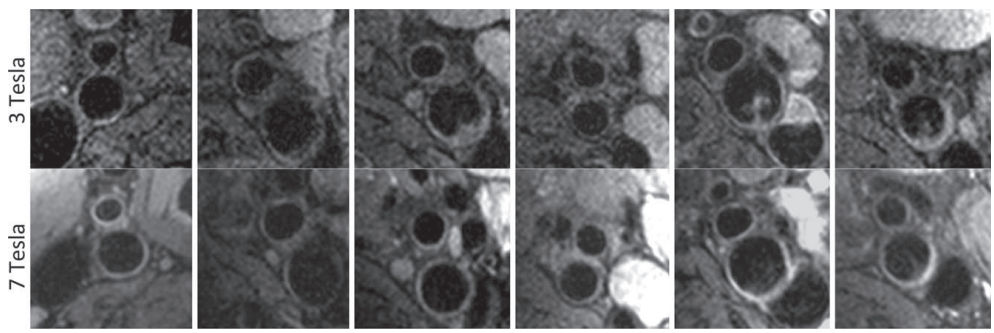

Figure 5. T_1 TSE images at 3.0 T (upper row) and 7.0 T (lower row) of all 6 healthy subjects.

Results

Figure 1 demonstrates representative examples of coronal and transversal actual flip angle maps at 3.0 T and 7.0 T. The flip angle distribution at 7.0 T was always much less homogeneous, reflecting an inhomogeneous $B1^+$. Figure 2 shows examples of the bilateral $B1^+$ shimming procedure for a 24-year-old female and a 25-year-old male. The measured actual flip angle in the ROIs after $B1^+$ shimming, did not deviate more than 20% from 100% flip angle, in all subjects. The SNR maps that were corrected with the flip angle maps are shown in Figure 3, illustrating an improved SNR at 7.0 T, particularly at the periphery.

SNR profile lines averaged over subjects are shown in Figure 4a. As can be observed from the larger standard deviation, the SNR at 7.0 T is more variable between subjects than at 3.0 T, but remains stronger. Figure 4b shows the SNR ratio between 7.0 T and 3.0 T. Up to 2 cm penetration depth, there is a high average gain (>7/3) in SNR at the 7.0 T setup. At a depth of 3 cm, the average SNR gain was found to be a factor 2.0.

T_1 weighted TSE scans for all subjects are shown in Figure 5. 7.0 T subjective SNR was better than that of 3.0 T in all cases. Figure 6 shows T1W, PDW, and T2W images, and $B1^+$ maps after $B1^+$ shimming, of two patient cases with carotid stenosis. Figure 7 shows the T_1 and T_2 maps of the carotid artery of a 26-year-old female, together with the T_1 and T_2 recovery curves and the individual Ti and TE images of the same subject. The mean and standard deviation T_1 and T_2 over the vessel wall of each subject is given in Table 1, together with the mean and standard deviation T_1 and T_2 over all subjects.

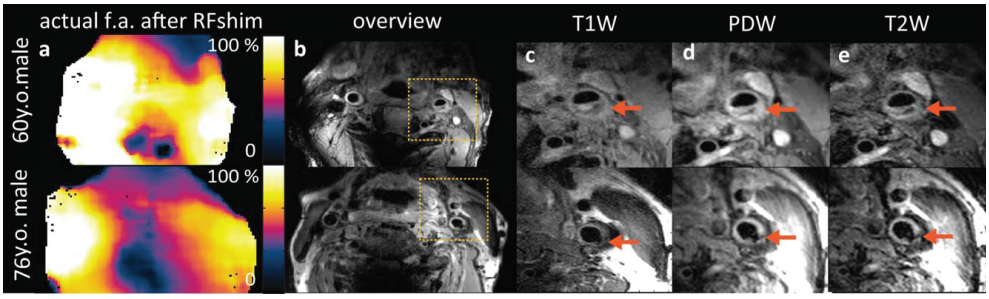

Figure 6. Two cases of patients (both male, age 60 and 76) with atherosclerotic plaques in the carotid artery. Actual flip angle maps after $B1^+$ shimming (a), overview PDW image (b), and zoomed image showing T_1 (c), PDW (d), and T_2 (e) images.

The combined effect on the SNR ratio 7.0 T/3.0 T of the changed T_1 and T_2 values, together with the gain in SNR, is shown in Figure 8. It shows that signal loss due to increased T_1 and reduced T_2, result in a reduction of SNR gain at 7.0 T, depending on the chosen TE and TR.

Additional signal loss due to coupling is shown in Figure 9. Figure 9a and 9b show the coupled and the uncoupled image, respectively. The ratio of these is given in Figure 9c. In the center of the phantom an SNR ratio of 0.6 is measured, suggesting a SNR loss of 40% through noise coupling and noise

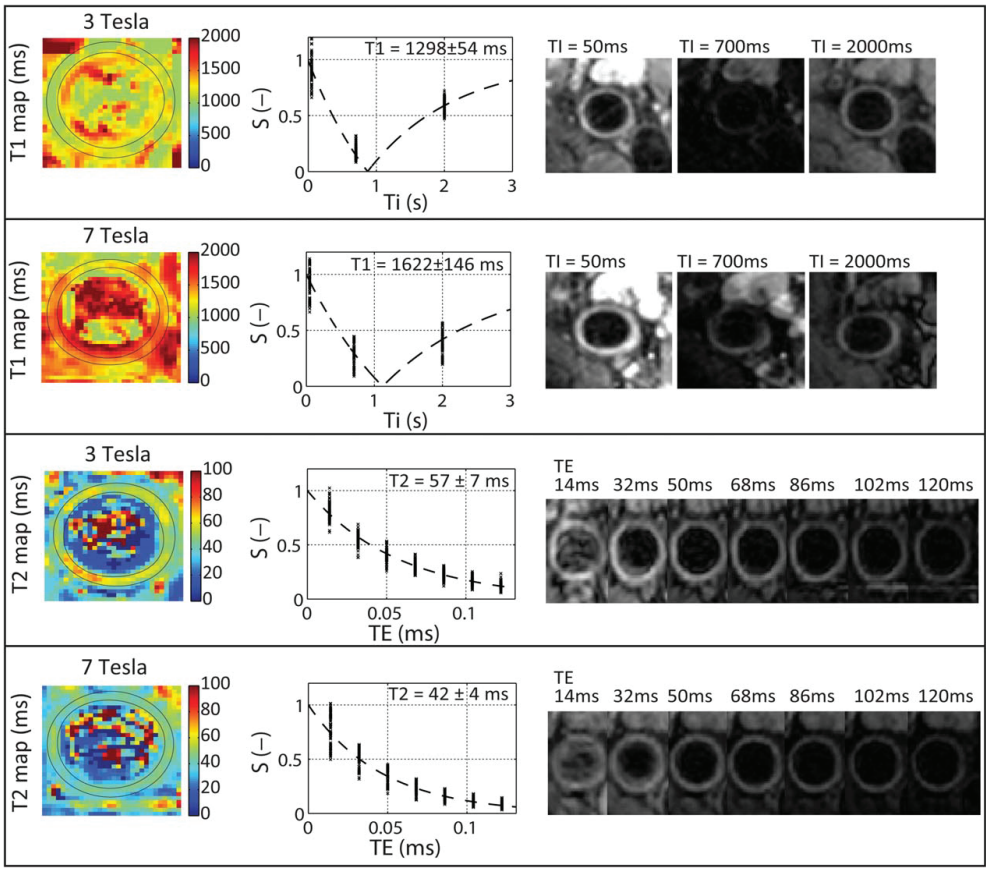

Figure 7. T_1 and T_2 relaxation time measurements in a normal carotid vessel wall at 3.0 T and 7.0 T. The left column shows the calculated T_1 and T_2 maps at both field strengths. Correspondingly, the middle column shows the relative intensities over the vessel wall, together with a fitted curve. The individual images for each inversion time (T_1 measurements) and echo time (T_2 measurements) are shown in the right column.

The 7.0 T carotid MRI was evaluated by means of a quantitative comparison with 3.0 T MRI. At both field strengths, a current RF coil was used. An overall improved quality of 7.0 T carotid MRI as compared to 3.0 T was shown. The SNR improvement in the anatomical images was the result of different effects, such as contributions by increased sensitivity of the receive arrays, changed T_1 and T_2 relaxation parameters and increased $B1^+$ field inhomogeneities.

Even after $B1^+$ shimming, there were still large differences in $B1^+$ patterns between different subjects. This can be explained by the relatively small ROIs that were used for the $B1^+$ shimming optimization. Targets in $B1^+$ in the ROIs are met as far as possible with the available degrees of freedom of two transmit elements. Outside the ROIs, however, the $B1^+$ is left unconstrained and can, therefore, show random patterns. The variability in $B1^+$ patterns shows the capability of the multi transmit setup, to potentially optimize the $B1^+$ for other locations such as the spine. The effect of the gradient in $B1^+$ was not visible over a distance as small as the diameter of the carotid artery.

Table 1. T_1 and T_2 relaxation times in the normal carotid vessel wall at 3.0 T and 7.0 T

	T_1		T_2	
	3.0T	7.0 T	3.0 T	7.0 T
1	1266 ± 91	1498 ± 149	77 ± 19	48 ± 6
2	1187 ± 100	1759 ± 332	47 ± 6	46 ± 7
3	1298 ± 54	1622 ± 146	56 ± 7	42 ± 4
4	1210 ± 120	1448 ± 152	46 ± 9	39 ± 8
5	1177 ± 69	1748 ± 250	53 ± 8	50 ± 7
6	1229 ± 80	1691 ± 226	50 ± 10	45 ± 7
all subjects*	1227 ± 47	1628 ± 130	55 ± 11	46 ± 4

Mean and standard deviation over vessel wall in all separate subjects. * Mean and standard deviation of all subjects

We report T_1 and T_2 relaxation times in the normal carotid vessel wall at 7.0 T. The combination of in plane resolution of 0.5 x 0.5 mm^2, and a suppressed blood signal was chosen to avoid partial voluming effects. Even a small volume of blood in a voxel containing vessel wall, can have a large effect on the quantified T_1 or T_2. This strong partial voluming effect is caused by the high signal of the freshly inflowed blood. This is why we chose a single slice TSE sequence, having inherent blood suppression, as a basis for both the T_1 and the T_2 measurement. T_2 values in the normal carotid vessel wall at 3.0 T were in the expected range of previously published values.[12–14] However, the carotid vessel wall T_1 at 3.0 T found in the current study (1227 ± 47 ms) was considerable longer than the values found in earlier studies (685.9 ± 166 ms[13], and 869 ± 224 ms[15]) where faster methods were used to gain speed or cover a big volume. In the present study only one slice was acquired with a very long TR of 8000 ms to assure a straightforward T_1 assessment. Three inversion times resulted in a feasible scan time and a well determined fit using the two parameter model. It is a limitation of this study that only the relaxation parameters of the right carotid artery were acquired. The ROIs for the imaging and for the T_1 and T_2 measurements were too far apart to assure sufficient $B1^+$ in both imaging ROI (above bifurcation) and the ROI of the T_1 and T_2 measurements (below the bifurcation).

Another possible limitation of this study is the fact that the receive arrays used at both field strengths were not the same. A greater number of smaller elements were used at 7.0 T. However, the sizes of these elements were smaller than optimal for the depth of interest.[16,17] The ideal radius α of a loop coil for imaging an object at depth d is approximated by $\alpha = 5d/\sqrt{5}$.[17] Therefore, it was assumed that the additional SNR benefit of the small element receive array at 7.0 T was only present in the peripheral regions

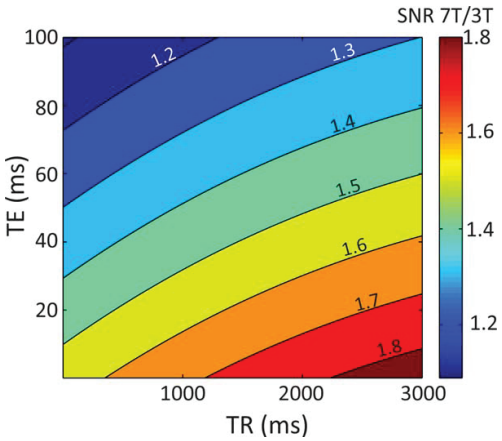

Figure 8. Theoretical signal gain 7.0 T/3.0 T for a spin echo sequence as a function of TE and TR (Eq. [4]) for the T_1 and T_2 values as given in Table 1 calculated for an SNR gain of 2.0, following the SNR measurements. It shows the theoretical gain from 3.0 T to 7.0 T in SNR including the extra signal loss due to increased T_2 and decreased T_1. For TR.1000 ms and TE.18 ms, equivalent to the T_1-weighted sequence shown in Figures 5 and 6, an SNR gain of 1.58 in the vessel wall is expected.

(at a depth of 2 cm and less). At greater depths, however, the individual elements of the 3.0 T setup were closer to optimal dimensions. From there, the parallel imaging reconstruction cancels out the bias of different individual element sizes[18], and SNR can be compared fairly. At the depths of the carotid artery, the only additional benefit of the density array at 7.0 T compared with the 3.0 T array, is not an increased SNR, but an increased acceleration possibility. In this research, this property was used for the timecostly T_1 maps, that were scanned with an acceleration factor of 2 at 3.0 T, whereas at 7.0 T an acceleration factor of 3 was applied. Overall, except for at the periphery (<3 cm depth), the SNR gain 7.0 T/3.0 T was lower than the expected 7/3. The possible effect of T_1 and T_2 were already excluded by the proton density weighted SNR scan. We showed in the phantom experiment that the combined effect of noise coupling and noise correlation of the dense receiver contributed to 40% of the total noise at deeper tissues. Although the preamps are not mounted on the individual coil elements, the coupling numbers were reasonably low.[7] Therefore, it is expected that most of this noise contribution is caused by intrinsic similarities in field patterns of these coils, hence causing the noise correlations.

A higher variance in SNR was observed at 7.0 T. A possible explanation could be that the small elements at 7.0 T are more sensitive to tissue loading. Therefore, less tight positioning onto the neck could have a greater effect on 7.0 T than it has on 3.0 T where the individual elements were bigger. Furthermore, the signal decreases faster with distance from the surface than for a receive array with larger elements. Hence, variation in depth of the carotid artery resulted in a larger variation in the respective SNR at 7.0 T than it is the case at 3.0 T.

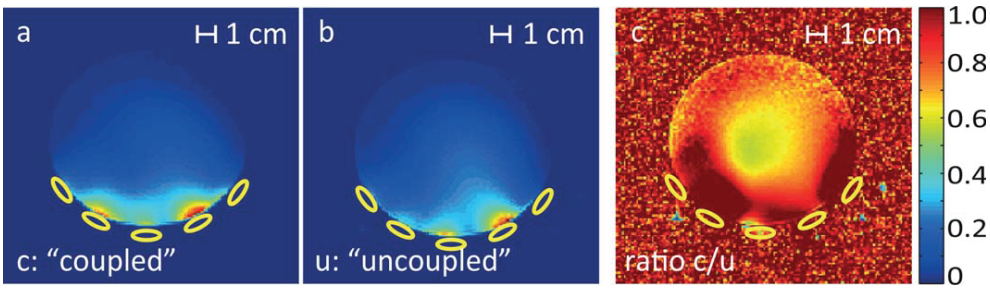

Figure 9. Phantom experiment giving a localized indication of the loss through coupling and noise correlation. The yellow circles indicate the high density receiver array at 7.0 T. A "coupled" image (gradient echo), acquired with all elements simultaneously (a), an ideal "uncoupled" image (b), and the ratio between the coupled and the uncoupled image (c). In the middle of the phantom, up to 40% loss is observed compared with the ideal perfectly uncoupled and noise decorrelated image.

An earlier study compared carotid MRI at 7.0 T and 3.0 T qualitatively[19] and showed good lumen area and vessel wall area reproducibility at both fields. However, these experiments were performed with one large single loop coil per side for reception at both field strengths, while other studies apply more dedicated receiver arrays with eight[20] or sixteen[21] elements. Another study focusing on a comparison of 3.0 T and 7.0 T intracranial angiography, reports an increase of contrast to noise ratio (CNR) between lumen and surrounding of the carotid arteries of 30 - 40%.[22] In that study, no tissue properties of the vessel wall itself were assessed, and the used headcoil prohibited imaging the carotid arteries at a level as low as the bifurcation. Even when a dedicated neck coil is used, the transmit field is localized to the neck. Due to the absence of a body coil[23], conventional blood suppression strategies (double inversion recovery[24] and quadruple inversion recovery[25]) could not be applied with this limited transmit field at 7.0 T. Instead, a TSE, which has inherent black blood contrast, was used as an alternative. At 7.0 T there is an increased SAR, which can reduce the efficiency of the SAR demanding sequences like TSE, by requiring increased TR. Alternatively, depending on the tissue T_1 and T_2 relaxation times, reducing the refocusing angles of an echo train in a TSE, can also effectively reduce SAR while controlling contrast and SNR.[26] Moreover, as T_1 and T_2 relaxation times will be different between the field strengths, sequences have to be optimized specifically for 7.0 T for optimal CNR and SNR. While the observed SNR at 7.0 T increased with a factor of 2.0 as compared to 3.0 T, the altered relaxation times also contributed to changes in SNR and tissue contrast.

In conclusion, an evaluation between 3.0 T and 7.0 T carotid MRI with optimized setups at both field strengths was performed. An increase in SNR of even greater than 7/3 was observed at the periphery of the neck. At an average depth of the carotids, still a considerable gain in SNR of a factor 2.0 was measured in a series of healthy subjects, though somewhat less than the theoretical factor of 2.33. Phantom experiments indicate that the high density receive array used at 7.0 T suffers some loss in SNR due to coupling, but at the same time benefits from higher acceleration factors using parallel imaging techniques. In all subjects, the 7.0 T subjective SNR was better than the 3.0 T SNR. For the first time, T_1 and T_2 in the healthy carotid vessel wall was documented for both 3.0 T and 7.0 T, which are needed to perform tailored sequence optimization in the future.

References

1. Leiner T, Gerretsen S, Botnar R, et al. Magnetic resonance imaging of atherosclerosis. Eur Radiol 2005;15:1087–1099.
2. Rothwell P, Gibson R, Warlow C. Interrelation between plaque surface morphology and degree of stenosis on carotid angiograms and the risk of ischemic stroke in patients with symptomatic carotid stenosis. Stroke 2000;31:615–621.
3. Saam T, Ferguson M, Yarnykh V, et al. Quantitative evaluation of carotid plaque composition by in vivo MRI. Arterioscler Thromb Vasc Biol 2005;25:234–239.
4. Cai JM, Hatsukami TS, Ferfuson MS, et al. Classification of human carotid atherosclerotic lesions with in vivo multicontrast magnetic resonance imaging. Circulation 2002; 106:1368–1373.
5. Shinnar M, Fallon JT, Wehrli S, et al. The diagnostic accuracy of ex vivo MRI for human atherosclerotic plaque characterization. Arterioscler Thromb Vasc Biol 1999;19:2756–2761.
6. Edelstein WA, Glover GH, Hardy CJ, et al. The intrinsic signal-to-noise ratio in NMR imaging. Magn Reson Med 1986;3: 604–618.
7. Koning W, Bluemink JJ, Langenhuizen EAJ, et al. High-resolution MRI of the carotid arteries using a leaky waveguide transmitter and a high-density receive array at 7 T. Magn Reson Med 2013;69:1186–1193.
8. Yarnykh VL. Actual flip-angle imaging in the pulsed steady state: a method for rapid three-dimensional mapping of the transmitted radiofrequency field. Magn Reson Med 2007;57:192–200.
9. Schar M, Kozerke S, Fischer SE, et al. Cardiac SSFP imaging at 3 Tesla. Magn Reson Med 2004;51:799–806.
10. The International Commission on Non-Ionizing Radiation Protection. Medical magnetic resonance (MR) procedures: protection of patients. Health Phys 2004;87:197–216.
11. Busse RF, Hariharan H, Vu A, Brittain JH. Fast spin echo sequences with very long echo trains: design of variable refocusing flip angle schedules and generation of clinical T2 contrast. Magn Reson Med 2006;55:1030–1037.
12. Sun B, Giddens DP, Long R, et al. Automatic plaque characterization employing quantitative and multicontrast MRI. Magn Reson Med 2008;59:174–180.
13. Mihai G, Giri S, Sharkey-Toppen TP, et al.Quantitative T1, T2 and T2 * mapping of carotid artery normal wall and atherosclerotic plaque. In: Proceedings of the 19th Annual Meeting of ISMRM, Montreal, Canada, 2011.
14. Biasiolli L, Lindsay AC, Chai JT, et al. Invivo quantitative T2 mapping of carotid arteries in atherosclerotic patients: segmentation and T2 measurement of plaque components. J Cardiovasc Magn Reson 201;15:69.
15. Coolen BF, Heijtel DF, Potters WV, et al. 3D carotid wall T1 quantification using variable flip angle 3D Merge with steadystate recovery. In: Proceedings of the 21st Annual Meeting of ISMRM, Salt Lake City, 2013.
16. Hoult DI, Phil D. Sensitivity and power desposition in a high-field imaging experiment. J Magn Reson Imaging 2000;12:46–67.
17. Bottomley PA, Lugo Olivieri CH, Giaquinto R. What is the optimum phased array coil design for cardiac and torso magnetic resonance? Magn Reson Med 1997;37:591–599.
18. Roemer PB, Edelstein WA, Hayes CE, et al. The NMR phased array. Magn Reson Med 1990;16:192–225.
19. Kroner ES, van Schinkel LD, Versluis MJ, et al. Ultrahigh-field 7-T magnetic resonance carotid vessel wall imaging: initial experience in comparison with 3-T field strength. Invest Radiol 2012; 47:697–704.
20. Balu N, Yarnykh VL, Scholnick J, et al. Improvements in carotid plaque imaging using a

new eightelement phased array coil at 3T. J Magn Reson Imaging 2009;30: 1209–1214.
21. Tate Q, Kim S-E, Treiman G, et al. Increased vessel depiction of the carotid bifurcation with a specialized 16-channel phased array coil at 3T. Magn Reson Med 2012;69: 1486–1493.
22. von Morze C, Xu D, Purcell DD, et al. Intracranial time-of-flight MR angiography at 7T with comparison to 3T. J Magn Reson Imaging 2007;26:900–904.
23. Schick F. Whole-body MRI at high field: technical limits and clinical potential. Eur Radiol 2005;15:946–959.
24. Edelman R, Chien D, Kim D. Fast selective black blood MR imaging. Radiology 1991;181:655–660.
25. Yarnykh VL, Yuan C. T1-insensitive flow suppression using quadruple inversion-recovery. Magn Reson Med 2002;48:899–905.
26. Hennig J, Weigel M, Scheffler K. Calculation of flip angles for echo trains with predefined amplitudes with the extended phase graph (EPG)-algorithm: principles and applications to hyperecho and TRAPS sequences. Magn Reson Med 2004;51: 68–80.

Chapter 5

7.0 T MRI of atherosclerotic plaque in the significantly stenosed carotid artery

AAJ de Rotte, W Koning, MTB Truijman, AG den Hartog, SM Bovens, A Vink, S Sepehrkhouy, JJM Zwanenburg, DWJ Klomp, G Pasterkamp, FL Moll, PR Luijten, J Hendrikse, GJ de Borst

Investigative Radiology. 2014;49:749-757

Abstract

Background and purpose:

The objective of this study was to assess the feasibility of carotid vessel wall imaging at 7.0 T magnetic resonance imaging (MRI) in a series of patients with a symptomatic greater than 70% stenosis of the internal carotid artery.

Methods:

First, a series of 6 healthy volunteers were scanned

at 3.0 T and 7.0 T MRI to perform a signal-to-noise ratio comparison between these 2 field strengths. Second, in patients with a greater than 70% stenosed carotid artery, a 7.0 T MRI protocol, consisting of a dual-echo turbo spin echo sequence (echo times of 45 and 150 milliseconds) and a T_1weighted turbo spin echo sequence, was obtained. Lumen and vessel wall were delineated for interobserver and intraobserver reproducibility, and signal intensity distribution in the most severely stenosed part of the internal carotid artery was correlated with different plaque components on histopathologic findings.

Results:

The mean (SD) signal-to-noise ratio in the vessel wall was 42 (12) at 7.0 T and 24 (4) at 3.0 T. Nineteen patients were included, but technical issues yielded carotid MRI data of 14 patients available for the final analysis. Of these patients, 4 were diagnosed with stroke, 7 were diagnosed with a transient ischemic attack, and 3 were diagnosed with amaurosis fugax. Intraclass correlation coefficient of the agreements of lumen and vessel wall determination between 2 observers and between the repeated measures of 1 observer were above 0.80 in both 3.0 T and 7.0 T data sets of the healthy volunteers and also in the 7.0 T data set of the patients. Signal hyperintensity in the 7.0 T magnetic resonance images was inversely proportional to calcification. Other correlations between plaque components and signal intensity could not be confirmed.

Conclusion:

This first series of patients with carotid atherosclerotic plaque who were scanned at 7.0 T MRI shows that 7.0 T MRI enables to adequately determine lumen and vessel wall areas. Signal hyperintensity in these 7.0 T magnetic resonance images was inversely proportional to calcification. However, at this stage, no other correlations between histologic findings and vessel wall contrast were found. Implementation of in vivo high-resolution 7.0 T MRI of plaque components for risk stratification remains challenging. Future development of hardware and software is still needed to attain a more robust setup and to enable complete plaque characterization, similar to what is currently possible with multiple MRI sequences at 1.5 T and 3.0 T MRI.

Introduction

Several magnetic resonance imaging (MRI) studies have shown that vulnerability of atherosclerotic carotid artery plaques can be determined by its components.[1-3] Hence, intraplaque hemorrhage (IPH) and a thin fibrous cap on top of a lipid-rich necrotic core (LRNC) can be used for risk stratification of the occurrence of cerebrovascular events.[4-8] The criterion standard to assess these different plaque components ex vivo is histopathology.[9] However, in vivo identification of different components may enable to identify subgroups of patients with a high risk for (recurrent) cerebrovascular ischemia.

Thus far, most MRI studies on in vivo carotid plaque imaging have been performed at field strengths of 1.5 and 3.0 T with successful results.[10-12] Multisequence MRI seems to be sufficient to reliably visualize different plaque components in vivo.[11,13,14] Still, the ability of MRI to detect local heterogeneity within a plaque, because of different components, strongly depends on signal-to-noise ratio (SNR) and contrast-to-noise ratio. Because histology shows that details of the plaque architecture often are at a submillimeter scale and beyond the resolution capacity of MRI in general, it is important to aspire for the highest possible spatial resolution. Accordingly, local surface coils in combination with an ultrahigh magnetic field strength of 7.0 T may provide an SNR enabling plaque imaging with an increased spatial resolution. Despite the fact that 1.5 and 3.0 T yield good results in plaque component imaging already,[1,3,4] an even higher field strength might enable the visualization of more subtle changes of the carotid artery wall in the early stages of plaque formation. In addition, changed relaxation parameters and susceptibility effects at 7.0 T may eventually lead to altered and increased contrast between different plaque components. Except for 1 study that showed 7.0 T MRI of an ulcerating plaque and 50% stenosis in the internal carotid artery in a single patient, no patient studies have been reported yet at 7.0 T MRI.[15]

The aim of the current study is to investigate the feasibility of carotid vessel wall imaging at 7.0 T MRI in a series of patients with a greater than 70% internal carotid artery stenosis, who were scheduled for carotid endarterectomy (CEA). All patients were symptomatic because the decision to perform CEA in daily practice is based on symptoms and the stenosis grade. Magnetic resonance image quality and signal intensity were evaluated and correlated with histopathologic assessment of the surgically derived carotid artery plaque. To assess a measure for performance and reproducibility relative to 3.0 T, an additional group of healthy volunteers was scanned at both 3.0 and 7.0 T.

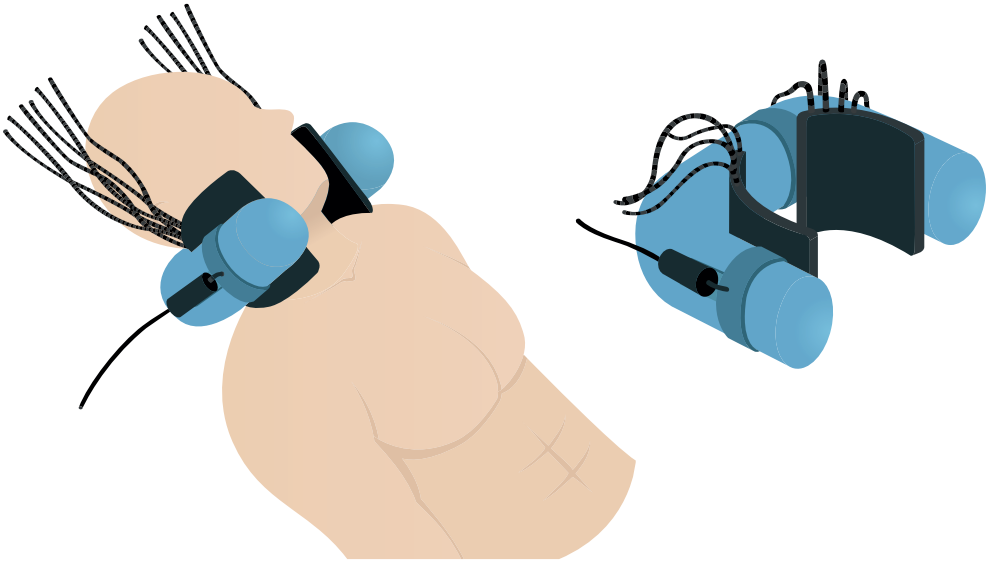

Figure 1. Carotid arteries setup at 7.0 T MRI. The leaky waveguide transmitter, illustrated in blue, is positioned around the neck as shown on the left. The high-density receive arrays, illustrated in gray, are positioned between the neck and the leaky waveguide transmitter.

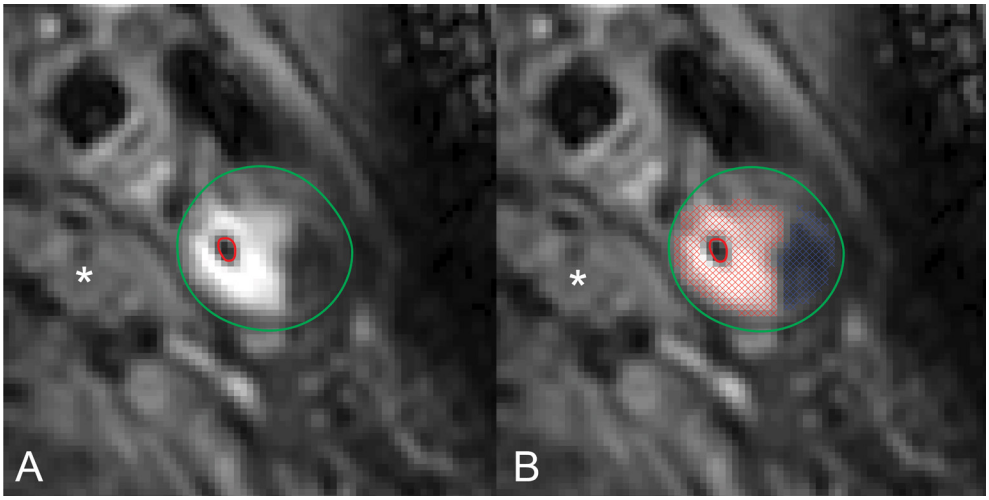

Figure 2. The Proton Density weighted TSE images of a patient with a symptomatic left carotid artery stenosis of greater than 70% (male; 73 years). Example of signal intensity analysis with original image (A) and image with analysis (B). Red markers indicate hyperintense voxels and blue markers indicate hypointense voxels. Voxels with no marker within the vessel wall represent isointense voxels relative to the adjacent muscle (*).

Methods

Participants

A 7.0 T MRI protocol dedicated for carotid vessel wall imaging was obtained in the patients. All patients were diagnosed with a symptomatic carotid artery stenosis of greater than 70% and were scheduled for CEA. Exclusion criteria were inability to undergo a 7.0 T MRI scan, due to contraindications for 7.0 T MRI (eg, pacemakers, nerve stimulators, and other metallic implants). In addition, the healthy volunteers without contraindications to undergo both 3.0 T and 7.0 T MRI were scanned for a 3.0 T versus 7.0 T SNR comparison. Institutional review board approval was obtained for this prospective study, as previously described,[16] and all participants gave written informed consent.

Magnetic Resonance Imaging

Ultra-high field strength MRI was performed on a 7.0 T whole-body MRI system (Philips Healthcare, Cleveland, OH) with a leaky waveguide transmitter and high-density receive array (MR Coils B.V., Drunen, The Netherlands), designed for high-resolution carotid artery imaging at 7.0 T MRI (Figure 1).[17] The receive array consisted of 30 receive channels bilaterally (15 elements per side). The optimal phase depends on both neck size as well as artery location and needed to be optimized for each individual participant. Because the transmit array consisted of 2 separate transmit channels, the B1 fields could be optimized for a certain desired region using B1 shimming.[17,18] For the B1 shimming procedure, actual flip angle imaging maps were acquired for each of the 2 transmit channels using a double repetition time (TR) method, with TR1/TR2 of 50/200 milliseconds, a nominal flip angle of 50 degrees, and a total duration of 1 minute 12 seconds.19 With the use of actual flip angle imaging maps, the B1 could be focused on both carotids or primarily on the carotid artery scheduled for CEA.

High-field strength MRI was performed on a 3.0 T wholebody MRI system (Philips Achieva; Philips Healthcare, Best, The Netherlands) with an 8-channel phased-array coil (Shanghai Chenguang Medical Technologies Co, Shanghai, China) dedicated for carotid artery imaging.

The imaging protocol on both 3.0 T and 7.0 T MRI consisted of a dual-echo turbo spin echo (TSE) sequence and a T_1 weighted TSE sequence. The black-blood T_1 TSE sequence was developed after the start of the study and therefore not obtained in all patients. Scan parameters of all used sequences are shown in Table 1. A specific absorption rate (SAR) model specific for this transmit array[17] was used to ensure that all 7.0 T protocols were acquired within the restrictions of the SAR guidelines, based on a maximum allowed SAR_{10g} of 10 $W \cdot kg^{-1}$.[20]

Table 1. Scan Parameters of the 3.0 T and 7.0 T protocol used for the healthy volunteers and the patients. Acquisition in transversal direction for each sequence.

	3.0 T		7.0 T	
	Dual-Echo TSE	T_1 TSE	Dual-Echo TSE	T_1 TSE
FOV, mm	150 x 179 x 31	180 x 180 x 26	150 x 179 x 31	180 x 180 x 26
Acquired voxel size, mm^3	0.50 x 0.51 x 2.00	0.40 x 0.41 x 1.50	0.50 x 0.51 x 2.00	0.40 x 0.41 x 1.50
Reconstructed voxel size, mm^3	0.28 x 0.28 x 2.00	0.19 x 0.19 x 1.50	0.28 x 0.28 x 2.00	0.19 x 0.19 x 1.50
TR/TI, ms	3000/-	1000/-	3000/-	1000/-
TE, ms	45*/150†	28	45*/150†	29
Equivalent TE, ms	27/70‡	18	27/70‡	19
Flip angle, degrees	90	100	90	100
Reduced refocusing angles, degrees	50	50	50	50
TSE factor	16	8	16	8
NSA	1	2	1	2
SENSE factor (AP x RL)	1 x -	2 x -	1 x -	2 x -
Fat suppression	SPIR	SPIR	SPIR	SPIR
Duration, min:sec	4:36	3:56	4:36	3:52

*First echo; †Second echo; ‡Equivalent echo time for a spin echo sequence with full 180-degree refocusing pulses, yielding similar T_2 weighting for tissues with T_1/T_2 approximately 2000/50 milliseconds; AP indicates anterior-posterior; FOV, field of view; NSA, number of signal averages; SENSE, factor in the AP direction and RL direction; RL, right-left; SPIR, spectral presaturation with inversion recovery; TE, echo time; TI, inversion time; TR, repetition time; TSE factor, echo train length (number of refocusing pulses); TSE, turbo spin echo.

SNR Analysis

The dual-echo TSE sequence as described previously and in Table 1 was used for the SNR analysis of the carotid vessel wall.[21] The first echo of this sequence yields a proton density weighted (PDW) image, in which the SNR analysis was performed, and was acquired with a readout bandwidth of 224 Hz. This measurement was performed in both carotid arteries of the 6 healthy volunteers at 7.0 and 3.0 T. MeVisLab 2.4 (MeVis Medical Solutions AG, Bremen, Germany) was used for vessel wall segmentation, noise determination, and SNR calculation.

Image Quality

In all participants, both the healthy volunteers and the patients, lumen and vessel wall were determined with VesselMass (Department of Radiology, Leiden University Medical Center, Leiden, The Netherlands). The available sequences were used to delineate both areas in all obtained slices, covering the common carotid artery and the internal carotid artery. The measurements were performed by 2 observers (AR and MT), both well trained in vessel wall analysis. With the assumption that a qualitative nondiagnostic image quality would give a lower intraclass correlation coefficient (ICC), this quantitative delineation of lumen and vessel wall is used to quantify the image quality.

Plaque Analysis

Histology Histology is analyzed according to the Athero-Express protocol previously described.[22] During the surgery, the distance between the distal side of the external carotid artery and the most severely stenosed part of the internal carotid artery was measured, as well as the length of the plaque. Both measurements were performed in situ and ex vivo after surgical removal. Subsequently, the internal and external carotid arteries as well as the most severely stenosed part of the internal carotid artery were marked with stitches. The endarterectomy specimens were fixed in formalin and embedded in paraffin. According to the Athero-Express protocol, only the most severely stenosed part of the internal carotid artery was analyzed. On this section, 4 different stainings were applied to identify different plaque components: hematoxylin and eosin for the identification of calcification, IPH, and thrombus; Sirius red for collagen identification and measurement of the fibrous cap thickness; α-actin for smooth muscle cells; and CD68 for macrophage identification. The slides were scanned with a ScanScope XT scanner (Aperio Technologies, Inc, Vista, CA) and analyzed using Imagescope (Aperio Technologies). The percentage of the different plaque components (atheroma, collagen, smooth muscle cells, and calcification) was determined. The

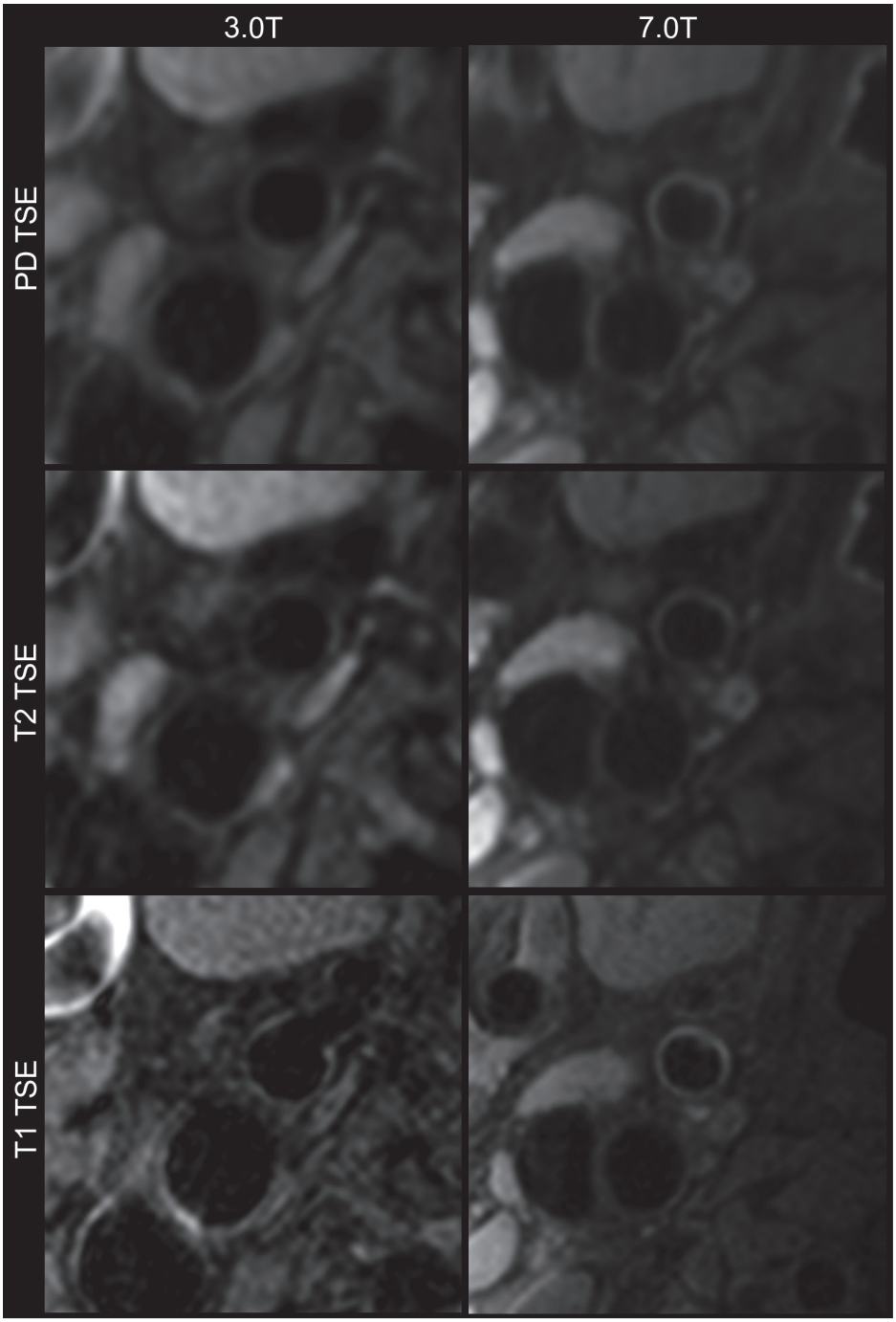

Figure 3. Example of 3.0 T and 7.0 T images of 1 healthy volunteer. Both series are just above the bifurcation of the right common carotid artery.

presence of IPH and luminal thrombus was determined, and macrophages were semi quantitatively scored as minor, moderate, or heavy. Subsequently, all plaques were classified according to the modified American Heart Association classification.[23] Finally, in plaques with a (thin) fibrous cap atheroma, the thickness of the fibrous cap was measured.

Magnetic Resonance Imaging

Seven Tesla MR images of the PDW sequence were used for signal intensity analysis (Figure 2). Signal intensities of the plaque were described, relative to the signal intensity of adjacent muscles, on the first echo of the dual-echo TSE sequence. Within the slice, associating with the most severely stenosed part of the internal carotid artery, each voxel of the vessel wall was defined as being hypointense, isointense, or hyperintense relative to the longus colli muscle. Hypointensity was defined as 2 standard deviations (SD) lower than longus colli muscle signal intensity and hyperintensity was defined as 2 SDs above longus colli muscle signal intensity. This signal intensity assessment was performed in a script build in MATLAB, version R2013a (The MathWorks, Inc, Natick, MA). A signal intensity correction was applied to correct for receive field inhomogeneity.

Statistics

For the interobserver and intraobserver reproducibility, 1 observer (AR) performed the analysis twice with 2 weeks in between. For the lumen and vessel wall, delineations were calculated. The ICC and Bland-Altman plots[24] were calculated for the intraobserver and interobserver reproducibility.

Associations between different histological characteristics and signal intensities on MRI were evaluated with a simple binary logistic regression.

Statistical analyses in this study were performed in IBM SPSS Statistics version 20 (IBM Corporation, Armonk, NY).

Results

In total, 19 symptomatic patients with severe stenosis (>70%) of the carotid artery, scheduled for CEA, were included between May 2011 and September 2013. Images of 2 patients were not available for the final analyses because of severe movement artifacts. In 1 patient, the B1 shimming procedure failed; in 1 patient, F0 determination failed; and in 1 patient, the histopathologic finding was not available because of fragmentation of the specimen. The final analyses were performed on 14 patients (10 men) with a mean age of 68 (range, 54 to 83) years. In 4 patients, stroke was diagnosed; in 7 patients, a transient ischemic attack was diagnosed; and in 3 patients, amaurosis fugax was

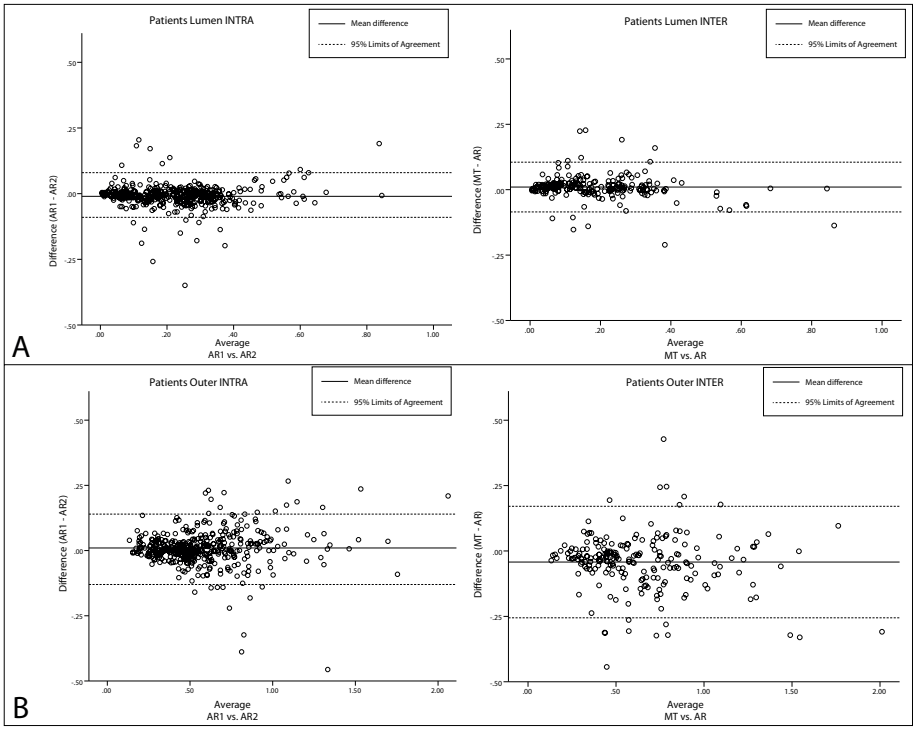

Figure 4. Bland-Altman plots of intraobserver and interobserver reproducibility of patient analysis. The plots of the healthy volunteers could be found in the Supplementary Material. Intraobserver (left) and interobserver reproducibility (right) of lumen determination in patients (7.0 T MRI) (A). Intraobserver (left) and interobserver reproducibility (right) of outer vessel wall determination in the patients (7.0 T MRI) (B).

Table 2. SNR Measurements of the Carotid Vessel Wall on 3.0 T and 7.0 T MRI in the 6 Healthy Volunteers

	Depth, mm^3		3.0 T			7.0 T		
	Right	Left	Right	Left	Mean	Right	Left	Mean
1	23	22	17.5	24.4	21.2	70.4	62.3	66.3
2	28	29	25.0	32.0	28.5	39.5	31.5	35.5
3	23	22	29.1	27.6	28.3	52.2	25.0	38.6
4	26	25	18.5	24.5	21.5	41.5	22.3	31.9
5	24	27	28.2	27.8	28.0	46.5	39.8	43.2
6	25	26	16.4	20.5	18.4	34.2	43.2	38.7

*Department of the common carotid artery, just beneath the bifurcation. Shortest distance from the middle of the arterial lumen to the skin surface is measured on the 3.0 T magnetic resonance images. MRI indicates magnetic resonance imaging; SNR, signal-to-noise ratio.

diagnosed. Carotid endarterectomy was planned on the left carotid artery in 9 patients and on the right side in the remaining 5 patients.

SNR Analysis

The SNR analysis was performed in the 6 healthy volunteers (2 men) with a mean age of 26 (range 23 to 33) years. Overview of all SNR measurements is given in Table 2. The mean (SD) SNR in the vessel wall was 42 (12) at 7.0 T and 24 (4) at 3.0 T.

Image Quality

First, 3.0 T and 7.0 T scans of the healthy volunteers were evaluated. An example of the 3.0 T and 7.0 T images of 1 healthy volunteer is given in Figure 3. For both interobserver and intraobserver agreement, the ICCs for the lumen and vessel wall delineation were strong. In all categories, scores were above 0.90, except for the interobserver agreement of the 7.0 T data in the healthy volunteers (lumen: ICC = 0.87, 95% confidence interval (CI) = 0.80 to 0.90, P = 0.001; outer vesselwall: ICC = 0.84, 95% CI = 0.70 to 0.91, P = 0.001) Regarding the patient data, the ICCs for both interobserver and intraobserver agreement of lumen and vesselwall delineationwere 0.95 or stronger. These strong ICCs in both the healthy volunteers and the patients correspond with a minimal difference between both observers and between the repeated measurements as can be seen from the Bland-Altman plots. The agreements in the lumen and vesselwall measurements are provided in Table 3. The Bland-Altman plots of the patient evaluation are shown in Figure 4; the Bland-Altman plots of the healthy volunteer evaluation can be found in the supplementary material.

Plaque Intensity

In Figure 5, an example of histopathologic finding with the corresponding slice on 7.0 T MRI is shown. Simple binary logistic regression analysis demonstrated that the odds of having calcification in the atherosclerotic plaque decreased proportionally to the increase of magnetic resonance signal hyperintensity in the corresponding slice of the carotid plaque (Nagelkerke $R^2 = 0.55$, $X^2 = 7.41$, P = 0.006, odds ratio = 0.92 [95% CI = 0.00 to 0.97, P = 0.02]). The P value and 95% CI were based on a bootstrap of 1972 samples. Although IPH was seen on the histopathologic analysis in 4 of the 14 patients, a similar analysis could not demonstrate a significant relation between signal intensity of the atherosclerotic plaque (on the PDW images) and IPH. A relation between signal intensity and macrophage infiltration and lipid accumulation in the most severely stenosed part of the internal carotid artery could not be demonstrated.

Interestingly, when looking at slices not representing the most severe stenosis, 2 cases showed a hyperintense signal in the plaque predominantly located in the region

of the plaque-lumen interface on the first and second echoes of the dual-echo TSE sequence (Figure 6). In 2 patients, a suggestion of discontinuity at the location of the plaque-lumen interface on the first echo of the dual-echo TSE sequence was found. This discontinuity was also not on the level of the most severe stenosis of the internal carotid artery. Bilateral images of one of these patients are demonstrated in Figure 7. Because these were findings on slices not representing the most severe stenosis, no comparison could be made with histopathologic findings.

Discussion

Our study confirms that 7.0 T MRI is feasible for carotid vessel wall imaging in a series of patients with a symptomatic highgrade carotid artery stenosis. An approximately 2-fold higher SNR in the carotid vessel wall was measured at 7.0 T compared with 3.0 T. Consequently, our study confirmed the accuracy of lumen and outer vessel wall delineation on 7.0 T magnetic resonance images in a series of patients with severely stenosed carotid arteries.

Previous studies have shown the feasibility of 7.0 T carotid vessel wall imaging in healthy volunteers.[15,17,25] A setup consisting of 1 unilateral local transmit/receive coil with a diameter of 15 cm resulted in reproducible vesselwall determination of the common carotid artery in healthy volunteers.[25] Second, with a rigid setup consisting of bilateral 8 surface loop transmit/receive coils, the first results of carotid vessel wall imaging in a single patient, with an ulcerating plaque and a 50% stenosis in the internal carotid artery, were presented.[15] In a third study, the combined transmit/receive coils were replaced by a separate transmit and receive coil, which yielded a more optimized setup with higher receive sensitivity while keeping SAR constraints low.[17] Together, these studies confirm that it is possible to cope with technical difficulties such as B1 inhomogeneities and SAR limitations. However, the current study is the first study that attempts to visualize plaque characteristics with the available black-blood sequences on 7.0 T MRI in a series of patients with a severe carotid artery stenosis.

The challenging setup of carotid artery imaging at 7.0 T with dedicated surface coils and no body transmit coil makes the transfer from healthy control participants to patients nontrivial. While testing the feasibility in this more clinical situation with a series of elderly patients with significantly stenosing carotid artery plaques, we encountered several challenges. Some challenges were technical issues of which the most important was the determination of the center Larmor frequency (F0) in the neck due to a very inhomogeneous B0 field and the large amounts of fat present in the neck. In 1 patient, the incorrect determination of F0 led to a nondiagnostic image quality. A second challenge comprised the B1 homogeneity. The image quality was often diminished by

the occurrence of local B1 inhomogeneity because of a suboptimal field of either the transmit array or the 30-channel receive array. The fact that a single-size transmitter was used for all sizes of neck resulted in some cases of suboptimal placement of the transmit elements. However, in most cases, the B1 shimming procedure enabled to correct this. Transmit B1 fields determine the flip angle distribution throughout the neck. This flip angle distribution was set by the B1 shimming procedure, in which the phases and powers of the transmit signal were determined for both transmit elements. Because of variation in neck size and depth of carotid arteries, the optimal phase sometimes varied up to 180 degrees between the participants. In case the available power was not sufficient to yield the desired flip angle in both the left and right carotid arteries, the carotid artery scheduled for CEA was given priority. In that case, the carotid artery at the contralateral side may end up in a region with very low B1, visible as a black band in the image. On the other hand, in case the carotids were located at a depth more than 5 cm from the surface of the neck, the low local receive field of the receive arrays resulted in a very low signal level, which also resulted in very low signal in the area of the carotids. Another important challenge was the inability of this setup to adequately fixate the patient's neck to avoid movement artifacts.

Although relaxation times are different at higher field strength, the same imaging sequences were used for the volunteer comparison at 3.0 T and 7.0 T. Because of the changed relaxation times, contrasts may turn out different between different field strengths. Therefore, the PDW scan, which has no additional contrast weighting, was used for the SNR analysis in the carotid vesselwall. The significantly higher SNR of the carotid vessel wall at 7.0 T MRI compared with 3.0 T is in agreement with the previous studies.[15,17,25] The SNR gain is slightly less than the expected gain in SNR of 7/3. However, although the first echo image of the dual-echo TSE was designed to be PDW, the TR of 3000 milliseconds and the echo time of 50 milliseconds can still cause some T_1- and T_2weighted signal loss, respectively. This effect is stronger at 7.0 T than it is on 3.0 T because T_1 increases and T_2 decreases with field strength and therefore explains more signal loss.[21] Although the SNR was still approximately twice as high and may allow the visualization of more subtle changes of the carotid artery wall in the early stages of plaque formation, this analysis is performed in young healthy volunteers. It is not guaranteed that the SNR ratio in elderly patients will be the same as the one found in the healthy volunteers, although elderly patients are more challenging at both field strengths. Nevertheless, the results of the image quality analysis have shown that lumen and vessel wall delineation remained adequate in both healthy volunteers and patients.

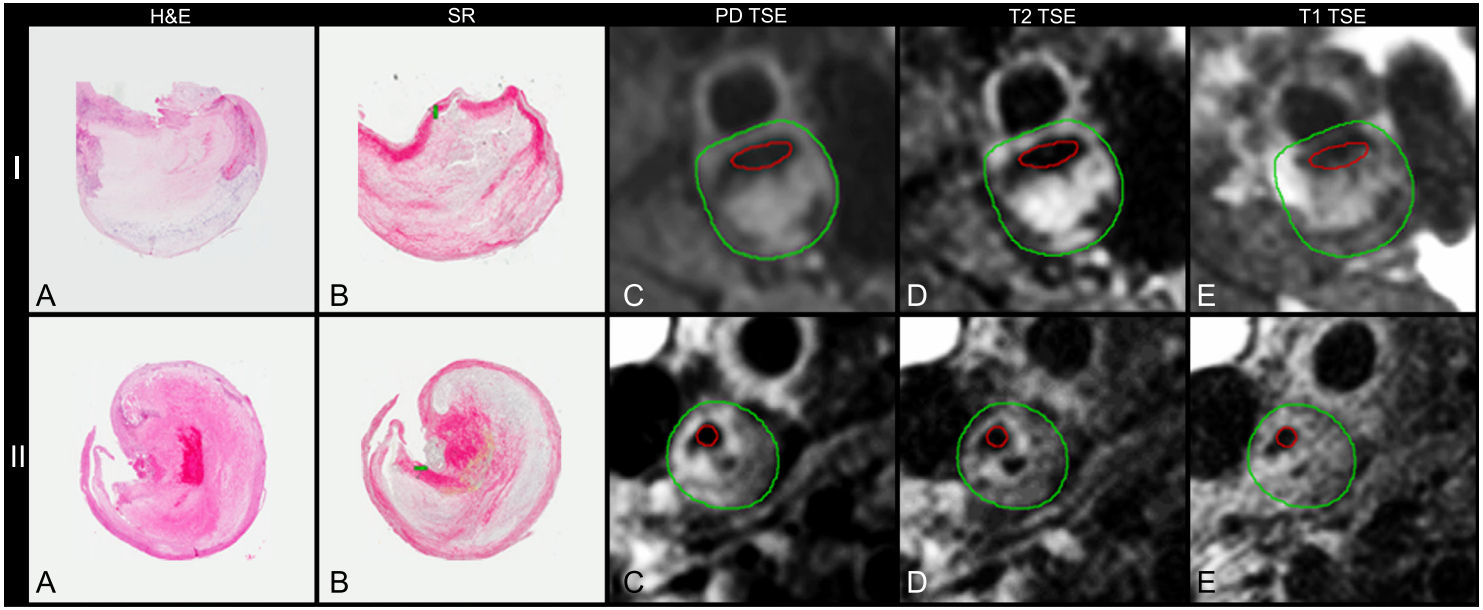

Figure 5. An overview of a 68-year-old patient (male) with a symptomatic stenosis in the left internal carotid artery (I) and an overview of a 75-year-old patient (male) with a symptomatic right internal carotid artery (II). Hematoxylin and eosin (A) and Sirus Red (B) stains of the most severely stenosed part of the internal carotid artery as well as Proton Density weighted (PD) TSE (C), T_2 TSE (D), and T_1 TSE (E) sequence of the corresponding slice on 7.0 T.

The high attainable SNR of this ultra-high field strength MRI should make it possible to obtain magnetic resonance images with an ultrahigh spatial resolution, needed for accurate plaque component imaging. Magnetic resonance imaging at a field strength of 1.5 and 3.0 T has been proven to enable detailed visualization of different components within atherosclerotic plaque.[4] Ultimately, for clinical use, different plaque components such as IPH and the fibrous cap status should be visualized in vivo with an even higher resolution at 7.0 T MRI. Previously described multisequence MRI protocols for 1.5 and 3.0 T recommend for IPH a highly T_1 weighted black-blood sequence or, at 1.5 T, a time-of-flight sequence. For LRNC and fibrous cap analysis, a T_1 weighted black-blood TSE before and after contrast administration is required, and for calcification, different sequences can be used, preferably TSE sequences.[26] Despite the fact that the current

Table 3. ICCs of Intraobserver and Interobserver Reproducibility for Determination of the Lumen and the Outer Vessel Wall

Intraobserver							
		ICC	95% CI Lower	95% CI Upper	Mean	95% LoA Lower	95% LoA Upper
7.0 T _patients	Lumen	0.95*	0.94	0.96	-0.01	-0.09	0.08
7.0 T _patients	Outer	0.97*	0.96	0.97	0.58	-0.13	0.14
3.0 T_volunteers	Lumen	0.98*	0.97	0.99	0.00	-0.05	0.04
3.0 T_volunteers	Outer	0.98*	0.96	0.99	0.02	-0.07	0.10
7.0 T_volunteers	Lumen	0.98*	0.97	0.99	0.00	-0.05	0.04
7.0 T_volunteers	Outer	0.98*	0.97	0.99	0.01	-0.05	0.08
Interobserver							
		ICC	95% CI Lower	95% CI Upper	Mean	95% LoA Lower	95% LoA Upper
7.0T_patients	Lumen	0.95*	0.93	0.96	0.01	-0.09	0.11
7.0 T_patients	Outer	0.94*	0.90	0.96	-0.04	-0.26	0.17
3.0 T_volunteers	Lumen	0.98*	0.96	0.98	-0.01	-0.06	0.04
3.0 T_volunteers	Outer	0.95*	0.70	0.98	-0.05	-0.14	0.05
7.0 T_volunteers	Lumen	0.87*	0.80	0.91	0.00	-0.12	0.11
7.0 T_volunteers	Outer	0.84*	0.70	0.91	-0.05	-0.24	0.14

A 2-way random-effects model was used, where both people effects and measures effects are random *P G 0.001. CI indicates confidence interval; ICC, intraclass correlation coefficient; LoA, limits of agreement.

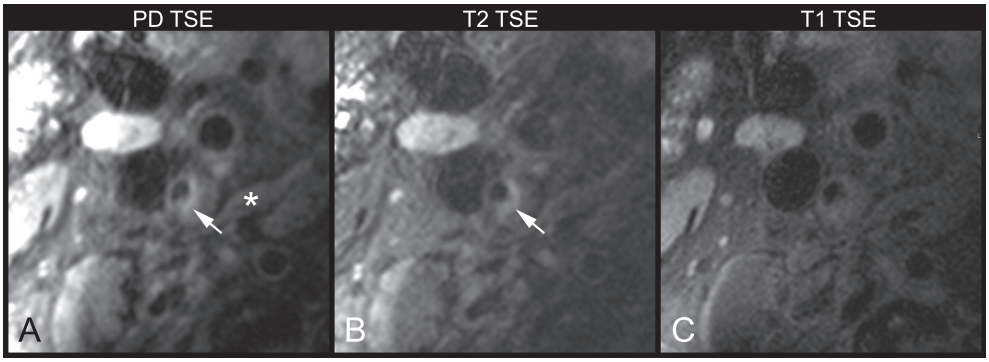

Figure 6. A Proton Density weighted (PD) TSE (A), a T_2 weighted TSE (B), and a T_1 weighted TSE (C) sequence of 75-year-old patient (male) with transient ischemic symptoms in the right hemisphere based on a greater than 70% stenosis of the right internal carotid artery. One slice (slice thickness, 2.0 mm) above the level of the most severely stenosed part of the internal carotid artery, which is histopathologically analyzed. A hyperintense signal, relative to the adjacent muscle (*), is visible on the plaque-lumen interface arrow). This hyperintense signal might be suggestive of a fibrous cap on top of a LRNC.

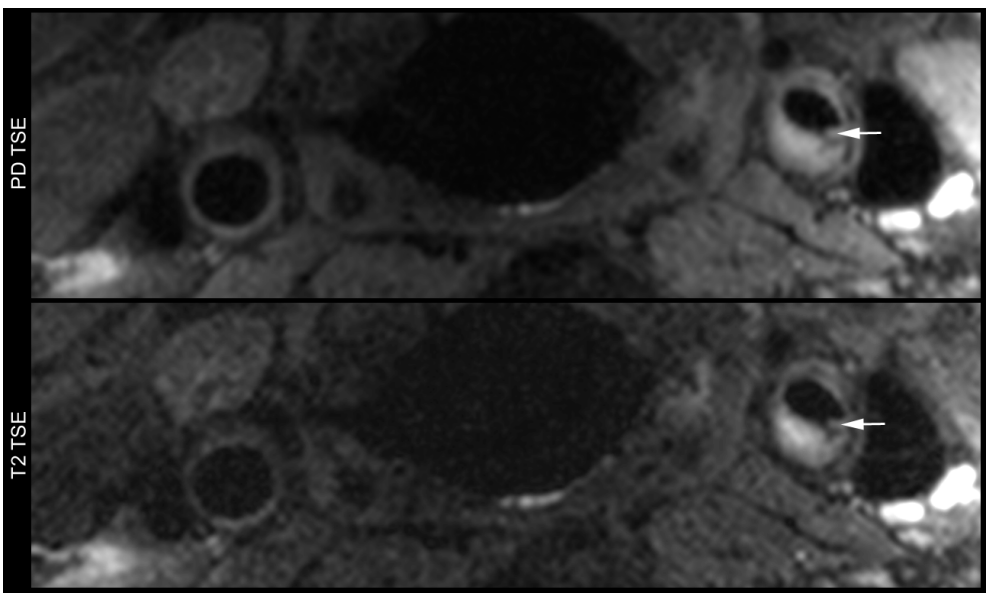

Figure 7. Bilateral images of a 68-year-old patient (male), consisting of a Proton Density weighted (PD) TSE (A) and a T_2 weighted TSE (B), 2 slices (slice thickness, 2.0mm) beneath the level of themost severely stenosed part of the internal carotid artery, which is histopathologically analyzed. A suggestion of discontinuity of the plaque-lumen interface (arrow).

study describes the first step toward clinical practice of even higher field strength MRI for plaque component imaging, there are 3 important limitations that have to be dealt with.

The first limitation is the lack of multiple contrast sequences at 7.0 T that are conventionally used at 1.5 T and 3.0 T for carotid plaque component detection. At 7.0 T, T_1 weighted TSE sequence has been subjected to T_2 contamination because of T_2 loss during the echo train, amplified by the decreased T_2 relaxation times at 7.0 T. This has reduced the observed T_1 contrast and might have been the reason why, in Figure 7C, the plaque shows little contrast. This T_1 weighted TSE sequence is used as an alternative to conventional black-blood T_1 weighted sequences, which rely on blood suppression prepulses, which, in turn, rely on a high-coverage body transmit coil.[26] At lower field strengths, an integrated body transmit coil is standardly available, but at 7.0 T, local excitation coils are used, which makes the conventional blood suppression more challenging. At this moment, the absence of dedicated black-blood sequences for plaque-component MRI at 7.0 T makes a correlation between plaque components on histology and on 7.0 T MRI difficult. However, the PDW sequence purely represents proton density of the visualized tissue, without additional contrast weightings. Because calcification has a low proton density and therefore should give a low signal, this sequence was used as a first validation of the contrast seen at 7.0 T magnetic resonance images of the carotid artery. In addition, with the available hardware setup, it still seems to be hard to consistently obtain images with a certain level of quality. This emphasizes the importance of future studies to develop dedicated T_1 weighted black-blood sequences and an evenmore robust hardware setup for 7.0 T MRI of the carotid arteries to enable plaquecomponent imaging.

Second, metallic implants have been an exclusion criterion for this ultra-high field strength MRI study. For this reason, a lot of patients were not considered for inclusion. Nevertheless, a recent study approves that not all metallic implants should be considered as a major contraindication for 7.0 T MRI.[27] In addition, for many patients eligible for inclusion in this prospective study, the preoperative schedule frequently was too exciting or the idea of an experimental setup of the 7.0 T MRI was too overwhelming, so they did not agree to undergo an extra MRI scan 1 day before surgery. These 2 factors caused a serious delay in the inclusion rate. Moreover, these factors were not present in the healthy volunteers, who hardly have any metallic implants and chose voluntarily to undergo the MRI. These problems underline that clinical implementation of a new imaging technique, such as 7.0 T carotid plaque MRI, remains challenging in the specific patient group we used.

Third, for the development of MRI sequences and analysis of the images,

comparison with histopathology is essential. Some patients did show a hyperintense lumen-vessel wall border (Figure 6) or a discontinuity in the lumen-vessel wall border (Figure 7). These images are suggestive of fibrous cap status information, but this could not be confirmed with histopathology because these findings were not found at the level of the most severely stenosed part of the internal carotid artery. Ideally, the whole plaque needs to be analyzed for a head-to-head comparison. However, according to the protocol of the Athero-Express study, only the most severely stenosed part was analyzed.[9]

Conclusion

This first series of patients with carotid atherosclerotic plaque who were scanned at 7.0 T MRI shows that 7.0 T MRI enables to adequately determine luminal and vesselwall areas. Signal hyperintensity in these 7.0 T magnetic resonance images was inversely proportional to calcification. However, at this stage, no other correlations between histology and vessel wall contrast were found. The implementation of in vivo high-resolution 7.0 T MRI of plaque components for risk stratification remains challenging. Future development of hardware and software is still needed to attain a more robust setup and to enable complete plaque characterization, similar to what is currently possible with multiple MRI sequences at 1.5 T and 3.0 T MRI.

References

1. Gupta A, Baradaran H, Schweitzer AD, et al. Carotid plaque MRI and stroke risk: a systematic review and meta-analysis. Stroke. 2013;44:3071-3077.
2. Hosseini AA, Kandiyil N, Macsweeney ST, et al. Carotid plaque hemorrhage on magnetic resonance imaging strongly predicts recurrent ischemia and stroke. Ann Neurol. 2013;73:774-784.
3. Saam T, Hetterich H, Hoffmann V, et al. Meta-analysis and systematic review of the predictive value of carotid plaque hemorrhage on cerebrovascular events by magnetic resonance imaging. J Am Coll Cardiol. 2013;62:1081-1091.
4. Kerwin WS, Hatsukami T, Yuan C, et al. MRI of carotid atherosclerosis. AJR Am J Roentgenol. 2013;200:W304-W313.
5. Yuan C, Mitsumori LM, Ferguson MS, et al. In vivo accuracy of multispectral magnetic resonance imaging for identifying lipid-rich necrotic cores and intraplaque hemorrhage in advanced human carotid plaques. Circulation. 2001;104:2051-2056.
6. Cai J, Hatsukami TS, Ferguson MS, et al. In vivo quantitative measurement of intact fibrous cap and lipid-rich necrotic core size in atherosclerotic carotid plaque: comparison of high-resolution, contrast-enhanced magnetic resonance imaging and histology. Circulation. 2005;112:3437-3444.
7. Yuan C, Kerwin WS, Ferguson MS, et al. Contrast-enhanced high resolution MRI for atherosclerotic carotid artery tissue characterization. J Magn Reson Imaging. 2002;15:62-67.
8. Cappendijk VC, Kessels AG, Heeneman S, et al. Comparison of lipid-rich necrotic core size in symptomatic and asymptomatic carotid atherosclerotic plaque: initial results. J Magn Reson Imaging. 2008;27:1356-1361.
9. Hellings WE, Pasterkamp G, Vollebregt A, et al. Intraobserver and interobserver variability and spatial differences in histologic examination of carotid endarterectomy specimens. J Vasc Surg. 2007;46:1147-1154.
10. Underhill HR, Yarnykh VL, Hatsukami TS, et al. Carotid plaque morphology and composition: initial comparison between 1.5- and 3.0-T magnetic field strengths. Radiology. 2008;248:550-560.
11. Cappendijk VC, Heeneman S, Kessels AG, et al. Comparison of singlesequence T1w TFE MRI with multisequence MRI for the quantification of lipid-rich necrotic core in atherosclerotic plaque. J Magn Reson Imaging. 2008;27:1347-1355.
12. den Hartog AG, Bovens SM, Koning W, et al. Current status of clinical magnetic resonance imaging for plaque characterisation in patients with carotid artery stenosis. Eur J Vasc Endovasc Surg. 2013;45:7-21.
13. Cappendijk VC, Cleutjens KB, Kessels AG, et al. Assessment of human atherosclerotic carotid plaque components with multisequence MR imaging: initial experience. Radiology. 2005;234:487-492.
14. Chu B, Ferguson MS, Chen H, et al. Magnetic resonance imaging features of the disruption-prone and the disrupted carotid plaque. JACC Cardiovasc Imaging. 2009;2:883-896.
15. Kraff O, Bitz AK, Breyer T, et al. A transmit/receive radiofrequency array for imaging the carotid arteries at 7 Tesla: coil design and first in vivo results. Invest Radiol. 2011;46:246-254.
16. den Hartog AG, Bovens SM, Koning W, et al. PLACD-7T study: atherosclerotic carotid plaque components correlated with cerebral damage at 7 tesla magnetic resonance imaging. Curr Cardiol Rev. 2011;7:28-34.
17. Koning W, Bluemink JJ, Langenhuizen EA, et al. High-resolution MRI of the carotid arteries using a leaky waveguide transmitter and a high-density receive array at 7 T. Magn Reson

Med. 2012;69:1186-1193.
18. Van de Moortele PF, Akgun C, Adriany G, et al. B(1) destructive interferences and spatial phase patterns at 7 Twith a head transceiver array coil. Magn Reson Med. 2005;54:1503-1518.
19. Yarnykh VL. Actual flip-angle imaging in the pulsed steady state: a method for rapid three-dimensional mapping of the transmitted radiofrequency field. Magn Reson Med. 2007;57:192-200.
20. Protection TiCoN-IR. Medical magnetic resonance (MR) procedures: protection of patients. Health Phys. 2004;87:197-216.
21. Koning W, de Rotte AA, Bluemink JJ, et al. MRI of the carotid artery at 7 tesla: quantitative comparison with 3 Tesla. J Magn Reson Imaging. 2014. [Epub ahead of print].
22. Verhoeven BA, Velema E, Schoneveld AH, et al. Athero-express: differential atherosclerotic plaque expression of mRNA and protein in relation to cardiovascular events and patient characteristics. Rationale and design. Eur J Epidemiol. 2004;19:1127-1133.
23. Virmani R, Kolodgie FD, Burke AP, et al. Lessons from sudden coronary death: a comprehensive morphological classification scheme for atherosclerotic lesions. Arterioscler Thromb Vasc Biol. 2000;20:1262-1275.
24. Altman DG, Bland JM. Comparison of methods of measuring blood pressure. J Epidemiol Community Health. 1986;40:274-277.
25. Kroner ES, van Schinkel LD, Versluis MJ, et al. Ultrahigh-field 7-T magnetic resonance carotid vessel wall imaging: initial experience in comparison with 3-T field strength. Invest Radiol. 2012;47:697-704.
26. Yuan C, Wang J, Balu N. High-field atherosclerotic plaque magnetic resonance imaging. Neuroimaging Clin N Am. 2012;22:271-284.
27. Wezel J, Kooij BJ,Webb AG. Assessing the MR compatibility of dental retainer wires at 7 Tesla. Magn Reson Med. 2013;72:1191-1198

Chapter 6

7.0 T MRI detection of cerebral microinfarcts in patients with a symptomatic high-grade carotid artery stenosis

AAJ de Rotte, W Koning, AG de Hartog, SM Bovens, JJM Zwanenburg, DWJ Klomp, G Pasterkamp, FL Moll, PR Luijten, GJ de Borst, J Hendrikse

Journal of Cerebral Blood Flow & Metabolism. 2014;34:1715-1719

Abstract

In the current study, the presence of cerebral cortical microinfarcts (CMIs) was evaluated in a series of 21 patients with a symptomatic high-grade <50% stenosis of the carotid artery. A T_2 weighted fluid-attenuated inversion recovery sequence and a T_1weighted turbo field echo sequence of the brain were obtained at 7.0 Tesla magnetic resonance imaging. Primary study endpoint was the number of CMIs and macroinfarcts. In total, 53 cerebral infarcts (35 macroinfarcts; 18 CMIs) were found ipsilateral to the symptomatic carotid artery, in 14 patients (67%). In four of these patients, both CMIs and macroinfarcts were visible. In the contralateral hemisphere, seven infarcts (five macroinfarcts and two CMIs) were found in five patients (24%). In the ipsilateral hemispheres, the number of CMIs and macroinfarcts were significantly correlated (P = 0.02). Unpaired comparison of medians showed that the number of CMIs in the ipsilateral hemisphere was significantly higher than the number of CMIs in the contralateral hemisphere (P = 0.04). No significant correlation was found between stenosis grade and the number of any infarct. The current study shows that in symptomatic patients with significant extracranial carotid artery stenosis, CMIs are part of the total cerebrovascular burden and these CMIs prevail with a similar pattern as observed macroinfarcts.

Introduction

Atherosclerosis of the carotid artery is an important risk for cerebral ischemia. In daily practice, patients are classified as high risk mainly based on the stenosis grade of the carotid artery.[1,2] Recent literature confirms that plaque characteristics may contribute to specify subgroups with an increased risk of (recurrent) ischemic cerebral events.[3–5] Moreover, the presence of infarcts in the brain parenchyma that downstream to these lesions may be important for accurate risk stratification. Patients with infarcts and cerebral symptoms were found to profit more from carotid endarterectomy (CEA), compared with patients with just ocular symptoms.[6,7] Therefore, sensitive detection of brain lesions in patients with carotid artery disease may be fundamental for identifying patient (sub)groups with the highest risk of recurrent stroke who might benefit most from carotid surgery. Magnetic resonance imaging (MRI) has a high distinctive capacity in the diagnosis of larger cortical and basal ganglia infarcts. However, from pathology studies it is known that smaller cerebral cortical microinfarcts (CMIs) can be too small for visualization with conventional in vivo imaging techniques.[8] Although 3.0 Tesla (T) MRI enables to visualize larger CMIs, the smallest lesions remain undetected.[9] However, recent publications have shown that sensitive detection of the total cerebrovascular burden, including very small CMIs of <3 mm in cortical length, is nowadays possible with stronger MRI field strengths, up to 7.0 T.[8,10] Until now, the presence of these CMIs is mainly associated with vascular cognitive impairment.[9,11]

The aim of the present study was to evaluate the presence of CMIs in a series of patients with a symptomatic high-grade stenosis of the carotid artery on high-resolution 7.0 T MRI.

Methods

Subjects

In patients who are scheduled for CEA, 7.0 T MR images of the brain were obtained <36 hours before surgery. In all patients, a symptomatic carotid artery stenosis of >50% was diagnosed, and the indication for revascularization was discussed within a multidisciplinary panel including neurologists, radiologists, and vascular surgeons. An exclusion criterion was inability to undergo 7.0 T MRI owing to the metallic implants not approved for ultra-high-field strength MR imaging. The medical ethics committee of the University Medical Center Utrecht gave approval for this prospective study, previously described,[12] and all patients gave written informed consent. The current study was conducted according to the guidelines of the Declaration of Helsinki.

Imaging

Ultra-high field strength MRI was performed on a 7.0 T MRI scanner (Philips Healthcare, Cleveland, OH, USA) with a 32-channel receive-coil and a volume transmit/receive-coil for transmission (Nova Medical, Wilmington, MA, USA). The MRI protocol consisted of a T_2 weighted fluid-attenuated inversion recovery (FLAIR) sequence[13] and a T_1 weighted turbo field echo (T_1 TFE) sequence. The FLAIR sequence was acquired in sagittal orientation with a field of view of 250 x 250 x 190 mm^3, an acquired voxel size of 0.8 x 0.8 x 0.8 mm^3, repetition time 8,000 ms, inversion time 2,250 ms, echo time 300 ms (equivalent echo time 154 ms), flip angle 100°, turbo spin echo factor 125, SENSE factor in anterior–posterior direction and right–left direction 2.5 x 2.5. Scanning time was 12 minutes 56 seconds. The T_1 TFE sequence was acquired in sagittal orientation with a field of view of 200 x 250 x 200 mm^3, an acquired voxel size of 1.0 x 1.0 x 0.5 mm^3 repetition time 4.8 ms, echo time 2.2 ms, flip angle 8° and scanning time was 1 minute 37 seconds.

Image analysis

Image analysis was performed with MeVisLab 2.4 (MeVis Medical Solutions AG, Bremen, Germany). The presence of CMIs and macroinfarcts on the high-resolution FLAIR images and T_1 TFE images of the brain were described, relative to the side of the scheduled CEA. The brain was systematically divided in seven regions: frontal, parietal, occipital, temporal, caudate nucleus, lentiform nucleus, and thalamus. For each of these regions, presence or absence and number of CMIs and macroinfarcts in both hemispheres were determined. CMIs were defined as infarcts <3 mm in cortical length. Two observers (JH and AR), masked for each other's assessment, performed the image analysis; the intraclass correlation coefficient and 95% confidence interval of ipsilateral infarcts (macro and micro) has been evaluated for interobserver agreement. In a consensus meeting, final decision of all infarcts was made; the final infarcts were used for statistical analyses.

Statistics

First, the relation between number of infarcts and baseline characteristics (age, type of symptoms, and stenosis grade) was evaluated by a Kendall's tau test. Second, the relation between number of macroinfarcts and CMIs was evaluated by the Kendall's tau test and the median difference in number of CMIs and macroinfarcts in the ipsilateral and the contralateral hemisphere by a Mann–Whitney U-test.

Statistical analyses were performed in IBM SPSS Statistics version 20 (IBM Corporation, Armonk, NY, USA).

Results

Subjects

Twenty-one patients with a symptomatic stenosis in the carotid artery, scheduled for CEA between May 2011 and September 2013, were included. Carotid endarterectomy was planned on the left carotid artery in 12 patients and on the right side in the remaining 9 patients. Of these patients, seven were diagnosed with a stroke, nine with a transient ischemic attack and five with amaurosis fugax. Mean age of the patients (14 male) was 69 ± 8 years. Baseline characteristics are presented in Table 1. Imaging was performed 1 day before surgery in 20 patients; for one patient, imaging and surgery were on the same day. The median interval between symptoms and imaging was 21 days (range 11 - 78 days). At increasing delays, the findings on MRI can less certainly be linked to the clinical symptoms. Nevertheless, the delay of 78 days was one single case. For the rest of the cohort, the range of delays between symptoms and imaging was 10 - 38 days. As the number of macro- and microinfarcts in this patient was not outlying, we decided not to exclude this patient from analysis.

None of the patients had a previous CEA of the ipsilateral carotid artery and none of the patients had a previous carotid revascularization or a history of symptoms on the contralateral carotid artery.

Cerebral burden

The determined interobserver agreement was strong for macroinfarcts and CMIs. The intraclass correlation coefficient was 0.78 (95% confidence interval = 0.53 to 0.90) for macroinfarcts and 0.80 (95% confidence interval = 0.55 to 0.92) for CMIs.

Both for the ipsilateral and contralateral hemisphere, no significant correlation was found between number of infarcts (macroinfarcts and CMIs) and stenosis grade. Both macroinfarcts and CMIs are also seen in patients with only ocular symptoms (amaurosis fugax). However, for both the ipsilateral and contralateral hemisphere, no significant correlation was found between number of infarcts (macroinfarcts and CMIs) and type of symptoms. In the ipsilateral hemisphere, no significant correlation was found between number of infarcts (macroinfarcts and CMIs) and age. In the contralateral hemisphere, a significant correlation only was found between macroinfarcts and age ($P = 0.04$), not between CMIs and age ($P = 0.32$). Results are shown in Table 2.

In 14 patients, 53 cerebral infarcts (18 macroinfarcts; 35 CMIs) were found ipsilateral to the carotid artery scheduled for CEA, compared with 7 infarcts in the

Table 1. Baseline characteristics of all included patients (n = 21)	
Gender, male	14 (67%)
Age, years	69 ± 8
Cerebrovascular accident type	
Stroke	7 (33%)
TIA	9 (43%)
Amaurosis fugax	5 (24%)
Interval event - MRI	16 (10-78)
Interval event - surgery	17 (11-79)
Stenosis, left	12 (57%)
Stenosis grade	
Symptomatic side	70 (50 - 99)
Asymptomatic side	25 (0 - 90)
Symptomatic history on asymptomatic side	0 (0%)
No. patients with infarcts ipsilateral to symptomatic side	
Macroinfarcts	14 (67%)
Microinfarcts	6 (29%)
Any infarcts	14 (67%)
No. Patients with infarcts contralateral to symptomatic side	
Macroinfarcts	4 (19%)
Microinfarcts	1 (4%)
Any infarcts	5 (24%)
No. infarcts ipsilateral to symptomatic side	53
Macroinfarcts	1 (0 - 6)
Microinfarcts	1 (0 - 7)
Any infarcts	1 (0 - 13)
No. infarcts contralateral to symptomatic side	7
Macroinfarcts	0 (0 - 2)
Microinfarcts	0 (0 - 2)
Any infarct	0 (0 - 2)

MRI, magnetic resonance imaging; TIA, transient ischemic attack. Median (range) or mean ± standard deviation or number of (No.) patients (% from total).

Table 2. Results of Kendalls tau correlation test, assessing the correlation between the stenosis grade and the number of infarcts and the correlation between CMIs and macroinfarcts

	Ipsilateral		Contralateral	
	τ	P	τ	P
Age versus macroinfarcts	-0.07	0.71	0.39	0.04
Age versus CMIs	0.09	0.62	-0.19	0.32
CVA type versus macroinfarcts	-0.024	0.20	-0.22	0.29
CVA type versus CMIs	0.02	0.94	0.04	0.48
Stenosis grade versus macroinfarcts	-0.18	0.29	-0.19	0.33
Stenosis grade versus CMIs	-0.03	0.88	0.26	0.20
CMIs versus macroinfarcts	0.45	0.02	-0.11	0.63

CMI, cerebral cortical microinfarct; CVA, cerebrovascular accident.

contralateral hemisphere (5 macroinfarcts; 2 CMIs). An example of two CMIs in the ipsilateral hemisphere is given in Figure 1 and an example of one macroinfarct in the ipsilateral hemisphere is given in Figure 2.

In all 14 patients with visible infarcts in the ipsilateral hemisphere, macroinfarcts were visible and CMIs were present in 4 of these patients. The presence of CMIs in the ipsilateral hemisphere was significantly correlated with the presence of macroinfarcts ($P = 0.02$) (Table 2). Furthermore, both the number of CMIs and the number of macroinfarcts were significantly higher in the ipsilateral hemisphere compared with the contralateral hemisphere ($P = 0.04$ and $P = 0.001$, respectively) (Table 3).

Discussion

The current study is the first study that presents in vivo visualization of CMIs in patients with extensive atherosclerosis of the extracranial vessels. The results show that CMIs prevail with the same pattern as macroinfarcts. Although the number of CMIs is less than the number of macroinfarcts, a siginificant correlation between the presence of CMIs and macroinfarcts was observed and CMIs were significant more prevalent in the hemisphere ipsilateral to the symptomatic carotid artery stenosis compared with the contralateral hemisphere.

CMIs are thus far mainly investigated in relation to dementia.[8,11] However, recently, autopsy studies showed that CMIs are not limited to patients with dementia; in 6% to 43% of patients without dementia CMIs were found.[11] Besides, also a strong correlation

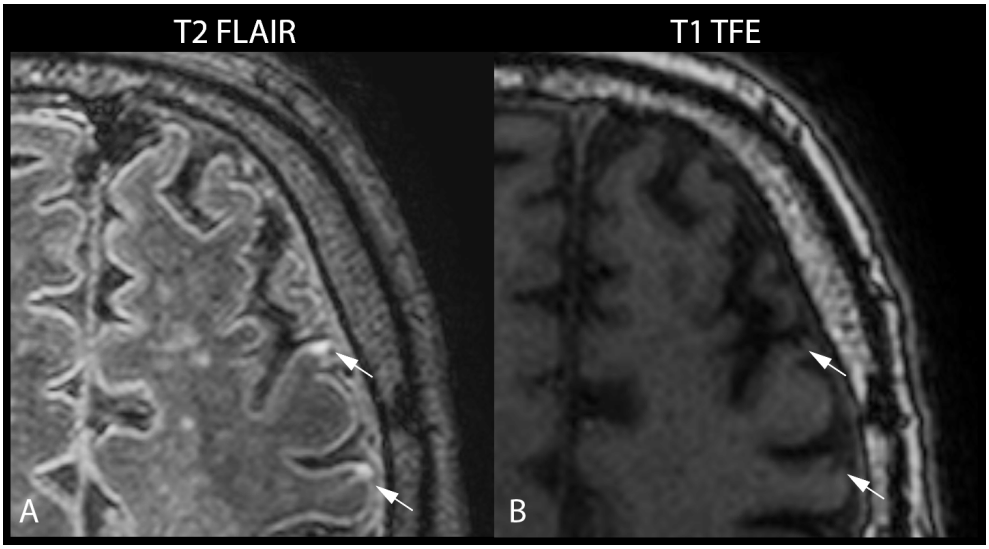

Figure 1. A 7.0 Tesla T_2 fluid-attenuated inversion recovery (FLAIR) image (A) and a T_1 turbo field echo (TFE) image (B) of a 74-year-old male with a symptomatic high-grade stenosis of the left carotid artery scheduled for carotid endarterectomy. Two cortical microinfarcts (arrows) ipsilateral to the symptomatic carotid artery are visualized in transversal plane.

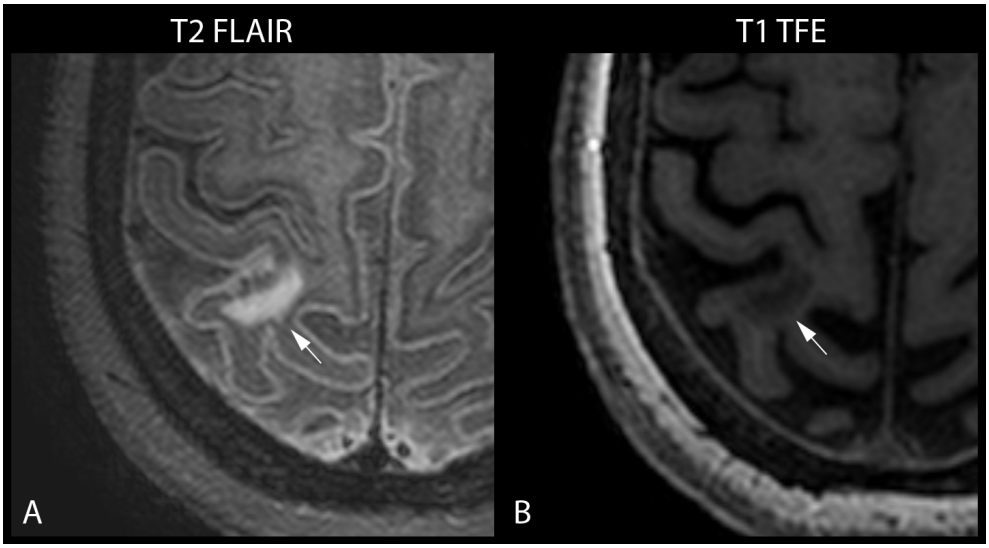

Figure 2. A 7.0 Tesla T_2 fluid-attenuated inversion recovery (FLAIR) image (A) and a T_1 turbo field echo (TFE) image (B) of a 58-year-old female with a symptomatic high-grade stenosis of the left carotid artery scheduled for carotid endarterectomy. One macroinfarct (arrows) ipsilateral to the symptomatic carotid artery is visualized in transversal plane.

was found between intracranial atherosclerosis and CMIs.[14] A prevalence of 43% in non-demented patients was found in a postmortem study in a general population cohort of people with an age of 75 years and older.[15] As the slice thickness in their specimens was already 10 micrometer, the size of microinfarcts visualized in this study were assumed to be much smaller than feasible for high-resolution 7.0 T MRI. In the current study, the prevalence of CMIs was 29% in the ipsilateral hemisphere and 5% in the contralateral hemisphere in a series of patients with a symptomatic high-grade atherosclerotic stenosis of the carotid artery. Because the CMIs in our study were found both in the ipsilateral and contralateral hemisphere and even in patients with only ocular symptoms, these infarcts may be the result of more generalized atherosclerosis. The significant higher prevalence of CMIs in the ipsilateral hemisphere in combination with the significant correlation between CMIs and macroinfarcts in the ipsilateral hemisphere is in agreement with the presence of a high-grade and possible vulnerable carotid plaque and patient symptoms.

In addition to the detection of CMIs, the current study is the second study thus far that evaluate cerebral (macro)infarcts at an ultra-high-field strength of 7.0 T. A previous study has shown that 7.0 T MRI enable to depict normal brain anatomy and ischemic lesions in patients with subacute and chronic stroke with a higher spatial resolution and more anatomic details.[16] In the current study, this high-spatial resolution was used to depict both macroinfarcts and CMIs.

In vivo visualization of CMIs was described first on ultra-highfield strength 7.0 T MRI.[10,11] Nevertheless, recent literature has shown that 3.0 T MRI is also able to visualize these ultra-small lesion.[9] However, in this study, only cognitive impaired patients were analyzed and the smallest CMIs were still not visible. In literature, a certain range of definitions of CMIs is used, deferring from invisible with the naked eye to <5 mm.[8,17] Although, the feasibility of imaging CMIs at 3.0 T MRI would make it more applicable in clinical settings, the clinical value of these microscopic lesions must be clarified first, which also implies that it must be clarified which size is clinically relevant.

As it is not guaranteed to find visible cerebrovascular damage in patients with a transient ischemic attack or amaurosis fugax, the finding that stroke patients have more often visible cerebral damage can be expected. However, both the number of macroinfarcts and CMIs are significantly higher in the symptomatic hemisphere, also in patients with only ocular symptoms. These findings suggest that CMIs prevail with the same pattern as macroinfarcts, and might also be an effect of the symptomatic vulnerable carotid plaque. The correlation between number of macroinfarcts and CMIs suggests that CMIs comprise a relevant part of the total cerebrovascular burden. Consequently, the ability to visualize CMIs *in vivo* enables to assess the cerebrovascular burden

more accurate, which makes visualization of more subtle differences between patients possible. Furthermore, as CMIs are mainly associated with cognitive impairment, this might suggest that the presence of CMIs gives additional information about the cognitive state of patients with a symptomatic carotid artery stenosis. More research is needed to evaluate this hypothesis and to clarify whether surgical or medical treatment of these patients prevents increasing prevalence of CMIs and thus further development of cognitive impairment.

Although this is the first study that describes in vivo visualization of CMIs in a group of patients with extensive extracranial atherosclerosis at 7.0 T, the current study has also limitations. First of all, it is a series of highly selected patients. As performing 7.0 T MRI with metallic implants is still restricted, the included patients might have been the more vital patients within this series of patients. Nevertheless, for future studies, this might be less of an issue, as recent literature confirms that not all metallic implants should be considered as a major contraindication for 7.0 T MRI.[18] Second, the current study is performed in a non-consecutive small group of patients with a symptomatic, high-grade stenosis. To validate the clinical benefit of visualizing CMIs more extensive research is warranted with asymptomatic patients, patients with a lower stenosis grade and healthy volunteers. Besides a head-tohead comparison with 3.0 T MRI is needed to explore the optimal clinical applicability.

Previous studies have shown that surgical treatment in the form of CEA is preferred over conservative treatment in patients with a symptomatic carotid artery stenosis of >70% and moderately beneficial for patients with a symptomatic carotid artery stenosis of >50%.[19–22] Outcome of these studies was a clinical cerebrovascular event, whether visible on computer tomography (CT) or not. As CMIs are too small to visualize on CT, they were not taken into account in this setting. Thereby, in previous studies, CMIs are mainly related to global cognitive impairment and not to acute symptoms.[11] In the current study, no correlation was found between the stenosis grade and the visible CMIs (Table 2). This could be explained by the small range of stenosis grades in the current study because only patients with a high-grade symptomatic carotid artery stenosis are included. Although CMIs are seen with a similar pattern as macroifarcts, the clinical value of CMIs for risk stratification of patients with carotid artery atherosclerosis remains unknown.

In conclusion, the current study shows that in symptomatic patients with significant extracranial carotid artery stenosis, CMIs also impress as a relevant part of the total cerebrovascular burden and these CMIs prevail with a similar pattern as observed macroinfarcts. Assessment of this technique is needed in asymptomatic patients, patients with a lower stenosis grade, and healthy volunteers to explore and to validate the clinical benefit of visualizing cortical microinfarcts in these patients.

References

1. Rothwell PM, Eliasziw M, Gutnikov SA, et al. Endarterectomy for symptomatic carotid stenosis in relation to clinical subgroups and timing of surgery. Lancet 2004; 363: 915–924.
2. Rothwell PM, Gibson R, Warlow CP. Interrelation between plaque surface morphology and degree of stenosis on carotid angiograms and the risk of ischemic stroke in patients with symptomatic carotid stenosis. On behalf of the European Carotid Surgery Trialists' Collaborative Group. Stroke 2000; 31: 615–621.
3. Saam T, Hetterich H, Hoffmann V, et al, Poppert H et al. Metaanalysis and systematic review of the predictive value of carotid plaque hemorrhage on cerebrovascular events by magnetic resonance imaging. J Am Coll Cardiol 2013; 62: 1081–1091.
4. Hosseini AA, Kandiyil N, Macsweeney ST, et al. Carotid plaque hemorrhage on magnetic resonance imaging strongly predicts recurrent ischemia and stroke. Ann Neurol 2013; 73: 774–784.
5. Gupta A, Baradaran H, Schweitzer AD, et al. Carotid plaque MRI and stroke risk: a systematic review and meta-analysis. Stroke 2013; 44: 3071–3077.
6. Howard DP, van Lammeren GW, Redgrave JN, et al. Histological features of carotid plaque in patients with ocular ischemia versus cerebral events. Stroke 2013; 44: 734–739.
7. Verhoeven B, Hellings WE, Moll FL, et al. Carotid atherosclerotic plaques in patients with transient ischemic attacks and stroke have unstable characteristics compared with plaques in asymptomatic and amaurosis fugax patients. J Vasc Surg 2005; 42: 1075–1081.
8. Brundel M, de Bresser J, van Dillen JJ, et al. Cerebral microinfarcts: a systematic review of neuropathological studies. J Cereb Blood Flow Metab 2012; 32: 425–436.
9. Ii Y, Maeda M, Kida H, et al. In vivo detection of cortical microinfarcts on ultrahigh-field MRI. J Neuroimaging 2013; 23: 28–32.
10. van Veluw SJ, Zwanenburg JJ, Engelen-Lee J, et al. In vivo detection of cerebral cortical microinfarcts with high-resolution 7T MRI. J Cereb Blood Flow Metab 2013; 33: 322–329.
11. Smith EE, Schneider JA, Wardlaw JM, et al. Cerebral microinfarcts: the invisible lesions. Lancet Neurol 2012; 11: 272–282.
12. den Hartog AG, Bovens SM, Koning W, et al. PLACD-7T study: atherosclerotic carotid plaque components correlated with cerebral damage at 7 Tesla magnetic resonance imaging. Curr Cardiol Rev 2011; 7: 28–34.
13. Visser F, Zwanenburg JJ, Hoogduin JM, et al. High-resolution magnetization-prepared 3D-FLAIR imaging at 7.0 Tesla. Magn Reson Med 2010; 64: 194–202.
14. Zheng L, Vinters HV, Mack WJ, et al. Cerebral atherosclerosis is associated with cystic infarcts and microinfarcts but not Alzheimer pathologic changes. Stroke 2013; 44: 2835–2841.
15. Brayne C, Richardson K, Matthews FE, et al. Neuropathological correlates of dementia in over-80-year-old brain donors from the population-based Cambridge city over-75s cohort (CC75C) study. J Alzheimers Dis 2009; 18: 645–658.
16. Madai VI, von Samson-Himmelstjerna FC, Bauer M, et al. Ultrahigh-field MRI in human ischemic stroke--a 7 tesla study. PLoS One 2012; 7: e37631.
17. Haglund M, Passant U, Sjobeck M, et al. Cerebral amyloid angiopathy and cortical microinfarcts as putative substrates of vascular dementia. Int J Geriatr Psychiatry 2006; 21: 681–687.
18. Wezel J, Kooij BJ, Webb AG. Assessing the MR compatibility of dental retainer wires at 7 Tesla. Magn Reson Med; advance online publication, 11 November 2013; doi:10.1002/mrm.25019.
19. European Carotid Surgery Trialists' Collaborative Group. Randomised trial of

endarterectomy for recently symptomatic carotid stenosis: final results of the MRC European Carotid Surgery Trial (ECST). Lancet 1998; 351: 1379–1387.
20. Barnett HJ, Taylor DW, Eliasziw M, et al. Benefit of carotid endarterectomy in patients with symptomatic moderate or severe stenosis. North American Symptomatic Carotid Endarterectomy Trial Collaborators. N Engl J Med 1998; 339: 1415–1425.
21. Rothwell PM, Gutnikov SA, Warlow CP. Reanalysis of the final results of the European Carotid Surgery Trial. Stroke 2003; 34: 514–523.
22. Rothwell PM, Eliasziw M, Gutnikov SA, et al. Analysis of pooled data from the randomised controlled trials of endarterectomy for symptomatic carotid stenosis. Lancet 2003; 361: 107–116.

Part II

High resolution MRI in patients with Cushing's disease

Chapter 7

Feasibility of high resolution pituitary MRI at 7.0 T

AAJ de Rotte, AG van der Kolk, DR Rutgers,
PMJ Zelissen, F Visser, PR Luijten, J Hendrikse

European Radiology. 2014;24:2005-2011

Abstract

Background and purpose:

Since the pituitary gland measures 3 - 8 mm, imaging with the highest possible spatial resolution is important for the detection of even smaller lesions such as those seen in Cushing's disease. In the current feasibility study, we tested a multi-sequence MRI protocol to visualize the pituitary gland in high resolution at 7.0 Tesla (T).

Methods:

Ten healthy volunteers were examined with a 7.0 T pituitary gland protocol. The protocol consisted of a T_1 weighted magnetization-prepared inversion recovery (MPIR) turbo spin echo (TSE) sequence and a T_2 weighted TSE sequence. Additionally, this protocol was tested in five patients with clinical and biochemical suspicion of a microadenoma.

Results:

The dedicated protocol was successful in visualizing normal pituitary anatomy. At 7.0 T compared to 1.5 T, four times asmany slices covered the pituitary gland in sagittal and coronal direction. In three patients, a lesion was diagnosed at 7.0 T, and was confirmed by histopathology to be a microadenoma.

Conclusion:

Head-to-head comparisons of 7.0 T with 1.5 T and 3.0 T are needed with larger samples of patients and with imaging times feasible for clinical settings. However, the current study suggests that high resolution 7.0 T MRI of the pituitary gland may provide new perspectives when used as a second-line diagnostic examination in the specific context of Cushing's disease.

Introduction

Magnetic Resonance Imaging (MRI), with its superior soft tissue contrast, is the preferred modality for visualization of the pituitary gland.[1,2] This imaging technique is able to achieve high contrast-to-noise ratio (CNR), even without the use of contrast agents, for normal anatomy as well as pathological lesions.[3–6] High-resolution imaging of the pituitary gland is necessary for pathologies such as Cushing's disease due to the presence of small microadenomas measuring less than 6 mm in the majority of cases.[7]

In clinical settings, 1.5 Tesla (T) MRI is commonly used for pituitary imaging. However, very small microadenomas often remain undetected with this standard low-field-strength MRI system due to the low spatial resolution that can be gained within reasonable examination time.[8] Furthermore, partial volume effects of the surrounding structures may result in false-positive diagnosis of microadenomas when using low-resolution MR imaging of the pituitary gland.

Higher-field-strength MRI systems – for instance, 3.0 T or 7.0 T – significantly improve the image quality as a result of higher attainable signal-to-noise ratio (SNR).[4,5,9–14] However, there are several negative consequences associated with higher magnetic field strength.[11,12] Because the pituitary gland is located in close proximity to the sphenoid sinus, susceptibility effects may pose a problem due to the airbrain interface. Furthermore, the relaxivity of gadoliniumbased contrast agents is lower with increased field strength.[15] The combination of prolonged T_1-values and the fast uptake and washout of gadolinium in the pituitary gland may affect the image contrast. Notwithstanding these effects, a series of studies has shown that high field strength MR imaging at 3.0 T is superior for detection of suspected pituitary gland pathology.[4,5,8,12–14] MR imaging at 7.0 T remains challenging, however, as the issues associated with the higher field strength may be even more pronounced. Additionally, safety test data for metallic implants at this strength are limited, resulting in most metallic implants being considered as a major contraindication for ultrahigh-field-strength MRI.

The aim of this study was to investigate whether it is feasible to visualize the pituitary gland with MRI at the ultrahigh field strength of 7.0 T. For protocol evaluation, 10 healthy volunteers were examined at 7.0 T. In addition, clinical 7.0 T MR images of the pituitary gland of five patients with no clear lesion at 1.5 T were shown.

Methods

Study population

Institutional Review Board (IRB) approval was obtained for this prospective study.

Healthy volunteers with any metallic implant considered as a major contra-indication were excluded. All included volunteers gave written informed consent.

Imaging techniques

Imaging was performed on a 7.0 T whole-body MRI system (Philips Healthcare, Cleveland, OH, USA) with a 32-channel receive-coil and a volume transmit/receive coil for transmission (Nova Medical, Inc., Wilmington, MA, USA). The final protocol consisted of a three-dimensional (3D) magnetization-prepared turbo field-echo (TFE) sequence (duration 8:08 minutes), a 3D T_2 weighted turbo spin echo (TSE) sequence (duration 10:24 minutes), and a 3D T_1 weighted magnetization-prepared inversion recovery (MPIR) TSE sequence (duration 10:40 minutes), each with whole-brain coverage. The latter sequence was based on the MPIR-TSE sequence for vessel wall imaging and imaging of the hippocampal anatomy.[16–18] This MPIR TSE sequence was used because of the low artefacts in the pituitary gland region, which is close to the air in the sphenoid sinus. Total imaging time, including preparation sequences, was approximately 37 minutes. Detailed imaging parameters of all 7.0 T MRI sequences used can be found in Table 1.

Table 1. Imaging parameters of the 7.0 T protocol, used for healthy volunteers and patients. Acquisition in sagittal direction for each sequence

	T_1 TFE	T_1 MPIR-TSE	T_2 TSE
FOV, mm	200 x 250 x 200	250 x 250 x 190	250 x 250 x 190
Acquired resolution, mm	1.0 x 1.0 x 1.0	0.8 x 0.8 x 0.8	0.7 x 0.7 x 0.7
Acquired voxel size, mm^3	1.0	0.512	0.343
TR/TI, ms	8/1200	3952/1375	3200/-
TE/equivalent TE, ms	1.97/-	37/19	300/58
Flip angle, degrees	8	150	120
TFE/TSE-factor	140	158	182
NSA	1	2	2
SENSE factor (AP x RL)	2 x 3	2 x 3	2 x 2.8
Duration (min:sec)	8:08	10:40	10:24

Image analysis

Images of the healthy volunteers were processed on an offline workstation (Philips). Coronal, axial, and sagittal reconstructions were made of all obtained sequences; care was taken to use identical angulations with all of the sequences for each individual volunteer. Slice thickness was based on the acquired resolution, and no gap was applied. The images of these final 7.0 T protocol sequences were analysed for image quality and pituitary gland coverage.

Image quality for 10 healthy volunteers was assessed by two observers (JH and AR). In the case of differences in assessment between the two observers, consensus was reached. For each sequence, 10 items were scored[12], divided into three categories. Each item was evaluated according to a four-point scale: 0 = non-diagnostic, 1 = poor, 2 = moderate, and 3 = good. In the first category, 'anatomy,' four items were assessed: a) border between pituitary gland and cavernous sinus, b) border between anterior and posterior pituitary gland, c) visualization of cranial nerves in cavernous sinus, and d) visualization of optic nerve. The second category, 'artefacts,' comprised four items: a) susceptibility artefacts, b) pulsation artefacts, c) movement artefacts, and d) B1 inhomogeneity artefacts. In this category, an evaluation of 'good' was assigned when there was no loss of image quality due to the specific type of artefact; conversely 'poor' indicated diminished image quality due to the specific type of artefact. The last category, 'image quality,' consisted of two items: total image quality and diagnostic image for clinical purpose. Mean scores were calculated for these items.

Patient evaluation

Additionally, the protocol dedicated for pituitary gland imaging was tested in five patients in whom a clinical 1.5 T MRI of the pituitary gland was not sufficient to diagnose a highly expected microadenoma. A post-contrast T_1 TFE and T_1 MPIR TSE sequence after administration of 0.1 mL/kg of a gadoliniumcontaining contrast agent (gadobutrol/Gadovist 1.0 mmol/mL, Bayer Schering Pharma, Newbury, UK) was added to the protocol in all patients. The 1.5 T and 7.0 T MR images of these five patients were retrospectively evaluated by a single observer (JH). On both field strengths, diagnosis of a visible lesion was based on the combination of sequences.

IRB approval was obtained for 7.0 T MRI for clinical purposes in the event that the better differentiating capacity of 7.0 T MRI would lead to more accurate diagnosis. Approval was based on the FDA consideration that a magnetic resonance diagnostic device up to a field strength of 8.0 Tesla is of non-significant risk in adults, children, and infants >1 month of age. (http://www. f d a . g o v / d o w n l o a d s / M e d i c a l D e v i c e s /DeviceRegulationandGuidance/GuidanceDocuments/UCM072688.pdf).

Coverage analysis

For both healthy volunteers and patients, the sequences performed at 7.0 T were analysed for pituitary gland coverage. These results were compared with the pituitary gland coverage on 1.5 T images of the patients in order to assess differences in potential partial volume effects. Coverage was assessed by counting the number of slices covering the pituitary gland, which was performed in all three directions. An increase in the number of slices covering the pituitary gland suggested a lower potential of partial volume effects.

Results

Study population

The mean age of 10 included healthy volunteers (4 males) was 25 years (range 19–28 years).

Image analysis

Results of quality analysis can be found in Table 2. The T_1 MPIR TSE and T_2 TSE sequence scored superior in anatomy, artefacts, and image quality. Figure 1 provides an overview of the 7.0 T MR images obtained in a healthy volunteer, which demonstrate highresolution and highly detailed images with an overall good quality of the T_2 TSE sequence and the T_1 MPIR TSE sequence. Due to susceptibility artefacts, the overall image quality of the T_1 TFE sequence was poor. This effect was visible in 9 of 10 healthy volunteers.

Patient evaluation

An overview of all patients is provided in Table 3. In four of the five patients, a small hyperintense lesion suggestive of a microadenoma was visible on the 7.0 T images of the pituitary gland (Figure 2). All four patients underwent surgery. A lesion was found in three of these patients, and was confirmed by histopathological examination to be an adrenocorticotropic hormone (ACTH)-producing microadenoma. The fourth patient was treated in another hospital, where the 7.0 T MR images were not available. Blind surgery yielded no resection of the expected microadenoma, and the patient still suffers from Cushing's disease. In the absence of follow-up imaging, we are not able to determine whether the visualized lesion is still present.

Coverage analysis

Results of the pituitary gland coverage are shown in Table 2. The coverage at 7.0 T was 16 (range 13–19), 12 (range 9–15), and 7 (range 6–9) slices in sagittal,

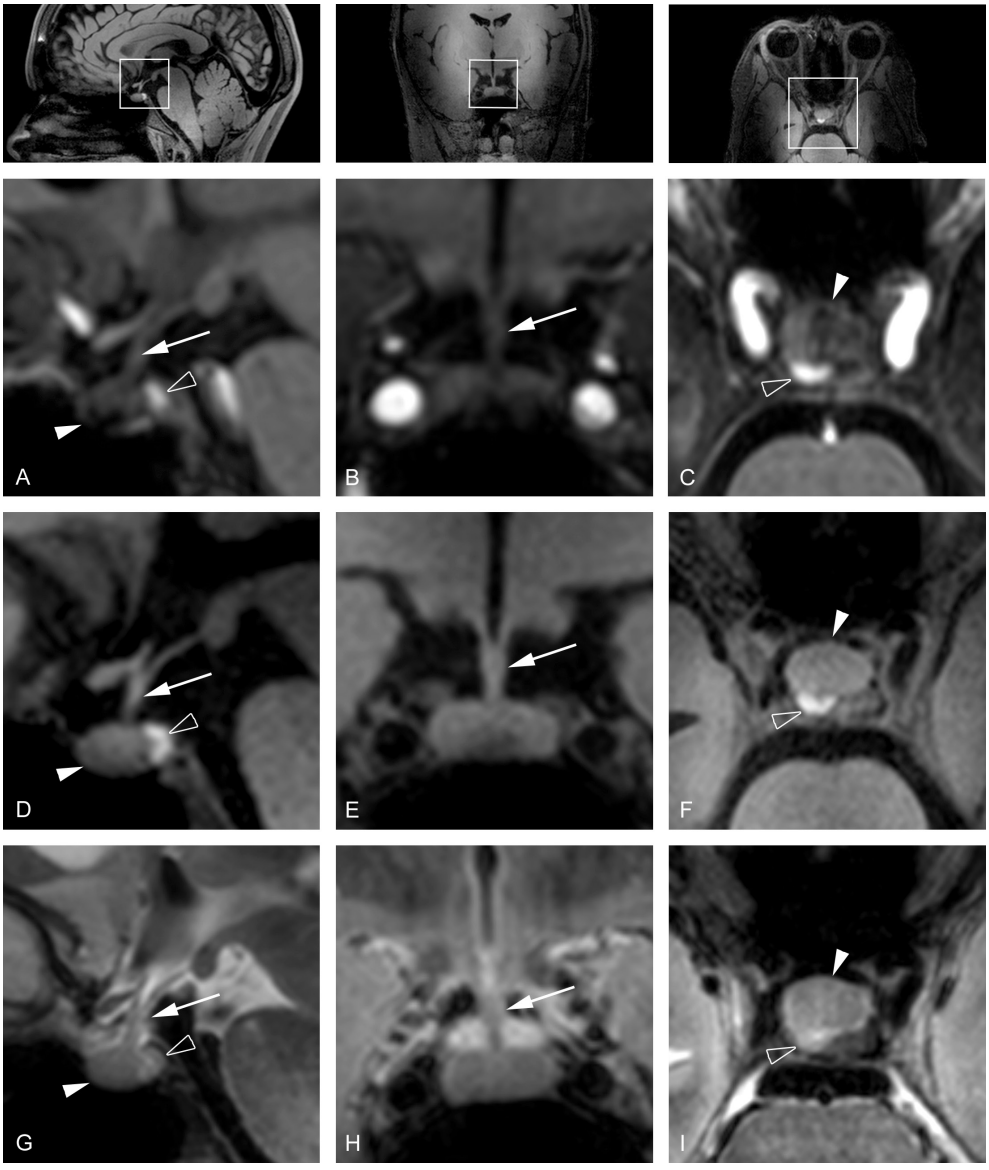

Figure 1. All obtained 7.0 T MR images of a 26-year-old healthy volunteer, consisting of a T_1 TFE sequence (a, b, c), T_1 MPIR TSE sequence (d, e, f) and T_2 TSE sequence (g, h, i) in sagittal (a, d, g), coronal (b, e, h) and transversal (c, f, i) direction, showing the anterior (white arrowhead) and posterior pituitary gland (open arrowhead) as well as the pituitary stalk (white arrow)

coronal, and transversal direction, respectively. In comparison, the pituitary gland coverage on 1.5 T MRI on average was 4 (range 3 - 5) slices in sagittal direction and 3 (range 2 - 4) slices in coronal direction.

Table 2. Qualitative scores

	T_1 TFE	T_1 MPIR TSE	T_2 TSE
Anatomy			
Border pituitary gland - cavernous sinus	0.2 (0 - 2)	2.9 (2 - 3)	3.0 (3)
Border anterior - posterior pituitary gland	1.4 (0 - 3)	3.0 (3)	1.8 (0 - 3)
Visualization cranial nerves	1.3 (0 - 2)	2.4 (1 - 3)	1.3 (0 - 3)
Visualization optic nerve	1.6 (0 - 3)	2.6 (1 - 3)	2.4 (1 - 3)
Artefacts			
Susceptibility effects	0.3 (0 - 2)	2.7 (1 - 3)	2.6 (1 - 3)
Pulsation artefacts	3.0 (3)	3.0 (3)	3.0 (3)
Movement artefacts	2.9 (2 - 3)	2.8 (1 - 3)	3.0 (3)
B1 inhomogeneity artefacts	3.0 (3)	3.0 (3)	3.0 (3)
Overal image quality			
Total image quality	0.7 (0 - 3)	2.9 (2 - 3)	2.8 (2 - 3)
Diagnostic for clinical purpose	0.7 (0 - 3)	3.0 (3)	2.9 (2 - 3)

Scores according to 10 items, divided into three categories: anatomy, artefacts, overall image quality. Each item was evaluated according to a four-point scale consisting of 0 = non-diagnostic, 1 = poor, 2 = moderate, and 3 = good; TFE, turbo field echo;MPIR-TSE magnetization-prepared inversion recovery turbo spin-echo

Figure 2. T_2 TSE sequence and T_1 MPIR TSE sequence before and after contrast administration at 7.0 T MRI of a 42-year-old male (a), a 44-year-old female (b), a 40-yearold female (c) and a 14-year-old girl with MEN-1 syndrome, (d). All patients suffered from clinical symptoms suspected for Cushing's disease, and biochemical tests proved an ACTH-producing pituitary adenoma. Arrowheads point to the suspected lesion at these 7.0 T images. Histopathological examination confirmed the lesions of patient A and patient C to be an ACTH-producing microadenoma. The lesion in patient D was confirmed to be a prolactin-producing lesion. A second, smaller lesion in this patient was confirmed to be an ACTH-producing microadenoma

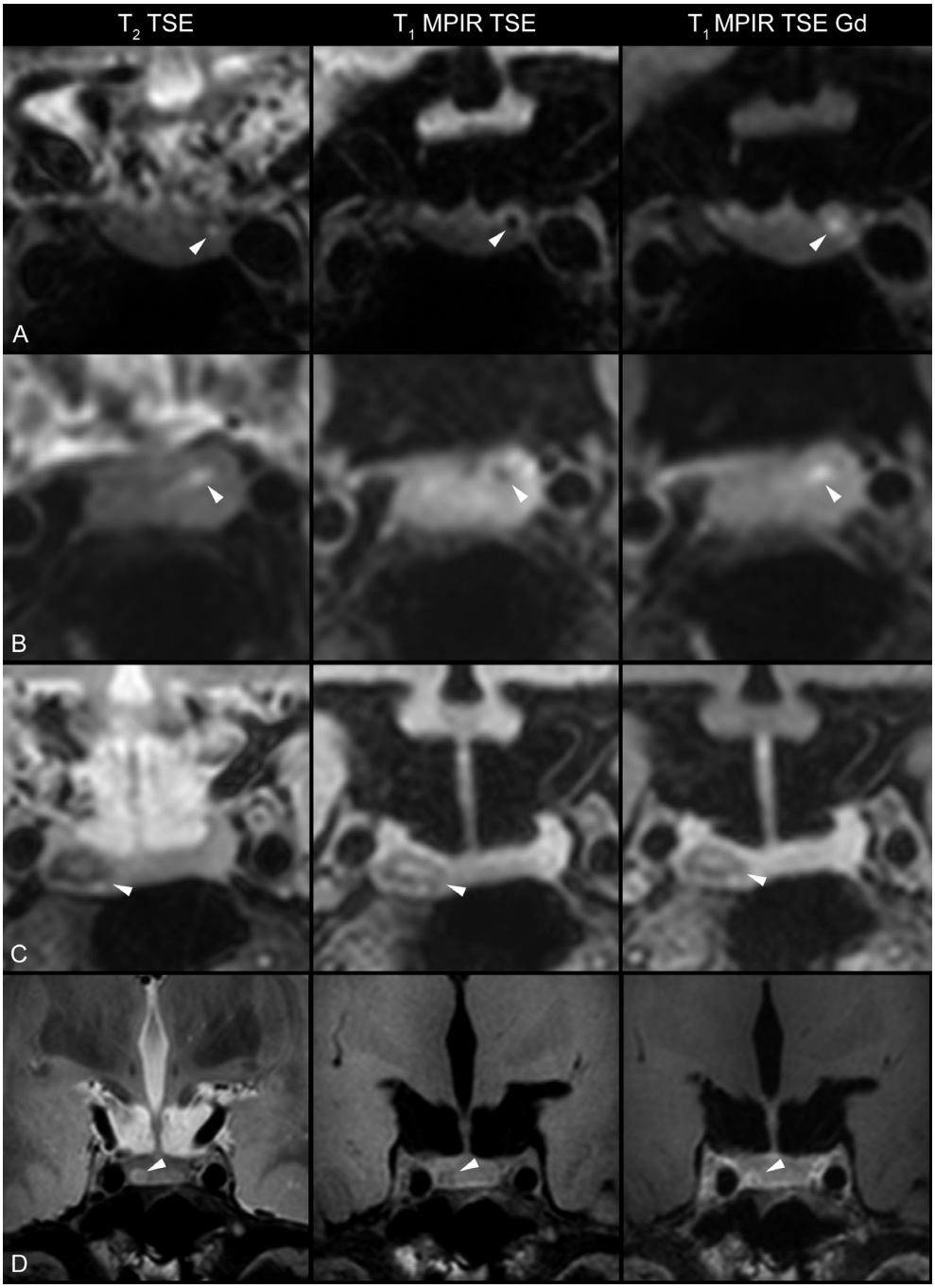
T2 TSE
T1 MPIR TSE
T1 MPIR TSE Gd
A
B
C
D

Discussion

We have shown that ultra-high field strength MRI of 7.0 T is feasible for imaging of the pituitary gland with high spatial resolution. Qualitative good high-resolution images of the pituitary gland can be obtained with a protocol consisting of a T_1 MPIR TSE sequence and a T_2 TSE sequence. Furthermore, in two patients, lesions that could not be diagnosed on the clinical 1.5 T MRI pituitary images were detected at 7.0 T MRI and confirmed with histopathology.

While this study suggests advantages in the use of ultra-high field strength MRI for imaging of the pituitary gland, there are several limiting factors. First, safety test data are limited for metallic implants at 7.0 T. In practice, this restricts the ability to perform 7.0 T MRI in most patients with postoperative status. However, although the procedure is currently contraindicated in patients with stents and other metallic implants, recent studies confirm that not all metallic implants should be considered as major contraindications for ultra-high field strength MRI.[19] In addition, patients with a pituitary microadenoma are typically young, and the presence of metallic implants is less common.

Second, issues such as longer T_1 values, sensitivity for pituitary enhancement, specific absorption rate (SAR) limitations, magnetic susceptibility artefacts around the air regions (sphenoid sinus) where the pituitary gland is located, and B0/B1 field heterogeneities are hurdles that must be dealt with at 7.0 T, as the pituitary gland is located deep in the middle of the skull and in close proximity to air in the sphenoid sinus. However, the T_1 MPIR TSE and T_2 weighted imaging methods that have been developed address these technical constraints and are able to provide images of the pituitary gland with limited amounts of artefacts. Since the pituitary gland is located in the middle of the head, the B0/B1 field heterogeneities were a minor issue with respect to the image quality of the pituitary gland itself. Susceptibility, meanwhile, was a more disturbing artefact due to the location of the pituitary gland close to the sphenoid sinus. Nevertheless, this effect does not result in overall non-diagnostic image quality of the T_1 MPIR TSE sequence. Another limiting artefact was movement. Due to the high spatial resolution, in combination with the relatively long duration of the sequences, the smallest movement can cause disturbing artefacts. The examination duration of the T_1 MPIR TSE sequence is approximately 10 minutes, which is more than twice that of a standard clinical T_1 TSE sequence at 1.5 T. However, in view of partial volume effects, it is important to acquire as many slices covering the pituitary gland as possible.

The third limitation is the rather small group of subjects who were evaluated and the lack of comparison with 3.0 T MR imaging, since the current study is a feasibility study of pituitary gland imaging at 7.0 T. While 1.5 T MRI is still the most common in

pituitary gland imaging, high field MRI of 3.0 T has been successfully described.[4,5,8,12–14] These studies demonstrate the superiority of 3.0 T over 1.5 T MR imaging for detection of suspected pituitary gland pathology. Since 3.0 T MRI is more widely available, future studies are warranted in which head-to-head comparisons of 1.5 T, 3.0 T, and 7.0 T, including pathological confirmation, are performed in larger groups of patients in order to assess actual clinical added value.[4,5,8,12]

Finally, while a lesion visible at 7.0 T MR images in two patients with Cushing's disease was confirmed by histopathology to be an ACTH-producing microadenoma, the higher spatial resolution of this pituitary gland MRI protocol will also increase the risk of finding incidentalomas. We know from previous studies that incidentalomas in the pituitary gland are present in approximately 20% of patients.[20] Therefore, it is possible that high-resolution imaging as proposed in the current study may be indicated only for selected patients with a high suspicion of pituitary microadenomas that cannot be visualized on lower- ield strength MRI.

Interestingly, on the T_1 MPIR TSE sequence, the pituitary gland lesions visualized in this study had a higher intensity compared to the surrounding pituitary gland after contrast administration. Classically, on lower field strengths, the majority ofmicroadenomas have a lower intensity than the surrounding pituitary gland on standard post-contrast images. There are several theories that may explain this reversedcontrast

phenomenon with hyperintense lesions. First, the amount of contrast used was the same as that for lowerfield-strength pituitary MR imaging, and it is possible that a

lower dose of contrast is needed when imaging at a higher field strength to produce the same contrast difference.[15] Second, the T_1 MPIR TSE sequence is not purely T_1weighted. A shine-through effect of the contrast agent's T_2* relaxation time may have changed the relative contrast in the images of the pituitary gland lesions. Finally, it is likely that the washout phase had already begun in the 7.0 T protocol due to differences in timing of imaging after contrast administration with the long (10: 40 minutes) post-contrast acquisition of the T_1 MPIR TSE sequence. More extensive research is needed to definitively identify the reason for this phenomenon.

In conclusion, normal anatomy of the pituitary gland can be depicted with a protocol consisting of a T_1 MPIR TSE sequence and a T_2 TSE sequence at 7.0 T MRI. The protocol dedicated for identification of normal pituitary anatomy also succeeded in identifying micropathology. In future studies, head-to-head comparisons of 7.0 T with 1.5 T and 3.0 T are needed with larger samples of patient and with imaging times feasible for clinical settings. However, the current study suggests that high-resolution 7.0 T MRI of the pituitary gland may provide new perspectives when used as a second-line diagnostic examination in the specific context of Cushing's disease.

Reference

1. Escourolle H, Abecassis JP, Bertagna X et al. (1993) Comparison of computerized tomography and magnetic resonance imaging for the examination of the pituitary gland in patients with Cushing's disease. Clin Endocrinol (Oxf) 39:307–313
2. Dwyer AJ, Frank JA, Doppman JL et al. (1987) Pituitary adenomas in patients with Cushing disease: initial experience with Gd-DTPAenhanced MR imaging. Radiology 163:421–426
3. Shah S, Waldman AD, Mehta A. Advances in pituitary imaging technology and future prospects. Best Pract Res Clin Endocrinol Metab 2012, 26:35–46
4. Kim LJ, Lekovic GP, White WL, et al. Preliminary experience with 3-Tesla MRI and Cushing's disease. Skull Base 2007, 17:273–277
5. Wolfsberger S, Ba-Ssalamah A, Pinker K et al. Application of three-tesla magnetic resonance imaging for diagnosis and surgery of sellar lesions. J Neurosurg 2004, 100:278–286
6. Plewes DB, Kucharczyk W Physics ofMRI: a primer. J Magn Reson Imaging 2012, 35:1038–1054
7. Newell-Price J, Trainer P, Besser M, et al. The diagnosis and differential diagnosis of Cushing's syndrome and pseudo-Cushing's states. Endocr Rev 1998, 19:647–672
8. Pinker K, Ba-Ssalamah A, Wolfsberger S, et al. The value of high-fieldMRI (3 T) in the assessment of sellar lesions. Eur J Radiol 2005, 54:327–334
9. Runge VM, Patel MC, Baumann SS et al. T1-weighted imaging of the brain at 3 tesla using a 2-dimensional spoiled gradient echo technique. Invest Radiol 2006, 41:68–75
10. Krautmacher C, Willinek WA, Tschampa HJ et al. Brain tumors: full- and half-dose contrast-enhanced MR imaging at 3.0 T compared with 1.5 T–Initial Experience. Radiology 2005, 237:1014–1019
11. SasakiM, Inoue T, TohyamaK, et al. High-field MRI of the central nervous system: current approaches to clinical and microscopic imaging. Magn Reson Med Sci 2003, 2:133–139
12. Kakite S, Fujii S, Kurosaki M et al. Three-dimensional gradient echo versus spin echo sequence in contrast-enhanced imaging of the pituitary gland at 3 T. Eur J Radiol 2011, 79:108–112
13. Erickson D, Erickson B, Watson R et al. 3 Tesla magnetic resonance imaging with and without corticotropin releasing hormone stimulation for the detection of microadenomas in Cushing's syndrome. Clin Endocrinol (Oxf) 2010, 72:793–799
14. Stobo DB, Lindsay RS, Connell JM, et al. Initial experience of 3 Tesla versus conventional field strength magnetic resonance imaging of small functioning pituitary tumours. Clin Endocrinol (Oxf) 2011, 75:673–677
15. Soher BJ, Dale BM,Merkle EM. A review of MR physics: 3 T versus 1.5 T. Magn Reson Imaging Clin N Am 2007, 15:277–290
16. van der Kolk AG, Zwanenburg JJ, Brundel M et al. Intracranial vessel wall imaging at 7.0-T MRI. Stroke 2011, 42:2478–2484
17. van der Kolk AG, Hendrikse J, Brundel M et al. Multisequence whole-brain intracranial vessel wall imaging at 7.0 tesla. Eur Radiol 2013, 23:2996–3004
18. Wisse LE, Gerritsen L, Zwanenburg JJ et al. Subfields of the hippocampal formation at 7 T MRI: in vivo volumetric assessment. Neuroimage 2012, 61:1043–1049
19. Wezel J, Kooij BJ,Webb AG. Assessing the MR compatibility of dental retainer wires at 7 Tesla. Magn Reson Med 2013 72: 1191-1198
20. Scangas GA, Laws ER Jr Pituitary incidentalomas. Pituitary 2014 17: 486-491

Chapter 8

High resolution pituitary MRI at 7.0 T: a clinical evaluation in Cushing's disease

AAJ de Rotte, A Groenewegen, DR Rutgers, ThD Witkamp, PMJ Zelissen, FJA Meijer, EJ van Lindert, A Hermus, PR Luijten, J Hendrikse

Under revision European Radiology

Abstract

Background and purpose:

Aim of the current retrospective study is to evaluate the detection of pituitary lesions with high resolution pituitary gland imaging at 7.0 T compared to 1.5 T MRI in patients with clinically and biochemically proven Cushing's disease.

Methods:

Data of 16 patients was evaluated. In 7 patients no lesion was visible on the initial 1.5 T MRI and in 9 patients an unclear lesion was visible. Firstly, two readers assessed the 1.5 T MRI and the 7.0 T MRI scans unpaired in a random order for the presence of lesions. Consensus reading with a third neuroradiologist was used to define final lesions in all MRI scans. Secondly, surgical outcome was evaluated by clinical remission and morning serum cortisol in the week after surgery. A comparison was made between the lesions visualized with MRI and the lesions found during surgery.

Results:

The probability adjusted interobserver agreement for lesion detection was good at 1.5 T MRI scans ($\kappa = 0.69$) and 7.0 T MRI scans ($\kappa = 0.62$). In 5 patients both the 1.5 T and 7.0 T MRI enabled to visualize a lesion on the correct side of the pituitary gland. In 3 patients 7.0 T MRI visualized a lesion on the correct side of the pituitary gland, while no lesion was visible at 1.5 T MRI.

Conclusion:

The interobserver agreement of image assessment for 7.0 T MRI in patients with Cushing's disease was good and lesions were detected more accurately with 7.0 T MRI.

Introduction

Endogenous Cushing's syndrome is a clinical condition in which the adrenal glands secrete excessive amounts of cortisol. In Cushing's disease, which is responsible for 80-85% of adrenocorticotrophic hormone (ACTH)-dependent Cushing's syndrome, an ACTH producing adenoma located in the pituitary gland stimulates the adrenal glands to secrete the excessive amounts of cortisol.[1] In the majority of cases these adenomas are small microadenomas, challenging to diagnose.[2] Therefore, final diagnosis is often based on central venous sampling and magnetic resonance imaging (MRI).[3] In case a pituitary origin of Cushing's syndrome is confirmed, treatment of choice is surgical removal of the lesion, for which visualization of the lesion is crucial.[4-6] Consequently, it is important to visualize the pituitary gland with the highest possible spatial resolution, which enables correct delineation of small anatomical structures and pathological lesions.

In routine clinical practice, MRI is the preferred imaging technique, since MRI enables to attain the highest spatial resolution, signal to noise ratio (SNR), and contrast to noise ratio (CNR) of the pituitary gland.[7,8] MRI at a field strength of 1.5 Tesla (T) is most commonly used, but pituitary microadenomas remain undetected in 36 - 63% of patients at this field strength.[9-13] The higher attainable SNR and spatial resolution at higher field strengths – for instance 3.0 T or 7.0 T – theoretically has the potential to significantly improve the tumor detection rate.[14,15]

Recently, a high resolution 7.0 T pituitary gland MRI protocol, with a 0.8 mm isotropic voxelsize, has been presented.[16] Feasibility was demonstrated in healthy control subjects and case examples of patients with Cushing's disease were given. Aim of the current retrospective study is to evaluate the detection of pituitary lesions with high resolution pituitary gland imaging at 7.0 T compared to 1.5 T MRI in patients with clinically and biochemically proven Cushing's disease with inconclusive lesions localization at 1.5 T MRI.

Methods

Subjects

Between January 2012 and July 2014 16 patients with clinically and biochemically proven Cushing's disease underwent 7.0 T MRI in the University Medical Center Utrecht. Patients were referred to Utrecht in case the standard 1.5 T MRI was inconclusive for the detection of an adenoma. An inconclusive diagnosis was defined as no pathologies visible or as an unclear lesion visible which both needed further investigation. The

institutional review board (IRB) of the University Medical Center Utrecht approved imaging at 7.0 T MRI for clinical purposes in case lower field strength MRI was inconclusive for diagnosis. All patients gave written informed consent. The Radboud University Medical Center referred 9 patients to Utrecht and the remaining 8 patients were patients from the University Medical Center Utrecht. IRB approval was obtained in both university medical centers to evaluate retrospectively the clinical information and 1.5 T and 7.0 T MR images of all patients. Data of five patients was previously published as part of clinical case examples of the high resolution pituitary protocol.(16)

Clinical evaluation

A pituitary origin of ACTH-dependent Cushing's syndrome was established by biochemical tests, including inferior petrosal sinus sampling (IPSS). A detailed description of these tests, used for diagnosis, is given in the supplementary material.

Magnetic Resonance Imaging

Initial imaging of all patients was performed on 1.5 T MRI scanners, using a local clinical protocol for depicting the pituitary gland. The protocol consisted of a pre- and post-contrast T_1 weighted turbo spin echo (TSE) sequence, a dynamic T_1 weighted TSE sequence and a T_2 weighted TSE sequence.

Note that 5 patients were referred from peripheral hospitals. In all patients the MRI scan from the peripheral hospital was of good quality and consequently used for the current retrospective analysis. In 6 patients the dynamic T_1 TSE sequence was lacking in the protocol. Besides, in 6 patients a proton density weighted sequence and in 2 patients a diffusion weighted sequence was added to the protocol.

All 7.0 T MRI scans were performed on a 7.0 T whole-body MRI system (Philips Healthcare, Cleveland, OH, USA) with a 32-channel receive-coil and a volume transmit/receive coil (Nova Medical, Inc., Wilmington, MA, USA). The imaging protocol was similar to the dedicated imaging protocol previously described.[16] Briefly, the protocol consisted of a three-dimensional (3D) T_2 weighted TSE sequence and a 3D T_1 weighted magnetization-prepared inversion recovery (MPIR) TSE sequence before and after contrast administration. A single dose, 0.1 mL/kg, gadolinium based contrast agent was used. Post-contrast imaging was started approximately 2 minutes after contrast injection. A dynamic contrast enhanced sequence was not performed.

Image analysis

Firstly, the images were evaluated by two experienced neuro-radiologists (ThW and DR) with 25 and 8 years' experience, respectively. All 1.5 T and 7.0 T scans were presented to the observers, unpaired and in a random order. Images were evaluated

for the presence and number of lesions in the pituitary gland and the precise location of all identified lesions. Secondly, consensus reading with a third neuro-radiologist (JH), with 10 years' experience, was used to evaluate the differences between both first observers and to make a final decision for every MRI scan. All observers were masked for patient characteristics, clinical and biochemical data and the initial MRI diagnoses. However, they were not masked for the diagnosis Cushing's disease.

Interobserver agreement for the presence of lesions was evaluated with Cohen's kappa coefficient. The kappa ranged from 0 (no agreement) to 1 (perfect agreement) and was divided in the following 5 categories: <0.20 (poor), 0.21 to 0.40 (fair), 0.41 to 0.60 (moderate), 0.61 to 0.80 (good) and 0.81 to 1.00 (very good). The statistical analysis was performed in IBM SPSS Statistics version 20 (IBM Corporation, Armonk, NY, USA).

Surgery

In case patients underwent surgery, the macroscopic and microscopic outcome of surgery, symptom status after surgery, and morning serum cortisol levels in the first week after surgery were used to evaluate the clinical outcome of surgery. Cure was defined as a morning serum cortisol of <0.14 µmol/L, based on previous published literature or as clinical remission.[17] The final results of 1.5 T MRI and 7.0 T MRI were compared with the surgical outcome. Histopathology was not taken into account for the current analysis because the surgical procedure was not standardized, which might result in a poor correlation between pathological outcome and actual remission.

Results

Subjects

In total, 16 patients underwent 7.0 T MRI of the pituitary gland. In 7 patients no lesion was visible on the initial 1.5 T MRI and in 9 patients an unclear lesion was visible.

Image analysis

There was absolute agreement between both observers for the results of 1.5 T MRI scans in 11 patients. In 5 patients both observers scored the 1.5 T MRI as no pathologies and in 6 patients both observers identified 1 identical lesion (n = 4) or 2 identical lesions (n = 2). In the remaining 5 patients one observer identified a lesion whereas the other observer did not (n = 1); both observers identified 1 identical lesion and only one observer identified a second lesion (n = 2); or a lesion in the right side of the pituitary gland was identified by one observer and a lesion in the left side of the pituitary gland was identified by the second observer (n = 2).

There was absolute agreement between both observers for the results of 7.0 T MRI scans in 10 patients. In 1 patient both observers scored the 7.0 T MRI as no pathologies and in 9 patients both observers identified 1 identical lesion (n = 6), or 2 identical lesions (n = 3). In the remaining 6 patients one observer identified a lesion whereas the other did not (n= 5) or both observers identified 1 identical lesion and only one observer identified a second lesion (n = 1). The probability adjusted interobserver agreement was good for 1.5 T MRI (κ = 0.69) and for 7.0 T MRI (κ = 0.62). The results were presented in Table 1, including the initial diagnosis on 1.5 T MRI.

After consensus reading, 13 lesions, in 9 patients, were identified on 1.5 T MRI scans, compared to 17 lesions, in 13 patients, on 7.0 T MRI. In 3 patients 2 lesions

Table 1. Patient overview with MRI results after consensus

Patient	Initial diagnosis	Study analysis		Surgery	Morning serum ortisol	Cure[a]
	1.5 T	1.5 T	7.0 T			
1	L	N	L	Unknown[b]	0.02	Yes
2	N	R/L	R/L	R	0.05	Yes
3	R	R	R	R	<0.02	Yes
4	L	L	L	L	<0.02	Yes
5	R	N	N	Both[c]	0.2	Yes
6	R	R	C	R	<0.02	Yes
7	N	N	N	n.a.	n.a.	n.a.
8	N	N	N	n.a.	n.a.	n.a.
9	L	L	L	n.a.	n.a.	n.a.
10	N	N	R/L	R	<0.02	Yes
11	N	N	R	R	<0.02	Yes
12	L/R	L	L/C	Both[c]	0.12	Yes
13	N	N	R	R	0.05	Yes
14	L/R	L	L	Both[c]	0.72	No
15	N	R/L	L	L	0.02	Yes
16	R	R/C	R/C	R	<0.02	Yes

Results are lesions found right (R), left (L) or central (C) in the pituitary gland or no pathologies (N), or a combination of those. n.a. = not applicable, these patients are not operated yet; a) Cure is defined as morning serum cortisol of <0.14 µmol/L or clinical remission; b) From these patients it is unknown from which side of the pituitary gland tissue has been excised; c) from these patients tissue is excised from both sides of the pituitary gland; morning serum cortisol (µmol/L) is determined in the week post-surgery.

were visible on both 1.5 T MRI and 7.0 T MRI. In 2 patients 2 lesions were visible only on 1.5 T MRI (n = 1) or only on 7.0 T MRI (n = 1). Comparison of the 1.5 T and 7.0 T results demonstrated in 10 patients an identical diagnosis on 1.5 T and 7.0 T. In the remaining 6 patients there was discrepancy between 1.5 T and 7.0 T. The exact results are demonstrated in Table 1.

In figure 1 an example is given (patient number 17). Initially no pathologies were identified on 1.5 T MRI. For the current study there was discrepancy between both observers for the 1.5 T MRI, only one observer identified a lesion. On 7.0 T, however, both observers identified this lesion. This case demonstrates that 7.0 T MRI might contribute to a more certain diagnosis.

Surgery

Transsphenoidal endoscopic microadenomectomy was performed in 13 patients and one patient underwent transsphenoidal total hypophysectomy. An overview of the outcome of surgery in all patients is demonstrated in Table 1. In 4 patients both sides of the pituitary gland were explored or the side of exploration was unclearly reported by the neurosurgeon. Since, for a correct correlation with MRI, it is crucial to know from which side a potential microadenoma has been excised during surgery, these 4 patients were not used for further analysis. For the remaining 9 patients, in 7 patients the right side of the pituitary gland was explored and in 2 patients the left side of the pituitary gland was explored. All 9 patients were cured after surgery with a morning serum cortisol level of <0.14 µmol/L after surgery. Exact values are demonstrated in Table 1. In 5 patients both the 1.5 T and 7.0 T MRI enabled to visualize a lesion on the correct side of the pituitary gland. In 3 patients 7.0 T MRI enabled to visualize a lesion on the correct side of the pituitary gland, while no lesion was visible at 1.5 T MRI. In 1 patient only 1.5 T MRI visualized the lesion on the correct side of the pituitary gland. In this patient a different lesion was visualized at 7.0 T MRI.

Discussion

The current study demonstrated that the interobserver agreement for the detection of microadenomas in patients with Cushing's disease is good, both at 1.5 T MRI and 7.0 T MRI. Additionally, in 5 patients 7.0 T enabled to confirm an unclear lesion at 1.5 T and in 3 patients 7.0 T enabled to visualize a lesion not visible at 1.5 T.

Previous literature has demonstrated that with high field strength 3.0 T MRI an increased detection rate of pituitary lesions is achieved compared to standard 1.0 and 1.5 T MRI.[15,18,19] This is important as there is evidence that a precise localization is associated with a more favorable outcome of surgery.[5,20] However, other studies could

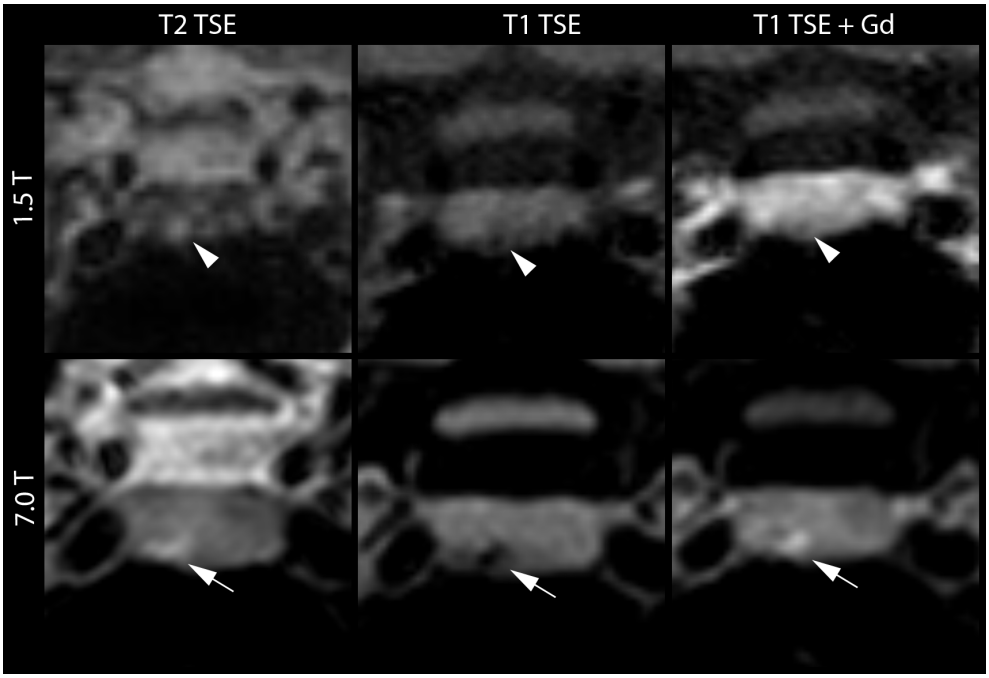

Figure 1. The 1.5 T and 7.0 T MR images of a 56 year-old woman with Cushing's disease. The lesion marked in the 1.5 T images (white arrow head) was identified by only one of the two observers. Note that this lesion was only visible on one slice. After consensus with a third observer the final decision was "no lesions". The lesion marked in the 7.0 T images (white arrow) was identified by both observers.

not demonstrate that the cure rate is higher in patients in whom the lesion is actually visualized before surgery.[4,18,21] Nevertheless, it is obvious that in patients with no visible lesion on MRI, a more extensive surgical procedure is needed.

A high spatial resolution 7.0 T MRI protocol has demonstrated a more detailed visualization of pituitary gland anatomy and promising results for detecting pathology.[16] Furthermore, the current study has demonstrated good interobserver agreement for both 1.5 T MRI and 7.0 T MRI, unless the limited experience with 7.0 T MRI of both observers. Although the initial diagnosis on 1.5 T in all patients was inconclusive in the current study there was absolute agreement for the diagnosis on those images in 11 patients. This high rate of agreement suggests that consensus reading in clinical practice might also confirm inconclusive diagnoses. However, the high spatial resolution of 7.0 T MRI enables to visualize more detail than standard 1.5 T MRI which might result in more visible lesions.

The current study has demonstrated that high resolution 7.0 T MRI indeed enables to visualize more pituitary lesions compared to 1.5 T MRI. In the small series of patients presented, the number of lesions visualized with 7.0 T MRI is higher compared to 1.5 T MRI. In addition, in the majority of cases the additional findings of 7.0 T MRI confirmed the unclear lesion on the initial 1.5 T MRI or enabled to visualize the actual lesion which was not visible at 1.5 T MRI. Consequently, we suggest that the predictive value of lesion detection on 7.0 T MRI is promising. However, it is important to note that with an increasing spatial resolution the chance of false-positive findings – incidentalomas – also increases. Incidentalomas occur in 10-20% of the patients, which potentially results in a higher percentage of false-positive findings with the improved lesion detection rate at higher field strengths.[22,23]

In addition to pituitary lesion detection, also the visualization of the surrounding pituitary anatomy may be used for neurosurgical planning.[14,24-26] Pituitary gland MRI at 3.0 T has demonstrated to improve the evaluation of the parasellar anatomy and the relation of the lesion to the adjacent structures.[14] For example, a clear delineation of the medial wall of the cavernous sinus can be seen only very rarely on 1.5 T MRI, while 3.0 T MRI can usually provide qualitatively good images of this medial border.[14,15] Moreover, 3.0 T MRI provides more detailed visualization of the optic chiasm and of the intracavernous segments of the cranial nerves.[14,15] However, 7.0 T MRI is expected to provide an even more detailed overview of the parasellar anatomy. [27-29] Nevertheless, with the current retrospective analysis it was not possible to evaluate the additional value for the performed surgical procedures.

The current study has several limitations. Firstly, a potentially confounding factor is the selection bias that is introduced by only scanning patients at 7.0 T MRI when the 1.5 T MRI was inconclusive. This means that only the difficult Cushing's disease cases were included in the current study. Thereby, it is important to notice that a conclusive Cushing's disease diagnosis may be challenging even for an experienced neuroradiologists. Secondly, different imaging protocols were used for clinical 1.5 T MRI of the pituitary gland because 1.5 T pituitary imaging was part of routine clinical practice of different referring hospitals. This implies that different vendors of MRI scanners and different scan parameters were used. Furthermore, the clinically acquired sequences were not equal in all patients. Still, we feel that the current study gives a realistic view of what can be expected from standard 1.5 T pituitary gland MRI compared with high resolution MRI at 7.0 T. Thirdly, the reports of the surgical procedure were incomplete in some patients. From these patients it is known whether they were cured after surgery or not. However, it remains unknown from which side of the pituitary gland the microadenoma was removed, which hindered a comparison between MRI and surgery

in 4 patients. Fourthly, a dedicated dynamic contrast enhanced (DCE) sequence was lacking in the current 7.0 T MRI protocol, whereas a DCE sequence at 1.5 T MRI was present in 10 patients. Previous literature demonstrates the clinical advantages of DCE imaging in lesion detection in patients with Cushing's disease.[30,31] Addition of a DCE sequence with high spatial resolution might increase the detection rate of the smallest lesions. Therefore, a DCE sequence might increase the interobserver agreement as well. Finally, the current retrospective analysis lacks the involvement of 3.0 T MRI. The improvement in SNR and the better spatial resolution by using 3.0 T MRI appears to establish a clear advantage in the localization of microadenomas and in the presurgical planning in patients suffering from Cushing's disease.[15,19] Still, 3.0 T MRI has not yet supplanted 1.5 T MRI as standard clinical workup for patients with Cushing's disease and a suspected pituitary microadenoma. A large-scale head-to-head comparison of 1.5 T, 3.0 T and 7.0 T MRI with dedicated scanning protocols is needed to evaluate the actual clinical advantages from high spatial resolution MRI in Cushing's disease. A prospective study should include an exact description of the surgical procedure, including the benefit of neurosurgical guidance based on the available detailed MR images.

To conclude, the interobserver agreement of image assessment for 7.0 T MRI in patients with Cushing's disease was good and lesions were detected more accurately with 7.0 T MRI.

References

1. Juszczak A, Grossman A. The management of Cushing's disease - from investigation to treatment. Endokrynol Pol. 2013;64:166-174.
2. Newell-Price J, Trainer P, Besser M, et al. The diagnosis and differential diagnosis of Cushing's syndrome and pseudo-Cushing's states. Endocr Rev. 1998;19:647-672.
3. Potts MB, Shah JK, Molinaro AM, et al. Cavernous and inferior petrosal sinus sampling and dynamic magnetic resonance imaging in the preoperative evaluation of Cushing's disease. Journal of neuro-oncology. 2014;116:593-600.
4. Maio SD, Biswas A, Vezina JL, et al. Pre- and postoperative magnetic resonance imaging appearance of the normal residual pituitary gland following macroadenoma resection: Clinical implications. Surg Neurol Int. 2012;3:67.
5. Witek P, Zielinski G. Predictive value of preoperative magnetic resonance imaging of the pituitary for surgical cure in Cushing's disease. Turk Neurosurg. 2012;22:747-752.
6. Yamada S, Fukuhara N, Nishioka H, et al. Surgical management and outcomes in patients with Cushing disease with negative pituitary magnetic resonance imaging. World Neurosurg. 2012;77:525-532.
7. Escourolle H, Abecassis JP, Bertagna X, et al. Comparison of computerized tomography and magnetic resonance imaging for the examination of the pituitary gland in patients with Cushing's disease. Clin Endocrinol (Oxf). 1993;39:307-313.
8. Guy RL, Benn JJ, Ayers AB, et al. A comparison of CT and MRI in the assessment of the pituitary and parasellar region. Clin Radiol. 1991;43:156-161.
9. Davis WL, Lee JN, King BD, et al. Dynamic contrast-enhanced MR imaging of the pituitary gland with fast spin-echo technique. J Magn Reson Imaging. 1994;4:509-511.
10. Patronas N, Bulakbasi N, Stratakis CA, et al. Spoiled gradient recalled acquisition in the steady state technique is superior to conventional postcontrast spin echo technique for magnetic resonance imaging detection of adrenocorticotropin-secreting pituitary tumors. J Clin Endocrinol Metab. 2003;88:1565-569.
11. Bartynski WS, Lin L. Dynamic and conventional spin-echo MR of pituitary microlesions. AJNR Am J Neuroradiol. 1997;18:965-972.
12. Buchfelder M, Nistor R, Fahlbusch R, et al. The accuracy of CT and MR evaluation of the sella turcica for detection of adrenocorticotropic hormone-secreting adenomas in Cushing disease. AJNR Am J Neuroradiol. 1993;14:1183-1190.
13. Ludecke DK, Flitsch J, Knappe UJ, et al. Cushing's disease: a surgical view. Journal of neuro-oncology. 2001;54:151-166.
14. Wolfsberger S, Ba-Ssalamah A, Pinker K, et al. Application of three-tesla magnetic resonance imaging for diagnosis and surgery of sellar lesions. J Neurosurg. 2004;100:278-286.
15. Pinker K, Ba-Ssalamah A, Wolfsberger S, et al. The value of high-field MRI (3T) in the assessment of sellar lesions. Eur J Radiol. 2005;54:327-334.
16. de Rotte AA, van der Kolk AG, Rutgers D, et al. Feasibility of high-resolution pituitary MRI at 7.0 tesla. Eur Radiol. 2014;24:2005-2011
17. Esposito F, Dusick JR, Cohan P, et al. Clinical review: Early morning cortisol levels as a predictor of remission after transsphenoidal surgery for Cushing's disease. J Clin Endocrinol Metab. 2006;91:7-13.
18. Stobo DB, Lindsay RS, Connell JM, et al. Initial experience of 3 Tesla versus conventional field strength magnetic resonance imaging of small functioning pituitary tumours. Clin Endocrinol (Oxf). 2011;75:673-677.
19. Kim LJ, Lekovic GP, White WL, et al. Preliminary Experience with 3-Tesla MRI and Cushing's Disease. Skull Base. 2007;17:273-277.
20. Bochicchio D, Losa M, Buchfelder M. Factors influencing the immediate and late outcome

of Cushing's disease treated by transsphenoidal surgery: a retrospective study by the European Cushing's Disease Survey Group. J Clin Endocrinol Metab. 1995;80:3114-1120.
21. Salenave S, Gatta B, Pecheur S, et al. Pituitary magnetic resonance imaging findings do not influence surgical outcome in adrenocorticotropin-secreting microadenomas. J Clin Endocrinol Metab. 2004;89:3371-3376.
22. Hall WA, Luciano MG, Doppman JL, et al. Pituitary magnetic resonance imaging in normal human volunteers: occult adenomas in the general population. Ann Intern Med. 1994;120:817-820.
23. Scangas GA, Laws ER, Jr. Pituitary incidentalomas. Pituitary. 2014;17:486-491.
24. Mori Y, Kobayashi T, Shibamoto Y. Stereotactic radiosurgery for metastatic tumors in the pituitary gland and the cavernous sinus. J Neurosurg. 2006;105 Suppl:37-42.
25. Nakazawa H, Shibamoto Y, Tsugawa T, et al. Efficacy of magnetic resonance imaging at 3 T compared with 1.5 T in small pituitary tumors for stereotactic radiosurgery planning. Jpn J Radiol. 2014;32:22-29.
26. Linn J, Peters F, Lummel N, et al. Detailed imaging of the normal anatomy and pathologic conditions of the cavernous region at 3 Tesla using a contrast-enhanced MR angiography. Neuroradiology. 2011;53:947-954.
27. van der Kolk AG, Hendrikse J, Luijten PR. Ultrahigh-field magnetic resonance imaging: the clinical potential for anatomy, pathogenesis, diagnosis, and treatment planning in brain disease. Neuroimaging Clin N Am. 2012;22:343-362, xii.
28. Umutlu L, Ladd ME, Forsting M, et al. 7 Tesla MR imaging: opportunities and challenges. Rofo. 2014;186:121-129.
29. Moser E, Stahlberg F, Ladd ME, et al. 7-T MR--from research to clinical applications? NMR Biomed. 2012;25:695-716.
30. Tabarin A, Laurent F, Catargi B, et al. Comparative evaluation of conventional and dynamic magnetic resonance imaging of the pituitary gland for the diagnosis of Cushing's disease. Clin Endocrinol (Oxf). 1998;49:293-300.
31. Kucharczyk W, Bishop JE, Plewes DB, et al. Detection of pituitary microadenomas: comparison of dynamic keyhole fast spin-echo, unenhanced, and conventional contrast-enhanced MR imaging. AJR Am J Roentgenol. 1994;163:671-679.

Chapter 9

General discussion and summary

General discussion and summary

Imaging is increasingly essential in modern diagnostic medicine. Among the available imaging modalities, MRI is one of the fastest developing imaging techniques. In this thesis different high resolution applications of MRI are presented in patients with ischemic stroke or as well as in patients with Cushing's disease. In the patients with ischemic stroke, MRI is used for both the imaging of the extracranial vasculature (carotid and vertebral arteries), the intracranial vasculature and the brain tissue. In the last decade more advanced MRI of carotid atherosclerosis and plaque is increasingly used for risk assessment of (recurrent) ischemic events. Furthermore, MRI is sensitive for the total burden of ischemic events (both recent and old). In the patients with Cushing's disease detailed pituitary MRI is used to detect microadenomas in the pituitary gland, in order to confirm the diagnosis and to plan surgical treatment. The results from the various studies presented in this thesis as well as the answers to the questions as formulated in the introduction are summarized and discussed here.

Are intraplaque hemorrhage and a thin/ruptured fibrous cap associated with cerebral infarcts on MRI and microembolic signals with transcranial Doppler?

MRI with a field strength of 3.0 T has been demonstrated to be accurate for visualizing plaque components.[1,2] Two plaque components associated with a high-risk of (recurrent) ischemic events are intraplaque hemorrhage (IPH) and a thin/ruptured fibrous cap (TRFC) on top of a lipid core.[3-8] Results in **Chapter 2** and **Chapter 3** demonstrate that the presence of IPH and a TRFC in the stenotic carotid artery are neither related to the presence of infarcts in the flow territory of the symptomatic carotid artery, nor to the microembolic signals (MES) on transcranial Doppler (TCD). Both studies are in contrast to previously published work.[9-11]

Firstly, a significant correlation between plaque components and infarcts on MRI was presented previously.[9-11] In **Chapter 2**, however, the infarcts are visualized with a fluid attenuated inversion recovery (FLAIR) sequence. The infarct volume on FLAIR images has been found to decrease over the time span of one month, but disappearance of infarcts on FLAIR has, to the best of our knowledge, never been reported.[12] Moreover, since the presence of IPH and TRFC also does not change over a time span of one year, it is unlikely that the long time lag between symptoms and imaging would be the explanation for the absent association mentioned above. This unless MRI would enable visualization of different stages of the plaque vulnerability.[8,13-15] The infarcts in the previously published studies, however, were visualized with diffusion weighted imaging (DWI). Consequently, results of these studies are focused on acute

infarcts, since DWI lesions only represent acute infarcts.[16] With FLAIR imaging, however, both old and recent infarcts are visualized. Consequently, the infarcts visualized with FLAIR are not only the infarcts related to the index event, which could explain the absence of a significant correlation, also described by Lindsay et al.[17]

Secondly, a highly significant relation between MES occurrence and the presence of a vulnerable plaque on MRI was presented previously.[11] In contrast to this previously published study, the study presented in **Chapter 3** was performed in patients with a symptomatic low-grade (30 - 69%) stenosis of the carotid artery and in addition a cardiac source of embolism was an exclusion criterion. Besides, the majority of patients in Chapter 3 used lipid-lowering therapy. Those three factors might have resulted in a lower prevalence of MES occurrence.[18-20] Moreover, it is also known that the occurrence of MES decreases over time after symptoms.[21] Since the time between symptoms and imaging in **Chapter 3** was approximately 52 days, this might explain the absence of a significant correlation between MES and the presence of high-risk plaque components as well.

Is it possible to visualize atherosclerotic carotid plaque with 7.0 T MRI?

From the early days of MRI it is known that MRI scanners with a higher magnetic field strength theoretically might enable to obtain images with a higher spatial resolution within acceptable scanning time.[22] In **Chapter 4** we have demonstrated a quantitative comparison of 7.0 T and 3.0 T carotid MRI. An overall improved quality and an increase in SNR of 7.0 T carotid MRI was demonstrated as compared to 3.0 T. The gain in SNR was 2.0 at the average depth of the carotid arteries, which was slightly less than the expected gain factor of 7/3. Theoretically, a lower gain in SNR could be explained by the combination of increased T_1 relaxation time and the decreased T_2 relaxation time at 7.0 T. However, a proton density weighted sequence was used to acquire the SNR maps, therefore the effect of increased T_1 relaxation times and decrease T_2 relaxation times where already excluded in the experiments. Nevertheless, phantom experiments indicated that the high density receive array, used at 7.0 T, caused some loss in SNR due to magnetic coupling effects of the individual coil elements.

Previously published studies have demonstrated that 7.0 T MRI enables to obtain qualitatively good anatomical images, and that these images are indeed accurate for vessel wall determination in healthy volunteers.[23-25] In **Chapter 5** we obtained MR images in a series of patients with a severely stenosed symptomatic carotid arteries one day prior to CEA. In addition, anatomical MR images were obtained with 3.0 T and 7.0 T in 6 healthy volunteers. A quality analysis was performed on all the obtained 3.0 T and 7.0 T anatomical images. Quality assessment was performed by delineating

the outer and inner boarders of the vessel wall. A strong inter- and intra-observer agreement for vessel wall delineation confirmed the previously published results. In addition, the specimens collected during CEA were histopathologically analyzed for vulnerable plaque components. Unfortunately, the absence of a dedicated black-blood sequence for plaque component imaging hampered accurate visualization of the plaque components with MRI. Consequently, a correlation of all plaque components visualized with MRI compared to histology was not possible. Since calcifications have a low proton density and therefore a low signal on proton density weighted sequences this sequence was used as a first validation of the contrast seen at 7.0 T MRI of the carotid arteries. Furthermore, with the currently available hardware setup, it appeared to be difficult to obtain images with a certain consistency in the level of quality.

To conclude, imaging the carotid vessel wall including atherosclerotic plaques is possible at 7.0 T. However, for the actual plaque component imaging a more robust hardware setup is needed and more dedicated sequences for plaque imaging need to be developed. This means that at present 3.0 T MRI is still superior over 7.0 T MRI in atherosclerotic plaque component imaging.

Are cortical microinfarcts related to macroinfarcts in patients with extracranial atherosclerosis?

Recently published work has demonstrated that cortical infarcts as small as 1.67 mm in length can be visualized with standard clinical MRI scanners with a field strength up to 3.0 T.[26] Nevertheless, ultra-high field strength scanners with a field strength of 7.0 T enable to visualize even smaller cortical microinfarcts, previously only visible in post mortem ex vivo studies.[27,28] These cortical microinfarcts (CMIs) are mainly associated with cognitive impairment. However, previously published ex vivo post mortem studies have demonstrated that CMIs are also present in patients without cognitive impairment such as dementia.[28] A prevalence of 6 - 43% is found in the non-demented population and one ex vivo study has demonstrated a statistically significant correlation of CMIs with extracranial atherosclerosis.[29] **Chapter 6** presents the first study that demonstrates in vivo visualization of CMIs in patients with extensive atherosclerosis of the extracranial vessels. The results demonstrate that CMIs occur in the same pattern as macroinfarcts. Although the number of CMIs is less than the number of macroinfarcts, a significant correlation between the presence of CMIs and macroinfarcts was observed and CMIs were significantly more prevalent in the hemisphere ipsilateral to the symptomatic carotid artery stenosis compared with the contralateral hemisphere.

It is possible to visualize pituitary microadenomas with 7.0 T MRI?

In **Chapter 7** we have demonstrated that 7.0 T MRI is feasible for imaging the pituitary gland with a high spatial resolution. Qualitative good high-resolution images of the pituitary gland can be obtained with a protocol consisting of a T1 MPIR TSE sequence and a T_2 TSE sequence. Hence, the feasibility of 7.0 T pituitary MRI has been demonstrated.

In **Chapter 8**, we have demonstrated that the interobserver agreement for the detection of microadenomas in patients with Cushing's disease is good, both at standard 1.5 T MRI and 7.0 T MRI. Additionally, in 5 patients 7.0 T enabled to confirm an pituitary lesion unclear at 1.5 T and in 3 patients the 7.0 T MRI enabled to visualize a lesion which was not visible at 1.5 T. To conclude, 7.0 MRI seems to be helpful in certain patients in whom the diagnosis of the suspected microadenoma with standard 1.5 T MRI is not conclusive. However, a large-scale head-to-head comparison of 1.5 T, 3.0 T and 7.0 T MRI is needed to evaluate the actual clinical relevance of high spatial resolution MRI in Cushing's disease.

Is high resolution 7.0 T MRI of the carotid arteries, the brain and the pituitary gland clinically relevant?

With 3.0 T MRI it is possible to obtain high-detailed images of carotid plaque components. Consequently, in the last decade literature had demonstrated that visualization of plaque components enables to differ groups of symptomatic patients with a difference in future stroke risk but similar degrees of carotid artery stenosis. However, these results cannot be translated to higher field strength MRI of 7.0 T until we are able to obtain dedicated plaque component images with a certain level of quality. The results in **Chapter 4** and **Chapter 5** demonstrate that the challenges of 7.0 T MRI field strength in the neck region. These challenges hamper the consistency and accuracy of 7.0 T MRI of carotid plaques.

It is feasible to visualize macroinfarcts at low field strength MRI of 1.5 T. For CMIs, however, 7.0 T or 3.0 T MRI with dedicated (3D) protocols is needed. CMIs are seen more frequently in patients with cognitive impairment compared to patients without cognitive impairment.[30] Furthermore, **Chapter 6** demonstrates that CMIs, depicted with 7.0 T MRI, occur with the same pattern as macroinfarcts. Since all patients with CMIs have macroinfarcts as well, the diagnosis of CMIs has limited added diagnostic value for the clinical setting. However, the burden of CMIs in patients with macroinfarcts may be related to (future) cognitive impairment. Therefore, a large-scale evaluation of CMI prevalence in stroke patients, including clinical and cognitive follow-up, is needed to evaluate the clinical value of CMIs in this specific group of patients.

The visualization of microadenomas is important for establishing the diagnosis of a pituitary origin of Cushing's syndrome as well as for the visualization of the actual location of the microadenoma in the pituitary gland, which in turn is crucial for surgical planning. In the retrospectively multicenter study presented in **Chapter 8** the 7.0 T images enabled the confirmation of some uncertain pituitary lesions obtained with 1.5 T. Furthermore, some lesions which were not visible with 1.5 T were indeed visualized with 7.0 T. These results suggest that 7.0 T MRI of the pituitary gland in patients with Cushing's disease and with inconclusive results on standard 1.5 T MRI, is the first clinically relevant application of high resolution 7.0 T MRI. However, a prospective study is needed to evaluate whether there are more patients with Cushing's disease who might benefit from 7.0 T MRI. Besides, to answer the question if 7.0 T MRI is clinically relevant, we first need to evaluate whether 3.0 T MRI performs as good as 7.0 T MRI and whether consensus reading of the 1.5 T MR images is as good as high field strength MRI. If one of these options would be qualitatively equal to the 7.0 T MRI, this would naturally be a far better applicable, more available and cheaper option in clinical medicine.

REFERENCES

1. Saam T, Hetterich H, Hoffmann V, et al. Meta-analysis and systematic review of the predictive value of carotid plaque hemorrhage on cerebrovascular events by magnetic resonance imaging. J Am Coll Cardiol. Sep 17 2013;62:1081-1091.
2. Gupta A, Baradaran H, Schweitzer AD, et al. Carotid plaque MRI and stroke risk: a systematic review and meta-analysis. Stroke. Nov 2013;44:3071-3077.
3. Yuan C, Mitsumori LM, Ferguson MS, et al. In vivo accuracy of multispectral magnetic resonance imaging for identifying lipid-rich necrotic cores and intraplaque hemorrhage in advanced human carotid plaques. Circulation. Oct 23 2001;104:2051-2056.
4. Saba L, Mallarini G. Fissured fibrous cap of vulnerable carotid plaques and symptomaticity: are they correlated? Preliminary results by using multi-detector-row CT angiography. Cerebrovasc Dis. 2009;27:322-327.
5. Moody AR, Murphy RE, Morgan PS, et al. Characterization of complicated carotid plaque with magnetic resonance direct thrombus imaging in patients with cerebral ischemia. Circulation. Jun 24 2003;107:3047-3052.
6. Hosseini AA, Kandiyil N, Macsweeney ST, et al. Carotid plaque hemorrhage on magnetic resonance imaging strongly predicts recurrent ischemia and stroke. Annals of neurology. Jun 2013;73:774-784.
7. Altaf N, Daniels L, Morgan PS, et al. Detection of intraplaque hemorrhage by magnetic resonance imaging in symptomatic patients with mild to moderate carotid stenosis predicts recurrent neurological events. J Vasc Surg. Feb 2008;47:337-342.
8. Chu B, Kampschulte A, Ferguson MS, et al. Hemorrhage in the atherosclerotic carotid plaque: a high-resolution MRI study. Stroke. May 2004;35:1079-1084.
9. Zhao H, Zhao X, Liu X, et al. Association of carotid atherosclerotic plaque features with acute ischemic stroke: A magnetic resonance imaging study. Eur J Radiol. May 13 2013;82:e465-e470.
10. Ouhlous M, Flach HZ, de Weert TT, et al. Carotid plaque composition and cerebral infarction: MR imaging study. AJNR Am J Neuroradiol. May 2005;26:1044-1049.
11. Altaf N, Goode SD, Beech A, et al. Plaque hemorrhage is a marker of thromboembolic activity in patients with symptomatic carotid disease. Radiology. Feb 2011;258:538-545.
12. Tourdias T, Renou P, Sibon I, et al. Final cerebral infarct volume is predictable by MR imaging at 1 week. AJNR Am J Neuroradiol. Feb 2011;32:352-358.
13. Underhill HR, Yuan C, Yarnykh VL, et al. Arterial remodeling in the subclinical carotid artery disease. JACC Cardiovasc Imaging. Dec 2009;2:1381-1389.
14. Takaya N, Yuan C, Chu B, et al. Presence of intraplaque hemorrhage stimulates progression of carotid atherosclerotic plaques: a high-resolution magnetic resonance imaging study. Circulation. May 31 2005;111:2768-2775.
15. Kwee RM, Truijman MT, van Oostenbrugge RJ, et al. Longitudinal MRI study on the natural history of carotid artery plaques in symptomatic patients. PLoS One. 2012;7:e42472.
16. Lansberg MG, O'Brien MW, Tong DC, et al. Evolution of cerebral infarct volume assessed by diffusion-weighted magnetic resonance imaging. Arch Neurol. Apr 2001;58:613-617.
17. Lindsay AC, Biasiolli L, Lee JM, et al. Plaque features associated with increased cerebral infarction after minor stroke and TIA: a prospective, case-control, 3-T carotid artery MR imaging study. JACC Cardiovasc Imaging. Apr 2012;5:388-396.
18. Spence JD, Coates V, Li H, et al. Effects of intensive medical therapy on microemboli and cardiovascular risk in asymptomatic carotid stenosis. Arch Neurol. Feb 2010;67:180-186.
19. Sliwka U, Job FP, Wissuwa D, et al. Occurrence of transcranial Doppler high-intensity transient signals in patients with potential cardiac sources of embolism. A prospective study. Stroke. Nov 1995;26:2067-2070.
20. Jayasooriya G, Thapar A, Shalhoub J, et al. Silent cerebral events in asymptomatic carotid

stenosis. J Vasc Surg. Jul 2011;54:227-236.
21. Forteza AM, Babikian VL, Hyde C, et al. Effect of time and cerebrovascular symptoms of the prevalence of microembolic signals in patients with cervical carotid stenosis. Stroke. Apr 1996;27:687-690.
22. Edelstein WA, Glover GH, Hardy CJ, et al. The intrinsic signal-to-noise ratio in NMR imaging. Magn Reson Med. Aug 1986;3:604-618.
23. Kroner ES, van Schinkel LD, Versluis MJ, et al. Ultrahigh-field 7-T magnetic resonance carotid vessel wall imaging: initial experience in comparison with 3-T field strength. Invest Radiol. Dec 2012;47:697-704.
24. Kraff O, Bitz AK, Breyer T, et al. A transmit/receive radiofrequency array for imaging the carotid arteries at 7 Tesla: coil design and first in vivo results. Invest Radiol. Apr 2011;46:246-254.
25. Koning W, Bluemink JJ, Langenhuizen EA, et al. High-resolution MRI of the carotid arteries using a leaky waveguide transmitter and a high-density receive array at 7 T. Magn Reson Med. Jul 3 2012;69:1186-1193.
26. Ii Y, Maeda M, Kida H, et al. In vivo detection of cortical microinfarcts on ultrahigh-field MRI. J Neuroimaging. Jan 2013;23:28-32.
27. van Veluw SJ, Zwanenburg JJ, Engelen-Lee J, et al. In vivo detection of cerebral cortical microinfarcts with high-resolution 7T MRI. J Cereb Blood Flow Metab. Mar 2013;33:322-329.
28. Smith EE, Schneider JA, Wardlaw JM, et al. Cerebral microinfarcts: the invisible lesions. Lancet Neurol. Mar 2012;11:272-282.
29. Zheng L, Vinters HV, Mack WJ, et al. Cerebral atherosclerosis is associated with cystic infarcts and microinfarcts but not Alzheimer pathologic changes. Stroke. Oct 2013;44:2835-2841.
30. Brundel M, de Bresser J, van Dillen JJ, et al. Cerebral microinfarcts: a systematic review of neuropathological studies. J Cereb Blood Flow Metab. Mar 2012;32:425-436.

Supplementary material

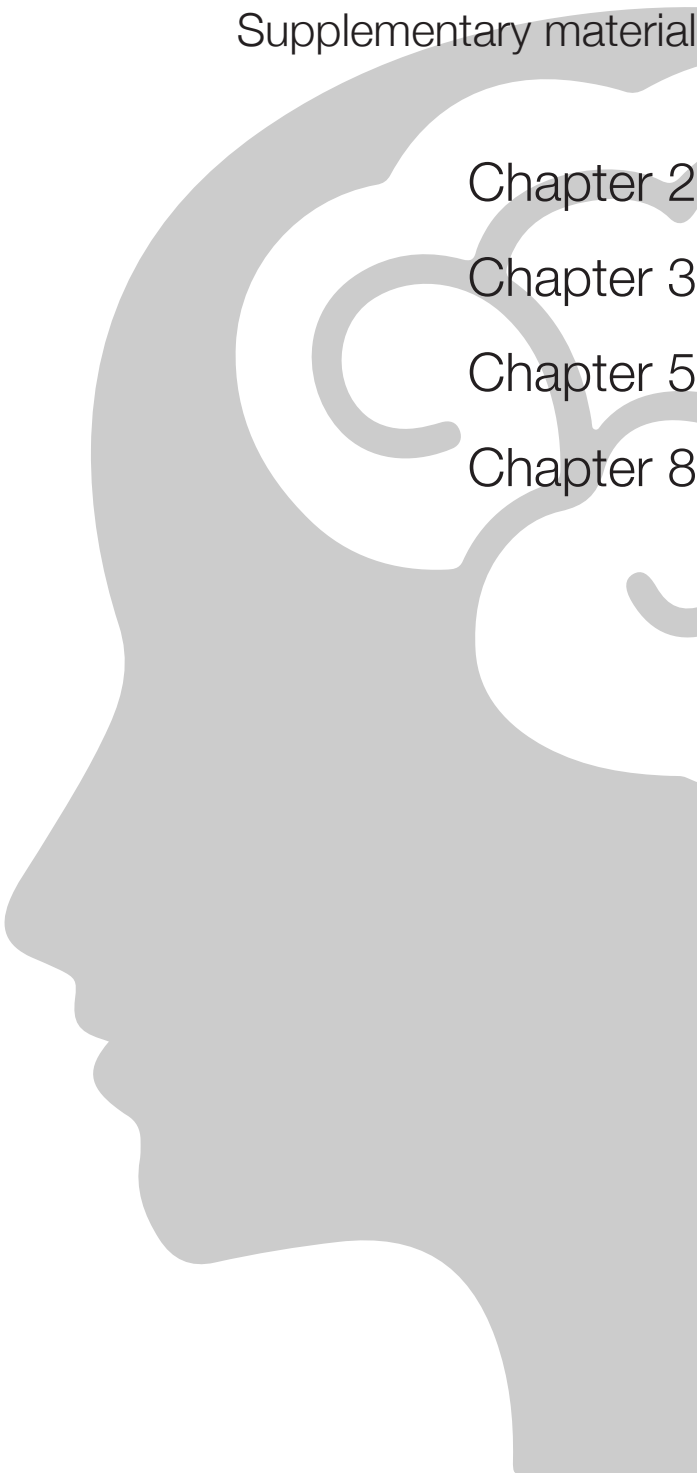

Chapter 2

Chapter 3

Chapter 5

Chapter 8

Chapter 2: Plaque components in symptomatic moderately stenosed carotid arteries related to cerebral infarcts; the PARISK study

Methods

Inclusion In the current study patients with a symptomatic 30-69% stenosis of the carotid artery were included. Briefly, the stenosis grade was based on both the European Carotid Surgery Trial criteria (lower cutoff value of 30%) and the North American Symptomatic Carotid Endarterectomy Trial criteria (upper cutoff value of 70%), as previously described.[1] Measurements were determined on clinically obtained Doppler ultrasound or computed tomography angiography.

Imaging hardware Imaging was performed on 3.0 Tesla whole-body MRI scanners (Achieva or Ingenia, Philips Healthcare, Best, The Netherlands, or a Discovery MR750 system, GE Healthcare, Milwaukee, Wisconsin, United States). For carotid artery imaging dedicated phased-array carotid surface coils were used (Shanghai Chenguang Medical Technologies Co, Shanghai China or Machnet B.V., Roden, The Netherlands) and for brain imaging dedicated head coils were used.[1]

Imaging protocols Carotid arteries. The imaging protocols for carotid artery imaging have been described previously.[1] Briefly, a pre- and post-contrast T_1 weighted quadruple inversion recovery (QIR) turbo spin echo (TSE) or a T_1 weighted double inversion recovery (DIR) Fast Spin Echo (FSE) sequence, on respectively Philips or GE scanners, was used for assessment of the fibrous cap status. Post-contrast images were acquired 6 minutes after administration of 0.1 mmol/kg gadolinium based contrast agent with an injection rate of 0.5 mL/min. A time-of-flight (TOF) sequence and a T_1 weighted inversion recovery turbo field echo (TFE) or a T_1 weighted spoiled gradient echo (SGR) sequence, on respectively Philips or GE scanners, were used to identify IPH.

Brain. The imaging protocols for brain imaging have been described previously as well.[1] Briefly, the sequences used for infarct detection are a T_2 weighted fluid attenuated inversion recovery (FLAIR) sequence and a T_2 weighted TSE or FSE sequence.

Image analysis All imaging data were evaluated by trained readers blinded to the results of other imaging modalities, clinical data, and baseline characteristics. Each reader was trained on test sets of 15 patients.[1] Trained readers could only perform final data analyses after achieving acceptable interobserver agreement with experts on the test sets. Since the test sets were rather small a cut-off value of kappa ≥ 0.4 was

used. The interobserver agreement of IPH was good (both readers kappa = 0.7). The interobserver agreement for TRFC was good for one observer (kappa = 0.7) and fair for the other reader (kappa = 0.4).

Carotid arteries In all patients the presence or absence of IPH in the ipsilateral carotid artery was determined and the fibrous cap status was scored binary as thick or thin/ruptured. The presence of IPH was scored as a region of hyperintense signal, relative to the adjacent sternocleidomastoid muscle, in the bulk of the plaque on the TOF sequence or on the T_1 TFE or SGR sequence, according to previously published criteria.[2-5] Fibrous cap status was determined on pre- and post-contrast T_1 weighted images. The fibrous cap was scored as thick in case of a continuous signal enhancement between lumen and lipid rich necrotic core (LRNC) and as thin/ruptured in case of an interrupted or absent signal enhancement between lumen and LRNC.

The carotid images were analyzed by two independent readers (MT and AD), with three years of experience in carotid MRI reading. Each patient was analyzed once. In case of doubt a third reader, with >10 years of experience in carotid MRI reading, was consulted (MK or AL).

Statistical analysis Since there is a large variety in delay between symptoms and imaging (median 45 days, range 7 - 100) the relationship between plaque components, presence of infarcts and time between symptoms and imaging was evaluated with an unpaired samples T-test. Additionally, patients were divided in imaged before 45 days and imaged after 45 days. A Fisher's Exact test was used to evaluate the difference in plaque components between these two groups.

Results

The mean time between symptoms and imaging in patients with ≥1 infarcts in the flow territory of the symptomatic carotid artery was 44 days, compared to 52 days in patients without infarcts in the flow territory of the symptomatic carotid artery. This difference was, based on a unpaired samples T-test not statistically significant.

IPH was present in 20 patients imaged before 45 days, compared to 20 patients imaged after 45 days. IPH was absent in 32 patients imaged before 45 days, compared to 29 patients imaged after 45 days. TRFC was present in 25 patients imaged before 45 days, compared to 24 patients imaged after 45 days. A thick fibrous cap was present in 16 patients imaged before 45 days, compared to 21 patients imaged after 45 days. Both, the prevalence of IPH (P = 0.84) and TRFC (P = 0.52), were not significantly different in patients imaged before and after 45 days.

Discussion

In histological literature a fibrous cap of <200 µm is considered to be a thin fibrous cap. In a previous MRI study, however, is demonstrated that the accuracy of measurements of fibrous caps <310 µm decreases significantly.[6] Besides, a good reproducibility for fibrous cap assessment based on the differentiation between thin/ruptured and thick fibrous caps is demonstrated in previous literature.[5] This classification also seems to be useful for risk assessment in patients with a high risk on recurrent cerebral ischemia.[7] For this reason we decided to classify the plaques between a thin/ruptured or a thick fibrous cap.

Table. Distribution of infarcts, compared to classification of index event

	Clinical diagnosis	Infarcts (cortical + subcortical)	Cortical infarcts
Stroke (minor)	49	34	19
TIA	42	12	4
AFX	10	1	1

Data are number of patients; TIA = transient ischemic attack; AFX = amaurosis fugax

References

1. Truijman MT, Kooi ME, van Dijk AC, de Rotte AA, van der Kolk AG, Liem MI, Schreuder FH, Boersma E, Mess WH, van Oostenbrugge RJ, Koudstaal PJ, Kappelle LJ, Nederkoorn PJ, Nederveen AJ, Hendrikse J, van der Steen AF, Daemen MJ, van der Lugt A. Plaque at risk (parisk): Prospective multicenter study to improve diagnosis of high-risk carotid plaques. Int J Stroke. 2013;9:747-754
2. Chu B, Kampschulte A, Ferguson MS, Kerwin WS, Yarnykh VL, O'Brien KD, Polissar NL, Hatsukami TS, Yuan C. Hemorrhage in the atherosclerotic carotid plaque: A high-resolution mri study. Stroke. 2004;35:1079-1084
3. Saam T, Ferguson MS, Yarnykh VL, Takaya N, Xu D, Polissar NL, Hatsukami TS, Yuan C. Quantitative evaluation of carotid plaque composition by in vivo mri. Arterioscler Thromb Vasc Biol. 2005;25:234-239
4. Yuan C, Mitsumori LM, Ferguson MS, Polissar NL, Echelard D, Ortiz G, Small R, Davies JW, Kerwin WS, Hatsukami TS. In vivo accuracy of multispectral magnetic resonance imaging for identifying lipid-rich necrotic cores and intraplaque hemorrhage in advanced human carotid plaques. Circulation. 2001;104:2051-2056
5. Kwee RM, van Engelshoven JM, Mess WH, ter Berg JW, Schreuder FH, Franke CL, Korten AG, Meems BJ, van Oostenbrugge RJ, Wildberger JE, Kooi ME. Reproducibility of fibrous cap status assessment of carotid artery plaques by contrast-enhanced mri. Stroke. 2009;40:3017-3021
6. Nieuwstadt HA, Geraedts TR, Truijman MT, Kooi ME, van der Lugt A, van der Steen AF, Wentzel JJ, Breeuwer M, Gijsen FJ. Numerical simulations of carotid mri quantify the accuracy in measuring atherosclerotic plaque components in vivo. Magn Reson Med. 2014;72:188-201
7. Kwee RM, van Oostenbrugge RJ, Mess WH, Prins MH, van der Geest RJ, ter Berg JW, Franke CL, Korten AG, Meems BJ, van Engelshoven JM, Wildberger JE, Kooi ME. Mri of carotid atherosclerosis to identify tia and stroke patients who are at risk of a recurrence. J Magn Reson Imaging. 2013;37:1189-1194

Chapter 3: Intraplaque hemorrhage, fibrous cap status, and microembolic signals in symptomatic patients with mild to moderate carotid artery stenosis: the PARISK study

Methods

Patient selection: Eligible for the study were patients with a transient ischemic attack, amaurosis fugax or minor stroke (modified Rankin scale ≤3) of the carotid artery territory and an atherosclerotic plaque with a < 70% stenosis of the ipsilateral internal carotid artery who were not scheduled for a revascularization procedure. Patients needed to be eligible for imaging within three months after initial ischemic event. Exclusion criteria were a probable cardiac source of embolism, a clotting disorder, severe comorbidity, standard contraindications for MRI, a documented allergy for MRI or CT contrast agent or a renal clearance of <30 ml/min. Degree of stenosis was be determined with clinically obtained Doppler US or CT angiography. The upper cutoff value of 70% was based on the North American Symptomatic Carotid Endarterectomy Trial criteria.[1] The lower cutoff value was an atherosclerotic plaque with a thickness of at least 2 - 3 mm, which corresponds to an European Carotid Surgery Trial stenosis of 30%.[2]

MRI protocol: All patients were scanned using 3.0 T scanners (Achieva and Ingenia, Philips Healthcare, Best, The Netherlands; Discovery MR750 system, GE Healthcare, Milwaukee, WI) and dedicated phased-array carotid surface coils (Shanghai Chenguang Medical Technologies Co, Shanghai, China or Machnet B.V., Roden, The Netherlands). T_1 weighted inversion recovery turbo field echo (IR-TFE) or spoiled gradient echo (SPGR) as well as T_1 pre- and postcontrast quadruple inversion recovery turbo spin echo (QIR TSE) or T_1 double inversion recovery fast spin echo (DIR FSE) images were obtained. The postcontrast images were acquired 6 minutes after the injection of 0.1 mmol/kg of a gadolinium-based contrast agent with an injection rate of 0.5 mL/s.

MRI analysis: IPH was scored as being present if a hyperintense signal (compared with the adjacent sternocleidomastoid muscle) was visible in the bulk of the plaque on IR-TFE or SPGR images. With the precontrast T_1 QIR TSE or T_1 DIR FSE image as baseline for comparison, lipid-rich necrotic core (LRNC) was identified on the postcontrast images as an area in the bulk of the plaque with no or slight contrast enhancement compared with the surrounding, more strongly enhanced fibrous tissues.

Subsequently, FC status was scored by comparing pre- and postcontrast images for the presence of a continuous signal enhancement on the postcontrast images between LRNC and the lumen (thick FC) or an interrupted or no continuous signal enhancement (thin/ruptured FC).

TCD recording: An axial sample volume setting of 5.1 mm was used, and probe aiming (2-axis servo-control), pulse repetition frequency, depth, and power were optimized using dedicated software on a laptop which was connected to the ambulatory unit. The automatic servo system for optimizing probe aiming was activated, and the laptop was disconnected. Raw quadrature Doppler data were stored on an SD-memory card. Patients were asked to turn the device off after four hours of ambulatory monitoring.

TCD analysis: Fast Fourier transforms (128 points) were performed with an overlap of 90-95%. The normal blood signal amplitude was monitored continuously and defined as the upper quartile of the spectral speckle peaks. At a preset speckle peak amplitude (15 dB in the present study) above this level, the signal was analyzed further by the software. In order to qualify the signal as a MES candidate, the mirror amplitude (negative velocity) had to be much lower (15 dB) than the positive velocity peak amplitude. Furthermore, the duration of the spectral peak had to be compatible with the expected duration given the sample volume size and the flow velocity. These criteria eliminated practically all artifacts due to probe and patient movements as well as spectral bands due to speech and vocalizations. The remaining possible MES events were saved in a separate file. These signals were inspected both audibly and visually (spectral analysis) by two independent observers (MT and WM). Only those events agreed upon by both were classified as MES (figure 2). To validate and optimize the algorithms, the first 40 hours or recordings were analyzed and listened to by two independent observers (MT and AR). All possible MES were listed and checked by a third observer (WM). The software settings were adjusted in such a manner that no MES detected by the human observers were missed.

References

1. North american symptomatic carotid endarterectomy trial. Methods, patient characteristics, and progress. Stroke. 1991;22:711-720
2. Rothwell PM. Randomised trial of endarterectomy for recently symptomatic carotid stenosis: Final results of the mrc european carotid surgery trial (ecst). Lancet. 1998;351:1379-1387

Table 1A: Crosstabs indicating the prevalence of MES in patients with and without IPH

		IPH		
		Yes	No	Total
MES	Yes	2	6	8
	No	42	55	97
	Total	61	44	105

Table 1B: Crosstabs indicating the prevalence of MES in patients with a thin/ruptured fibrous cap (FC) and with a thick FC

		FC		
		Thin/ruptured	Thick	Total
MES	Yes	2	6	8
	No	47	37	84
	Total	49	43	92

Chapter 5: 7.0 T MRI of atherosclerotic plaque in the significantly stenosed carotid artery

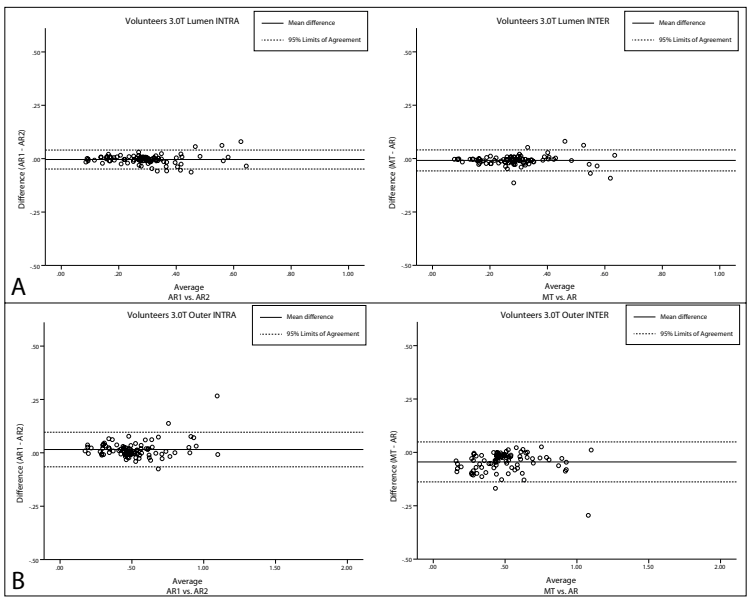

Figure 1A. Intra- (left) and inter-observer reproducibility (right) of lumen determination in healthy volunteers (3.0T MRI) (A). Intra- (left) and inter-observer reproducibility (right) of outer vessel wall determination in healthy volunteers (3.0T MRI) (B).

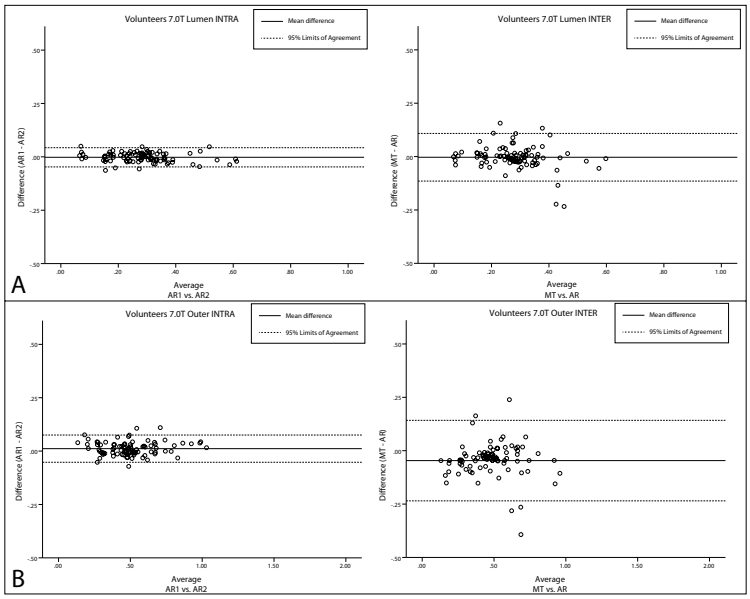

Figure 1B. Intra-(left) and inter-observer reproducibility (right) of lumen determination in healthy volunteers (7.0T MRI) (A). Intra- (left) and inter-observer reproducibility (right) of outer vessel wall determination in healthy volunteers (7.0T MRI) (B).

Chapter 8: High resolution pituitary MRI at 7.0 T: a clinical evaluation in Cushing's disease

Methods

Biochemical evaluation

Bilateral inferior petrosal sinus sampling (IPSS) of ACTH before and after stimulation with corticotrophin releasing hormone (CRH) and magnetic resonance imaging (MRI) both enable to confirm the diagnosis of adrenocorticotrophic hormone (ACTH) producing adenomas in the pituitary gland.

Discrimination between an ectopic and a pituitary origin of Cushing's syndrome was based on MRI or IPSS. In case a lesion of >6 mm was visualized with MRI this was conclusive for a pituitary origin of Cushing´s syndrome. IPSS was performed in case no lesions were visible on MRI or in case a small, unclear lesion was visible. Based on IPSS a pituitary origin was diagnosed in case the ratio between petrosal sinus sample and peripheral venous blood sample was ≥2.0 before and/or ≥3.0 after stimulation with CRH, based on previously published literature.[1] To determine lateralization of the IPSS results, the ratio between right and left petrosal sinus sample was calculated. A ratio of ≥1.4 was considered to be predictive for lateralization, based on previously published literature.[2] However, note that the reliability of lateralization with IPSS is limited.

Results

Clinical evaluation

All 17 patients presented with classical signs and symptoms of Cushing's syndrome. Endogenous cortisol hypersecretion was confirmed in all patients by demonstrating increased excretion of free cortisol in 24 hours urine collection, elevated plasma or salivary cortisol levels at midnight and failure to suppress endogenous cortisol after administration of 1 mg of dexamethasone. Plasma levels of ACTH were not suppressed in any of the 17 patients, demonstrating ACTH-dependent Cushing's syndrome. In order to differentiate between pituitary ACTH hypersecretion (Cushing's disease) and ectopic ACTH hypersecretion, bilateral IPSS was performed in 13 patients and unilateral IPSS was performed in 1 patient. In 2 patients IPSS was not performed because of an allergy for the contrast agent (patient 12) and because the lesion confirmed with 7.0 T MRI was >6 mm (patient 16). IPSS demonstrated the pituitary origin of ACTH hypersecretion in

all 14 patients. In patients who did not undergo IPSS, a 7 mg dexamethason infusion test and/or a CRH test were performed. Results of these tests raised a strong suspicion of a pituitary origin of ACTH hypersecretion in these patients. A complete overview of the IPSS results is presented in the Table below.

Table. Results inferior petrosus sinus sampling (IPSS)

Patient	IPSS Pituitary origin	IPSS Lateralization
1	+	R
2	+	R
3	+	L
4	+	L
5	+	R
6	+	R
7	+	R
8	+	R
9	+	L
10	+	R
11	+	R
12	n.a.	n.a.
13	+[a]	unknown
14	+	R
15	+	unknown[b]
16	n.a.	n.a.

Pituitary origin was considered positive (+) or negative (-), in 2 patients IPSS was not performed. [a]In patient 13 IPSS was performed unilateral. [b]In patient 15 the results from IPSS could not establish lateralization.

1. Oldfield EH, Doppman JL, Nieman LK, et al. Petrosal sinus sampling with and without corticotropin-releasing hormone for the differential diagnosis of Cushing's syndrome. N Engl J Med. 1991;325:897-905.
2. Wind JJ, Lonser RR, Nieman LK, et al. The lateralization accuracy of inferior petrosal sinus sampling in 501 patients with Cushing's disease. J Clin Endocrinol Metab. 2013;98:2285-2293.

Appendix

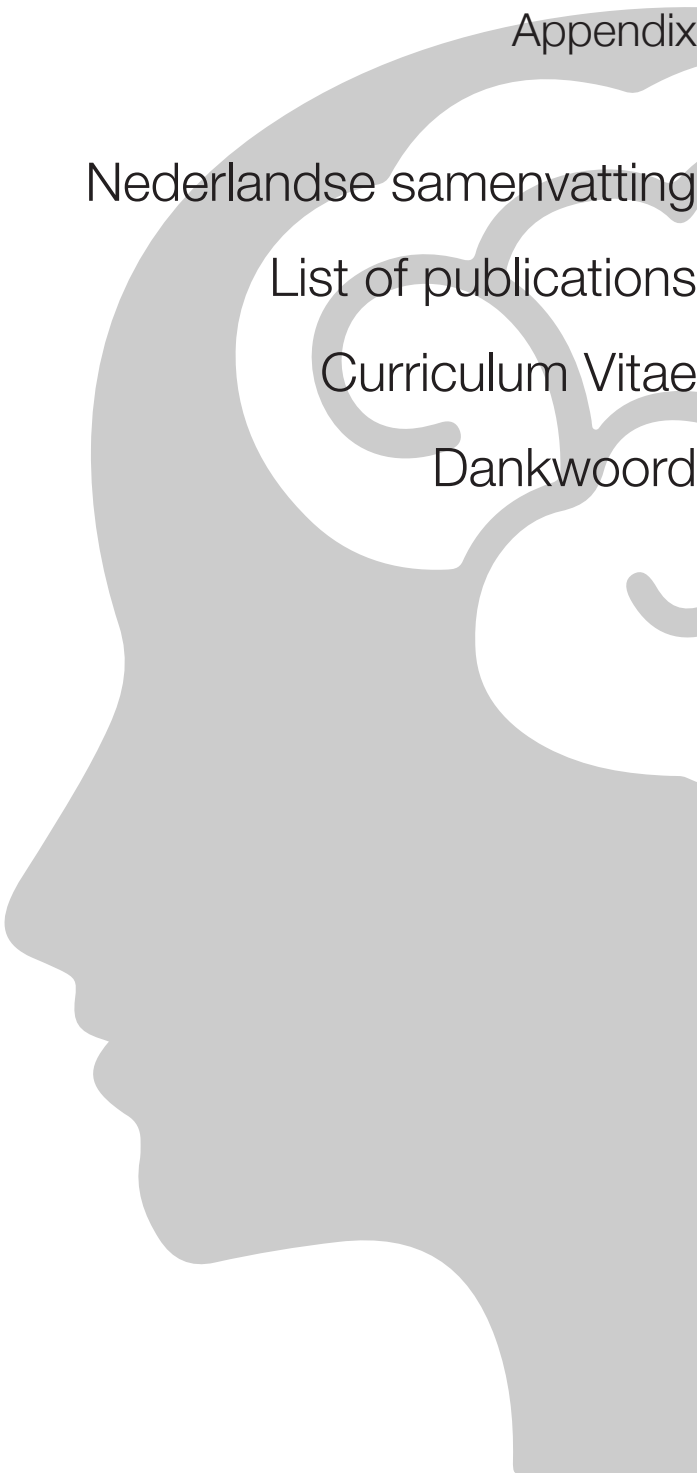

Nederlandse samenvatting

List of publications

Curriculum Vitae

Dankwoord

Samenvatting en algemene discussie

Beeldvorming is een diagnostisch middel dat in de moderne geneeskunde een belangrijke plaats inneemt. Er zijn verschillende beeldvormende technieken beschikbaar, zoals conventionele röntgen, echografie, CT (computertomografie) en MRI (magnetic resonance imaging). Elke van deze modaliteiten heeft voor- en nadelen, waardoor elke modaliteit zijn eigen specifieke toepassingen heeft. MRI is een van de snelst ontwikkelende technieken en drie belangrijke voordelen van MRI zijn de mogelijkheid om met een hoge resolutie te scannen, de sterke contrastverschillen die verkregen kunnen worden binnen zacht weefsel en MRI is niet gebaseerd op ioniserende straling. Dit maakt dat MRI een niet-schadelijke modaliteit is die gebruikt kan worden om kleine anatomische en pathologische structuren af te beelden. Aan de andere kant zijn twee belangrijke nadelen van MRI dat de scantijd lang is in vergelijking met bijvoorbeeld CT en dat het een dure techniek is.

In dit proefschrift zijn verschillende toepassingen besproken van hoge resolutie MRI bij patiënten met een ischemische beroerte of de ziekte van Cushing. Voor patiënten die een ischemische beroerte hebben gehad wordt MRI gebruikt om de extracraniële vaten (aa. carotis en vertebralis), de intracraniële vaten en het hersenparenchym in beeld te brengen. In de afgelopen 10 jaar zijn meer geavanceerde MRI technieken ontwikkeld om de atherosclerotische plaque in de carotis in beeld te brengen. Deze technieken worden in toenemende mate gebruikt om het risico op het ontwikkelen van een nieuw infarct in te schatten. Daarnaast is MRI uitermate geschikte om de totale schade als gevolg van een infarct, alsmede de schade van oude infarcten, in beeld te brengen.

Voor patiënten met de ziekte van Cushing wordt MRI gebruikt om zeer gedetailleerde afbeeldingen van de hypofyse te maken. Deze zeer gedetailleerde afbeeldingen worden gebruikt voor zowel het stellen van de diagnose als het plannen van de chirurgische behandeling.

De resultaten van de verschillende studies alsmede de antwoorden op de onderzoeksvragen uit de introductie worden hieronder samengevat en bediscussieerd.

Zijn intraplaque bloedingen en een dunne/geruptureerde fibreuze kap geassocieerd met cerebrale infarcten op MRI en met microembolische signalen op transcraniële Doppler?

Eerder gepubliceerde literatuur heeft aangetoond dat MRI op een veldsterkte van 3.0 tesla (T) in staat is om plaque componenten accuraat in beeld te brengen.[1,2] Twee van deze plaque componenten, geassocieerd met een verhoogd risico op het krijgen van een (nieuw) cerebraal ischemisch infarct, zijn een intraplaque bloeding en een dunne/geruptureerde fibreuze kap over een vetkern. [3-8] De resultaten in **Hoofdstuk 2**

en **Hoofdstuk 3** laten zien dat de aanwezigheid van een intraplaque bloeding of een dunne/geruptureerde fibreuze kap niet gerelateerd zijn aan infarcten in het stroomgebied van de betreffende symptomatische carotis stenose en ook niet aan microembolische signalen (MES) op transcraniële Doppler (TCD). Beide studies laten tegenovergestelde resultaten zien in vergelijking met voorgaande publicaties.[9-11]

Ten eerste hebben voorgaande studies juist een statistisch significante correlatie aangetoond tussen plaque componenten en infarcten op MRI. [9-11] In **Hoofdstuk 2** zijn de infarcten afgebeeld met een fluid-attenuated inversion recovery (FLAIR) sequentie. Het infarct volume op FLAIR beelden blijkt af te nemen in de tijd, maar verdwijning van een infarct op FLAIR beelden is nooit eerder beschreven.[12] Daarbij blijkt ook de aanwezigheid van een intraplaque bloeding en een dunne/geruptureerde fibreuze kap niet te veranderen over de tijd.[8,13-15] Dit maakt het onwaarschijnlijk dat het tijdsverschil tussen de symptomen en beeldvorming de afwezigheid van een significante associatie kan verklaren. De infarcten in de eerder gepubliceerde studies zijn echter afgebeeld met een diffusie gewogen sequentie (DWI). Dit impliceert dat deze studies slechts gericht zijn op acute infarcten, omdat laesies op DWI alleen zichtbaar zijn in de acute fase na een infarct.[16] Met FLAIR daarentegen worden zowel oude als nieuwe infarcten afgebeeld. Dit betekent dat de infarcten die met FLAIR afgebeeld worden dus niet allemaal gerelateerd hoeven te zijn aan het infarct waar het op dit moment om gaat. Dit zou de afwezigheid van de eerder genoemde associatie wel kunnen verklaren en is ook eerder beschreven door Lindsey en collega's.[17]

Ten tweede is er eerder een statistisch significante associatie aangetoond tussen MES en de aanwezigheid van kenmerken van een kwetsbare plaque op MRI.[11] Het is bekend dat het voorkomen van MES afneemt in de tijd na symptomen.[18] In **Hoofdstuk 3** was de tijd tussen symptomen en beeldvorming ongeveer 52 dagen en dit zou dus een belangrijke verklaring kunnen zijn dat er geen significante relatie gevonden wordt. Daarnaast is de studie in **Hoofdstuk 3** uitgevoerd in patiënten met een symptomatische laaggradige stenose (30 - 69%) van de carotis en was een cardiale emboliebron een exclusie criterium, in tegenstelling tot deze eerder gepubliceerde studie. Daarbij gebruikte een meerderheid van de patiënten in **Hoofdstuk 3** lipide verlagende middelen. Deze drie factoren hebben ook bij kunnen dragen aan de afwezigheid van een significante associatie.[19-21]

Is het mogelijk om atherosclerotische plaque in de carotis af te beelden met 7.0 T MRI?

Vanaf het ontstaan van de MRI techniek is het al bekend dat MRI scanners met een hogere veldsterkte theoretisch gezien in staat zijn om afbeeldingen met een hogere

resolutie te maken binnen een acceptabele scan tijd.[22] In **Hoofdstuk 4** hebben we een kwantitatieve vergelijking laten zien tussen 3.0 T en 7.0 T MRI voor het afbeelden van de carotiden. Een algehele verbetering van de kwaliteit en een toegenomen signaal ruis verhouding (SNR) werd gedemonstreerd op 7.0 T. De toename in SNR was 2.0 op de gemiddelde diepte van de carotiden, wat iets lager was dan de verwachte 7/3. Theoretisch gezien kan deze lagere winst in SNR verklaard worden door de combinatie van T_1 relaxatietijd verlenging en T_2 relaxatietijd verkorting op 7.0 T. Echter, in de experimenten in **Hoofdstuk 4** hebben we een proton density gewogen sequentie gebruikt om de SNR maps te maken, waardoor het effect van T_1 relaxatietijd verlenging en T_2 relaxatietijd verkorting niet meer van toepassing is. Daarentegen hebben de fantoom experimenten laten zien dat de zogenaamde high density receive array, die we op 7.0 T gebruikt hebben, enig SNR verlies veroorzaakte door magnetische koppeling van de individuele spoelelementen.

Eerder gepubliceerde studies hebben laten zien dat 7.0 T MRI het mogelijk maakt om kwalitatief goede anatomische afbeeldingen te maken van de carotis en dat deze afbeeldingen goed genoeg zijn voor het afgrenzen van de vaatwand bij gezonde vrijwilligers.[23-25] In **Hoofdstuk 5** hebben we een MRI van de carotiden gemaakt in een serie patiënten met een symptomatische hooggradige vernauwing, 1 dag voor de geplande carotis desobstructie. Daarnaast zijn er in deze studie 3.0 T en 7.0 T MRI afbeeldingen gemaakt van de carotiden in 6 gezonde vrijwilligers. Een kwaliteitsanalyse werd uitgevoerd op alle 3.0 T en 7.0 T afbeeldingen (patiënten en vrijwilligers). Een goede inter- en intraobserver reproduceerbaarheid van het intekenen van de vaatwand bevestigde de resultaten van de eerder gepubliceerde studies. Daarnaast zijn de plaques, verwijderd tijdens de carotis desobstructie, histopathologisch geanalyseerd voor de aanwezigheid van verschillende componenten. Helaas ontbreekt een gespecialiseerde sequentie met zwart bloed op 7.0 T MRI, om alle componenten goed in beeld te brengen. Hierdoor was het niet mogelijk om alle plaque componenten in beeld te brengen en dus ook niet om een één-op-één correlatie te maken met de histopathologie. Omdat calcificaties een lage proton dichtheid hebben en daardoor een laag signaal geven op proton density gewogen sequenties hebben we deze sequentie gebruikt als zijnde een eerste validatie van het contrast dat we zien in carotis plaque met 7.0 T MRI. Daarnaast blijkt het met de huidige hardware setup nog steeds moeilijk te zijn om afbeeldingen te maken met een zekere consistentie in het kwaliteitsniveau.

Concluderend kunnen we zeggen dat carotis vaatwand beeldvorming mogelijk is met 7.0 T MRI, maar dat voor het daadwerkelijk afbeelden van plaque componenten meer gespecialiseerde sequenties ontwikkeld moeten worden en dat er een robuustere hardware setup moet worden ontwikkeld. Dit betekent dat 3.0 T MRI vooralsnog

superieur is boven 7.0 T MRI als het gaat om carotis plaque beeldvorming.

Zijn corticale microinfarcten gerelateerd aan macroinfarcten in patiënten met extracraniële atherosclerose?

Recent gepubliceerd werk laat zien dat corticale infarcten met een minimale grootte van 1,67 mm in beeld gebracht kunnen worden op standaard MRI scanners met een veldsterkte van 3.0 T.[26] Daarentegen maken MRI scanners met een hogere veldsterkte het mogelijk om nog kleinere infarcten in beeld te brengen, waarvan het in het verleden alleen mogelijk was om ze in ex vivo post mortem studies aan te tonen.[27,28] Deze zogenaamde corticale microinfarcten zijn voornamelijk geassocieerd met cognitieve achteruitgang. Eerder gepubliceerde ex vivo studies hebben echter laten zien dat patiënten zonder cognitieve achteruitgang, zoals dementie, ook corticale microinfarcten hebben.[28] Een prevalentie van 6 - 43% is gevonden in een niet-dementerende populatie en één ex vivo studie heeft daarbij een statistisch significante associatie aangetoond van corticale microinfarcten met de aanwezigheid van extracraniële atherosclerose.[29] In **Hoofdstuk 6** hebben we corticale microinfarcten in vivo in beeld hebben gebracht bij patiënten met uitgebreide atherosclerose in de extracraniële vasculatuur. De resultaten laten zien dat coriticale microinfarcten in hetzelfde patroon voorkomen als macroinfarcten. Hoewel het aantal microinfarcten minder is dan het aantal macroinfarcten, wordt er wel een significante relatie gevonden tussen de aanwezigheid van microinfarcten en macroinfarcten. Daarnaast waren microinfarcten, net als macroinfarcten vaker aanwezig in de hemisfeer ipsilateraal aan de symptomatische carotis vernauwing, in vergelijking met de contralaterale hemisfeer.

Is het mogelijk om microadenomen in de hypofyse in beeld te brengen met 7.0 T MRI?

In **Hoofdstuk 7** hebben we laten zien dat het haalbaar is om met 7.0 T MRI de hypofyse met een hoge resolutie in beeld te brengen. Kwalitatief goede afbeeldingen met een hoge resolutie konden worden gemaakt met een protocol dat bestond uit een T_1 gewogen MPIR TSE sequentie en een T_2 gewogen TSE sequentie.

In **Hoofdstuk 8** hebben we laten zien dat de interobserver overeenkomst voor de detectie van microadenomen in patiënten met de ziekte van Cushing goed is, met 1.5 T en met 7.0 T MRI. Daarnaast heeft de 7.0 T MRI het in 5 patiënten mogelijk gemaakt om een laesie die niet duidelijk was met 1.5 T MRI beter zichtbaar te maken en in 3 patiënten heeft de 7.0 T MRI ervoor gezorgd dat een laesie zichtbaar werd die niet met 1.5 T zichtbaar was. Hieruit concluderen we dat 7.0 T MRI nuttig lijkt te zijn bij die patiënten waarin een sterke verdenking op een microadenoom met 1.5 T niet bevestigd

kan worden. Echter, een grootschalige vergelijking van 1.5 T, 3.0 T en 7.0 T MRI is nodig om de daadwerkelijk toegevoegde waarde van hoog resolutie MRI bij patiënten met de ziekte van Cushing te bepalen.

Is hoge-resolutie 7.0 T MRI van de carotiden, de hersenen en de hypofyse klinisch relevant?

Met 3.0 T MRI is het mogelijk om zeer gedetailleerde afbeeldingen te maken van carotis plaque, inclusief de verschillende componenten. In de laatste 10 jaar heeft literatuur laten zien dat de visualisatie van verschillende componenten in een plaque het mogelijk maakt om onderscheid te maken tussen patiënten met eenzelfde stenose graad van de carotis, maar een verschillend risico op cerebrale ischemie. Deze resultaten kunnen echt niet zondermeer vertaald worden naar 7.0 T MRI. De resultaten in **Hoofdstuk 4** en **Hoofdstuk 5** laten zien dat 7.0 T MRI in de nek regio nog steeds een uitdaging is en dat de problemen waar we tegenaan lopen het nog steeds niet mogelijk maken om met een zekere kwaliteit afbeeldingen van carotis plaque te maken met 7.0 T MRI.

Het is mogelijk om macroinfarcten met een lage veldsterkte van 1.5 T in beeld te brengen. Echter, voor microinfarcten zijn meer gespecialiseerde (3D) protocollen nodig. Microinfarcten worden vaker in patiënten met cognitieve achteruitgang gezien dan in patiënten zonder cognitieve achteruitgang.[30] Daarnaast komen microinfarcten voor in het zelfde patroon als macroinfarcten, zoals aangetoond in **Hoofdstuk 6**. Omdat alle patiënten met microinfarcten ook macroinfarcten hadden zal de diagnose van een microinfarct weinig toegevoegde waarde hebben in de diagnostiek. De schade van microinfarcten zou echter wel gerelateerd kunnen zijn aan (toekomstige) cognitieve achteruitgang. Daarom zou een grootschalige evaluatie van het voorkomen van microinfarcten in patiënten met een ischemische beroerte, inclusief klinische en cognitieve follow-up, nodig zijn om de toegevoegde waarde van microinfarcten in deze specifieke groep patiënten te evalueren.

Het in beeld brengen van microinfarcten is belangrijk voor het stellen van de diagnose van een hypofysaire oorzaak van het syndroom van Cushing en voor het visualiseren van de exacte locatie van het microadenoom in de hypofyse, wat vervolgens weer van belang is voor de chirurgische planning. In de retrospectieve studie in **Hoofdstuk 8** bleek 7.0 T MRI in staat te zijn enkele laesies in beeld te brengen die op 1.5 T onzeker of überhaupt niet zichtbaar waren. Deze resultaten suggereren dat 7.0 T MRI van de hypofyse in die patiënten met de ziekte van Cushing die een onzekere uitslag van de 1.5 T MRI hebben een eerste klinisch relevante toepassing van hoge-resolutie 7.0 T MRI zou zijn. Een prospectieve studie is echter nodig om te evalueren welke patiënten

met de ziekte van Cushing precies baat zouden hebben bij een 7.0 T MRI. Daarnaast is het belangrijk om na te gaan of 3.0 T MRI niet minstens zo goed is als 7.0 T MRI en of het laten beoordelen van de beelden door een tweede observer niet minstens zo effectief is. Indien een van deze twee opties kwalitatief gelijk is aan 7.0 T MRI dan zou dit uiteraard een beter toepasbare en beschikbare toepassing zijn en bovendien een veel goedkopere optie in de steeds duurder wordende gezondheidszorg.

References

1. Saam T, Hetterich H, Hoffmann V, et al. Meta-analysis and systematic review of the predictive value of carotid plaque hemorrhage on cerebrovascular events by magnetic resonance imaging. J Am Coll Cardiol. Sep 17 2013;62(12):1081-1091.
2. Gupta A, Baradaran H, Schweitzer AD, et al. Carotid plaque MRI and stroke risk: a systematic review and meta-analysis. Stroke. Nov 2013;44(11):3071-3077.
3. Yuan C, Mitsumori LM, Ferguson MS, et al. In vivo accuracy of multispectral magnetic resonance imaging for identifying lipid-rich necrotic cores and intraplaque hemorrhage in advanced human carotid plaques. Circulation. Oct 23 2001;104(17):2051-2056.
4. Saba L, Mallarini G. Fissured fibrous cap of vulnerable carotid plaques and symptomaticity: are they correlated? Preliminary results by using multi-detector-row CT angiography. Cerebrovasc Dis. 2009;27(4):322-327.
5. Moody AR, Murphy RE, Morgan PS, et al. Characterization of complicated carotid plaque with magnetic resonance direct thrombus imaging in patients with cerebral ischemia. Circulation. Jun 24 2003;107(24):3047-3052.
6. Hosseini AA, Kandiyil N, Macsweeney ST, Altaf N, Auer DP. Carotid plaque hemorrhage on magnetic resonance imaging strongly predicts recurrent ischemia and stroke. Annals of neurology. Jun 2013;73(6):774-784.
7. Altaf N, Daniels L, Morgan PS, et al. Detection of intraplaque hemorrhage by magnetic resonance imaging in symptomatic patients with mild to moderate carotid stenosis predicts recurrent neurological events. J Vasc Surg. Feb 2008;47(2):337-342.
8. Chu B, Kampschulte A, Ferguson MS, et al. Hemorrhage in the atherosclerotic carotid plaque: a high-resolution MRI study. Stroke. May 2004;35(5):1079-1084.
9. Zhao H, Zhao X, Liu X, et al. Association of carotid atherosclerotic plaque features with acute ischemic stroke: A magnetic resonance imaging study. Eur J Radiol. May 13 2013;82(9):e465-e470.
10. Ouhlous M, Flach HZ, de Weert TT, et al. Carotid plaque composition and cerebral infarction: MR imaging study. AJNR Am J Neuroradiol. May 2005;26(5):1044-1049.
11. Altaf N, Goode SD, Beech A, et al. Plaque hemorrhage is a marker of thromboembolic activity in patients with symptomatic carotid disease. Radiology. Feb 2011;258(2):538-545.
12. Tourdias T, Renou P, Sibon I, et al. Final cerebral infarct volume is predictable by MR imaging at 1 week. AJNR Am J Neuroradiol. Feb 2011;32(2):352-358.
13. Underhill HR, Yuan C, Yarnykh VL, et al. Arterial remodeling in the subclinical carotid artery disease. JACC Cardiovasc Imaging. Dec 2009;2(12):1381-1389.
14. Takaya N, Yuan C, Chu B, et al. Presence of intraplaque hemorrhage stimulates progression of carotid atherosclerotic plaques: a high-resolution magnetic resonance imaging study. Circulation. May 31 2005;111(21):2768-2775.
15. Kwee RM, Truijman MT, van Oostenbrugge RJ, et al. Longitudinal MRI study on the natural history of carotid artery plaques in symptomatic patients. PLoS One. 2012;7(7):e42472.
16. Lansberg MG, O'Brien MW, Tong DC, Moseley ME, Albers GW. Evolution of cerebral infarct volume assessed by diffusion-weighted magnetic resonance imaging. Arch Neurol. Apr 2001;58(4):613-617.
17. Lindsay AC, Biasiolli L, Lee JM, et al. Plaque features associated with increased cerebral infarction after minor stroke and TIA: a prospective, case-control, 3-T carotid artery MR imaging study. JACC Cardiovasc Imaging. Apr 2012;5(4):388-396.
18. Forteza AM, Babikian VL, Hyde C, Winter M, Pochay V. Effect of time and cerebrovascular symptoms of the prevalence of microembolic signals in patients with cervical carotid stenosis. Stroke. Apr 1996;27(4):687-690.
19. Spence JD, Coates V, Li H, et al. Effects of intensive medical therapy on microemboli and

cardiovascular risk in asymptomatic carotid stenosis. Arch Neurol. Feb 2010;67(2):180-186.
20. Sliwka U, Job FP, Wissuwa D, et al. Occurrence of transcranial Doppler high-intensity transient signals in patients with potential cardiac sources of embolism. A prospective study. Stroke. Nov 1995;26(11):2067-2070.
21. Jayasooriya G, Thapar A, Shalhoub J, Davies AH. Silent cerebral events in asymptomatic carotid stenosis. J Vasc Surg. Jul 2011;54(1):227-236.
22. Edelstein WA, Glover GH, Hardy CJ, Redington RW. The intrinsic signal-to-noise ratio in NMR imaging. Magn Reson Med. Aug 1986;3(4):604-618.
23. Kroner ES, van Schinkel LD, Versluis MJ, et al. Ultrahigh-field 7-T magnetic resonance carotid vessel wall imaging: initial experience in comparison with 3-T field strength. Invest Radiol. Dec 2012;47(12):697-704.
24. Kraff O, Bitz AK, Breyer T, et al. A transmit/receive radiofrequency array for imaging the carotid arteries at 7 Tesla: coil design and first in vivo results. Invest Radiol. Apr 2011;46(4):246-254.
25. Koning W, Bluemink JJ, Langenhuizen EA, et al. High-resolution MRI of the carotid arteries using a leaky waveguide transmitter and a high-density receive array at 7 T. Magn Reson Med. Jul 3 2012;69(4):1186-1193.
26. Ii Y, Maeda M, Kida H, et al. In vivo detection of cortical microinfarcts on ultrahigh-field MRI. J Neuroimaging. Jan 2013;23(1):28-32.
27. Van Veluw SJ, Zwanenburg JJ, Engelen-Lee J, et al. In vivo detection of cerebral cortical microinfarcts with high-resolution 7T MRI. J Cereb Blood Flow Metab. Mar 2013;33(3):322-329.
28. Smith EE, Schneider JA, Wardlaw JM, Greenberg SM. Cerebral microinfarcts: the invisible lesions. Lancet Neurol. Mar 2012;11(3):272-282.
29. Zheng L, Vinters HV, Mack WJ, Zarow C, Ellis WG, Chui HC. Cerebral atherosclerosis is associated with cystic infarcts and microinfarcts but not Alzheimer pathologic changes. Stroke. Oct 2013;44(10):2835-2841.
30. Brundel M, de Bresser J, van Dillen JJ, Kappelle LJ, Biessels GJ. Cerebral microinfarcts: a systematic review of neuropathological studies. J Cereb Blood Flow Metab. Mar 2012;32(3):425-436.

Peer-reviewed publications

- *Plaque Components in Symptomatic Moderately Stenosed Carotid Arteries Related to Cerebral Infarcts: The Plaque At RISK Study.*
  AAJ de Rotte, MTB Truijman, AC van Dijk, MI Liem, FHBM Schreuder, AG van der Kolk, JR de Kruijk, MJAP Daemen, AFW van der Steen, GJ de Borst, PR Luijten, PJ Nederkoorn, ME Kooi, A van der Lugt, J Hendrikse.
  Stroke. 2015 Feb;46(2):568-71.

- *Intraplaque hemorrhage, fibrous cap status, and microembolic signals in symptomatic patients with mild to moderate carotid artery stenosis: the Plaque at RISK study.*
  MTB Truijman, AAJ de Rotte, R Aaslid, AC van Dijk, J Steinbuch, MI Liem, FHBM Schreuder, AFW van der Steen, MJAP Daemen, RJ van Oostenbrugge, JE Wildberger, PJ Nederkoorn, J Hendrikse, A van der Lugt, ME Kooi, WHM Mess.
  Stroke. 2014 Nov;45(11):3423-6.

- *Plaque At RISK (PARISK): prospective multicenter study to improve diagnosis of high-risk carotid plaques.*
  MTB Truijman, ME Kooi, AC van Dijk, AAJ de Rotte, AG van der Kolk, MI Liem, FHBM Schreuder, E Boersma, WHM Mess, RJ van Oostenbrugge, RJ Koudstaal, LJ Kappelle, PJ Nederkoorn, AJ Nederveen, J Hendrikse, AFW van der Steen, MJAP Daemen, A van der Lugt.
  Int J Stroke. 2014 Aug;9(6):747-54.

- *7.0 T MRI detection of cerebral microinfarcts in patients with a symptomatic high-grade carotid artery stenosis.*
  AAJ de Rotte, W Koning, AG den Hartog, SM Bovens, JJM Zwanenburg, DWJ Klomp, G Pasterkamp, FL Moll, PR Luijten, GJ de Borst, J Hendrikse.
  J Cereb Blood Flow Metab. 2014 Oct;34(10):1715-9.

- *Seven-tesla magnetic resonance imaging of atherosclerotic plaque in the significantly stenosed carotid artery: a feasibility study.*
  AAJ de Rotte, W Koning, MTB Truijman, AG den Hartog, SM Bovens, A Vink, S Sepehrkhouy, JJM Zwanenburg, DWJ Klomp, G Pasterkamp, FL Moll, PR Luijten, J Hendrikse, GJ de Borst.
  Invest Radiol. 2014 Nov;49(11):749-57.

- *MRI of the carotid artery at 7 Tesla: Quantitative comparison with 3 Tesla.*
  W Koning, AAJ de Rotte, JJ Bluemink, TA van der Velden, PR Luijten, DWJ Klomp, JJM Zwanenburg.
  J Magn Reson Imaging. 2014 Feb 27.

- *Feasibility of high-resolution pituitary MRI at 7.0 tesla.*
  AAJ de Rotte, AG van der Kolk, DR Rutgers, PMJ Zelissen, F Visser, PR Luijten, J Hendrikse.
  Eur Radiol. 2014 Aug;24(8):2005-11.

Conference presentations (first authors only)

- *7.0 T MRI of cerebral microinfarcts in symptomatic patients with a significantly stenosed carotid artery*
  AAJ de Rotte, W Koning, AG den Hartog, SM Bovens, A Vink, S Sepehrkhouy, JJM Zwanenburg, DWJ Klomp, G Pasterkamp, FL Moll, PR Luijten, GJ de Borst, J Hendrikse
  Oral presentation at the 22nd ISMRM Annual Meeting & Exhibition 2014, Milan, Italy

- *High quality 7T MRI of atherosclerotic plaque in the significantly stenosed carotid artery*
  AAJ de Rotte, W Koning, MTB Truijman, AG den Hartog, SM Bovens, A Vink, S Sepehrkhouy, JJM Zwanenburg, DWJ Klomp, G Pasterkamp, FL Moll, PR Luijten, J Hendrikse, GJ de Borst
  E-poster presentation at the 22nd ISMRM Annual Meeting & Exhibition 2014, Milan, Italy

- *Feasibility of high resolution 7.0 T pituitary MRI*
  AAJ de Rotte, AG van der Kolk, DR Rutgers, PMJ Zelissen, F Visser, PR Luijten, Hendrikse J
  Oral presentation at the 5th Annual Meeting of the ISMRM Benelux Chapter 2013, Rotterdam, The Netherlands
  Poster presentation at the 21st ISMRM Annual Meeting & Exhibition 2013, Salt Lake City, UT, USA

Dankwoord

Allereerst wil ik Jeroen Hendrikse, een van mijn twee co-promotoren, bedanken voor de kans die ik heb gekregen om deel te kunnen nemen aan dit ontzettend bijzondere onderzoek. Onderdeel uitmaken van een grote multi-center studie die op zijn beurt weer een onderdeel is van een grote translationele studie is een ervaring die ik met beide handen aangegrepen heb, omdat ik het vermoeden had dat je die kans niet vaak krijgt. Het was niet altijd makkelijk om een poppetje te zijn tussen een heleboel andere grote en kleine spelers, maar van jou kreeg ik in ieder geval altijd de waardering voor mijn harde werken.

Gert Jan de Borst, mijn tweede co-promotor, ook jou wil ik hartelijk bedanken voor de samenwerking. Het includeren van patiënten in de PlaCD-7T studie was soms moeizaam, maar door jouw doorzettingsvermogen en enthousiasme werd ik aangestoken en ontzettend gemotiveerd om hier elke week weer werk van te maken. Ook wil ik je hartelijk danken voor het meedenken en kritisch lezen van alle artikelen uit Deel I van dit proefschrift.

Peter Luijten, mijn promotor, hartelijk dank voor het deel uit mogen maken van de 7T groep. Door aan het PlaCD-7T project mee te gaan werken kwam ik bij in de 7T groep terecht wat een hele bijzondere samenwerking is tussen technici en klinici. Bijzonder gaaf om daar 3 jaar lang deel van uit te mogen maken.

Leescommissie: prof. dr. F.L. Moll, prof. dr. G.J. Biessels, prof. dr. W.P.Th.M. Mali, prof. dr. C.H.J. Terhaard en prof. dr. W.H. Mess, hartelijk dank voor het lezen en beoordelen van mijn proefschrift.

Alle patiënten en vrijwilligers die het mogelijk hebben gemaakt om de onderzoeken uit dit proefschrift tot stand te laten komen wil ik ontzettend bedanken. Zonder jullie was niet alleen het onderzoek niet mogelijk geweest, ook dit proefschrift had dan nooit tot stand kunnen komen.

Lieve paranimfen, Anouk en papa, wat een feestje om jullie achter mij te hebben.

Noukster, ik ben zo blij dat jij bij ons bent komen werken, met lekker veel bombari binnen komen en een dijk van een project neerzetten. Ik denk dat niet veel mensen het je nadoen. Ik kijk uit naar onze gezamenlijke publicatie in Investigative Oncology, die moet er gewoon echt een keer komen. Bedankt voor al je koffiemomentjes om eieren kwijt te kunnen, dubbel te liggen van het lachen en uit te kijken naar en terug te kijken op een waanzinnig mooie toerskivakantie. Ik kijk nu al uit naar de volgende.

Paps, jij zegt altijd “jij lijkt het meeste op mij van alle vier”. Tijdens de co-schappen snapte

ik dat nooit, het was niet het makkelijkste onderdeel van de studie en ik had vaak het gevoel dat we elkaar niet begrepen. In de afgelopen drie jaar ben ik er achter gekomen waar de schoen wrong. Gelukkig maar, want daardoor ben ik nu met ontzettend veel plezier begonnen bij de sportgeneeskunde en nog veel belangrijker, ik heb het gevoel dat we elkaar begrijpen. Het is bijzonder leuk om nu bij de cardiologie te werken en daar zo af en toe over te sparren, maar ik kijk er stiekem ook alweer naar uit om weer een klusproject samen aan te pakken, 1 kastje smaakt naar meer.

Anja, ontzettend bedankt dat ik van jou de Parisk studie over kon nemen. Ik denk dat ik geen betere voorgangster had kunnen treffen. Zo goed als jij alles op orde had... Later begreep ik dat dat niet alleen voor de Parisk studie gold. Ik heb me altijd bijzonder goed vermaakt als ik samen met jou kon lachen over onze overeenkomsten en toch ook de gigantische verschillen. Weeerkelijk!! Het begon al goed, ik met mijn gipsvoetje sprintjes trekken voor de bus om maar op tijd in de perifere centra te zijn. Is het ons nou ooit gelukt? Wij zijn een goed team, al zeg ik het zelf.

Wouter, wat een relaxte baas ben jij. Ontzettend gaaf dat ik met jou de 7.0 T stukken over de carotis kon schrijven. De technische termen duizelen me nog steeds, maar na 14 april maakt dat niet meer uit, want dan is het alleen nog maar check in tha box, twee ellebogen op tafel en handen in de lucht!!

Anneke, Saskia, Shanta, helden van het trialbureau. Zonder jullie is het voor ons promovendi niet mogelijk om het onderzoek rond te krijgen. Anneke, jou wil ik in het bijzonder bedanken voor het afronden van de laatste onderzoeken van de Parisk studie.

Alle laboranten van de duplex, CT en MRI wil ik mega veel bedanken, want de protocollen die mijn vrienden van de Parisk studie bedacht hebben zijn voor de laboranten niet altijd de makkelijkste. De tijd die het kost om het protocol af te werken was meestal niet helemaal in balans met de tijd die ervoor ingepland was in het programma, maar desondanks waren jullie altijd bereid om het protocol af te maken met kwalitatief goede beelden als resultaat. Dank!

Bij het secretariaat radiologie kan je terecht met de meest uiteenlopende vragen, een faxsturen, zaaltje huren voor vergaderingen, voorraad pennen/mappen/blocnotes, regelen stages voor studenten, indienen declaraties en niet te vergeten het versturen van pakketjes. In het bijzonder wil ik graag Marja en Sylvia bedanken voor alle keren dat ik weer langs kwam met een vraag waarop eigenlijk altijd wel een toepasselijk antwoord kwam.

Multimedia, Roy, Karin, Chris, Jan en Eugene, mijn vaste hangplek gedurende een groot deel van mijn onderzoek. Altijd geestverruimend om even een babbeltje te maken bij jullie. In het bijzonder Roy, onwijs bedankt voor alle lol en goede gesprekken die wij samen hebben gehad en je hulp bij grafische of fotografische klussen die ik voor werk én privé heb gedaan. Je hebt op de meest onchristelijke tijden voor me klaar gestaan en altijd met een lach, echt super!

Dennis, Jaco en Fredy dank voor de hulp bij technische stukken. Vaak snapte ik het wel, maar begreep ik het nog niet helemaal. Jullie zijn altijd bereid geweest om mij uit te leggen wat ik wilde weten en mijn stukken nauwkeurig te lezen. Dennis, jouw manier van leiding geven, altijd met een glimlach, vind ik echt onwijs bijzonder en ontzettend inspirerend. Als ik ooit leiding mag geven aan een groep dan hoop ik dat het lukt om aan jouw manier te tippen. Misschien moet ik gewoon beginnen een loopgroep, doe je mee?

Pierre Zelissen, prof. dr. Ad Hermus, Dik Rutgers, Theo Witkamp en Amy Groenewegen, ontzettend veel dank voor jullie inzet voor de hypofyse stukken. Zonder jullie was Deel II van dit proefschrift nooit tot stand gekomen.

Parisk collega's Anja, Martine, Floris, Anouk, Madieke, wat was ik blij dat ik jullie als klankbord had. Promoveren doe je eigenlijk voor een groot gedeelte alleen, maar bij de Parisk studie heb ik dat gevoel eigenlijk nooit gehad. Ik hoop dat we de Parisk etentjes er in kunnen houden nu de meeste van ons in de kliniek gestart zijn.

De 7T groep/Q4, onwijs bedankt voor de heerlijke koffie, de spaarzame borrel en bbq momenten waar ik bij kon zijn en natuurlijk de ISMRM reisjes. Eén ISMRM blijft me in het bijzonder bij, Salt Lake City. De reis begon met een waanzinnige dag skiën in Snowbird en bijna elke dag van het congres begon met een bootcamp en werd afgesloten met een rondje hardlopen en een borrel in de hottub.

Kamergenootjes: begonnen met Hanke, Tijl en Alex, later Hanke, Hamza en Marlijne en als laatste Wouter, Wybe, Anita, Aryen en Remco, ik hoop dat jullie niet te veel last hebben gehad van mijn eindeloze telefoontjes naar het AMC en patienten. Ik heb gelukkig ook heel wat uurtjes stilletjes ruisluisterend doorgebracht, ik weet gelukkig zeker dat jullie in die uren weinig last van me hadden. Anita, in het bijzonder wil ik jou nog bedanken voor alle eieren die wij altijd bij elkaar kwijt konden. Ik kijk uit naar de voorgenomen fietstochtjes, hopen dat die beter aflopen dat onze eerste poging.

Alle radiologie onderzoekers, onwijs bedankt voor de koffie momentjes, dinertjes en

fietstochtjes de afgelopen drie jaar. Super tof om te merken dat de verhalen nu steeds meer verschuiven van ervaringen als onderzoeker naar ervaringen als assistenten. Ik zeg, we houden het erin!

Lieve tant, wat heerlijk om zo af en toe een hapje samen te eten, in de duinen te wandelen en de hort op te gaan, lekker slieren. Ik vind het altijd knots gezellig dat je er bij bent, je hoort er gewoon bij.

Lieve papa, mama, Maurits, Pieter en Francijn, met zijn zessen zijn wij echt een bijzonder goed team. Pap, mam onwijs bedankt dat jullie hiervoor het perfecte voorbeeld hebben gegeven en de voorwaarden hiervoor hebben gecreëerd. Het is altijd een feestje om naar Oegstgeest te gaan en hoe voller het huis hoe leuker. Pap, nogmaals, het is een eer dat je achter me staat, niet alleen vandaag. Moems, bedankt voor heit eindeloos luisteren, of het nou frustraties of positieve ervaringen waren, bij jou kan je altijd terecht. En je hebt mijn Nederlandse samenvatting gecorrigeerd, waarvoor uiteraard ook ontzettend bedankt. Je bent een top-mama. Mau, jij bent altijd de eerste die alles mee moet maken van ons vieren, maar dat doe je eigenlijk bijzonder goed mag ik wel zeggen. Promoveren, trouwen en nu een kleine op komst, drie mijlpalen waarvan ik straks de eerste mag afvinken. Piet, met jou gaat het gelukkig ook eens niet over iets medisch, maar gewoon over bouw, inrichting en hardlopen. Ik hoop dat we komend jaar weer een paar mooie loopevenementen af kunnen vinken en dat we nog een keer mooie creatieve ideeën kunnen uitwerken samen. Sis, als ik jou niet had...met jou is het altijd zo heerlijk. Wij hebben aan een half woord genoeg om te begrijpen wat we bedoelen. In de box begreep jij al dat ik eruit wilde en een opstapje nodig had. Met jou kan ik helemaal in een scheur te liggen, maar gelukkig ook door de modder kruipen, planken en 65 km langs de Hollandse kust rennen/fietsen. Ik zeg we maken er dit jaar 135 km van, ik heb de beker alvast besteld.

Lieve Björn, last, but definitly not least! Ik vind het altijd zo gaaf om te horen hoe jij plannen hebt gesmeden om mij in te pakken en te versieren, een strikje erom en klaar is kees, het is je gelukt. Zonder dat ik het wist heb ik zelf ruimte gecreëerd voor de laatste stap...naar Utrecht verhuizen. Het was legendarisch, als ik eraan terug denk krijg ik nog buikpijn van het lachen. Met jou samen op pad zijn voelde vanaf dat eerste moment al goed. Lief, bij jou kan ik mezelf zijn en je geeft me het gevoel speciaal te zijn en dat is zo'n bijzonder gevoel. Ik kijk er naar uit om nog heel veel met jou op pad te zijn en nog vele jaren in ons huisje te genieten. Je bent een toffe huisgenoot!!

Curriculum Vitae

De auteur van dit proefschrift werd geboren op 19 maart 1986 te Nijmegen. De lagere school heeft zij doorlopen aan de Gevers Deutz Terweeschool in Oegstgeest. Na het behalen van haar VWO diploma aan het Rijnlands Lyceum in Oegstgeest is zij in 2004 begonnen met de studie geneeskunde aan de Rijksuniversiteit Groningen. Op 31 januari 2008 heeft zij de bacheloropleiding van geneeskunde afgerond en kon zij beginnen met haar coassistentschappen. Haar junior-coschappen heeft zij gevolgd in het Universitair Medisch Centrum Groningen en de senior-coschappen volgden in het Deventer Ziekenhuis. In Deventer volgde zij ook de semi-artsstage bij de radiologie en de nucleaire geneeskunde onder begeleiding van dokter M.M.J.J.R. Jaspers, dokter J.C.N.M. Aarts en dokter J.M.B. Manders. Haar wetenschappelijke stage heeft zij gevolgd aan de faculteit Industrieel Ontwerpen van de Technische Universiteit Delft, onder begeleiding van prof. dr. H. de Ridder, in samenwerking met de afdeling maag-, darm- en leverziekten van het Catharina Ziekenhuis te Eindhoven (dr. E.J. Schoon). Het afsluitend examen van de masteropleiding geneeskunde werd succesvol afgelegd op 26 juli 2011.

Van januari 2012 tot en met december 2014 was de schrijfster werkzaam als promovenda bij de afdeling radiologie van het Universitair Medisch Centrum Utrecht, in welk kader dit proefschrift tot stand kwam.

In januari 2015 is de schrijfster begonnen met de vierjarige specialisatie sportgeneeskunde in het Universitair Medisch Centrum Utrecht. Momenteel is zij, in het kader van deze specialisatie, werkzaam als arts-assistent op de afdeling cardiologie van het Universitair Medisch Centrum Utrecht.